# Lawrence Berkeley National Laboratory

**Title**
COMPLETE DETERMINATION OF POLARIZATION FOR A HIGH-ENERGY DEUTERON BEAM

**Permalink**
https://escholarship.org/uc/item/8ms8k7f6

**Author**
Button, Janice.

**Publication Date**
1959-03-01

# UNIVERSITY OF CALIFORNIA

*Ernest O. Lawrence*

# Radiation Laboratory

## BERKELEY, CALIFORNIA

8691

## DISCLAIMER

UNIVERSITY OF CALIFORNIA

Lawrence Radiation Laboratory
Berkeley, California

# COMPLETE DETERMINATION OF POLARIZATION
## FOR A HIGH-ENERGY DEUTERON BEAM

Janice Button
(Thesis)

May 4, 1959

# COMPLETE DETERMINATION OF POLARIZATION
# FOR A HIGH-ENERGY DEUTERON BEAM

## Contents

# COMPLETE DETERMINATION OF POLARIZATION
# FOR A HIGH-ENERGY DEUTERON BEAM

Janice Button

Lawrence Radiation Laboratory
University of California
Berkeley, California

May 4, 1959

## ABSTRACT

Measurements have been made, by double scattering, of all parameters necessary to describe completely the interaction of the deuteron with complex nuclei. Tensor components of polarization, which characterize the scattering of spin-one particles and which were unobservable at low energies, were determined to be appreciably different from zero. Internal targets at two different positions were used to polarize beams undergoing differing amounts of magnetic bending in the field of the cyclotron in order to separate two polarization components included in the $\cos\phi$ term of the scattering cross section for a polarized beam.

Deuterons of 410 and 420 Mev were scattered from beryllium and carbon, respectively. Internal angles of scattering were 10 deg for beryllium and 11 deg for carbon; angles of second scattering extended from 6 to 18 deg. The usual spin polarization (vector polarization) normal to the plane of scattering was found to reach a maximum of about 70%.

The impulse approximation was employed to obtain estimates of deuteron cross section and polarization on the basis of nucleon-scattering data.

# I. INTRODUCTION

Although the phenomenon of deuteron polarization is much more complex than that of proton polarization, experimental research should lead to a better understanding of the spin-orbit interaction between nucleon and nucleus and, more particularly, of the relative importance of various effects in the scattering of the deuteron. Many studies have been made of the spin-orbit potential in nucleon interactions.[1] Experimental work on the scattering of deuterons has been rather limited; Baldwin et al.[2] measured cross sections and polarizations for various elements at 94, 125, and 157 Mev, but failed to observe any of the "tensor components" of polarization expected for a spin-one particle. Stapp made extensive theoretical studies of the application of the impulse approximation in various forms to deuteron scattering; he found good agreement with experiment only by assuming that simultaneous scattering of both nucleons of the deuteron was an important effect.[3] Neither his assumptions as to the form of the nucleon-nucleus potential nor the use of nucleon-scattering data gave vector-polarization predictions at all comparable to the large values observed by Baldwin, although the tensor components could be estimated as very close to zero. Tripp carried out an experiment on the $p + p \rightarrow \pi^+ + d$ reaction to analyze the polarization of the deuteron for determination of the phases of meson-production amplitudes and hence differences in p-p phase shifts; on the basis of the work of Baldwin and Stapp, he assumed that tensor components were zero.[4]

Scattering measurements at a deuteron energy above 400 Mev, available from the reconverted cyclotron, seemed desirable to determine whether the tensor components of polarization might be observable; further, a method of separating the two components of polarization appearing in the $\cos\phi$ asymmetry, heretofore considered very difficult,[5] had been suggested,[a] and it was thought that the complete determination of scattering-matrix components would be

---

[a] By Dr. Ronald Mermod, now at Cern Laboratory, Geneva.

of interest. It was to be expected that the impulse approximation would give better agreement with experiment at the higher deuteron energy, since nucleon polarization rises rapidly with energy near 100 Mev and the Born approximation has greater validity at higher energies.

The results of the scattering by beryllium and carbon of two polarized beams having different tensor components are reported here. An analysis is carried out on the basis of the impulse approximation and comparison made with Baldwin's results.

It should be a relatively simple matter to extend these measurements to lower energies by degrading before the second scattering and thus to determine the energy dependence of polarization components more exactly. Further, useful information on differences between p-p phase shifts could be obtained by analysis of deuteron polarization in the $p+p \rightarrow \pi^+ + d$ reaction at proton energies of 400 to 740 Mev.

## II.  THEORY

Because the deuteron is a particle of spin one, four parameters in addition to the unpolarized cross section are needed to specify the intensity after double scattering.  These parameters are dependent upon the angles of first and second scattering and may be expressed in terms of the expectation values, after single scattering, of certain operators in the spin space of the deuteron.  Two of them may be determined immediately from differential-cross-section measurements, as was done by Baldwin at lower energies;[2] the other two, however, are combined as the coefficient of a $\cos\phi$ term (where $\phi$ is the azimuthal angle between the normals to the first and second scattering planes) and can be separately determined only by double scattering with and without a magnetic field between the first and second targets.

The theory of polarization of the deuteron was given first by Lakin[5] and subsequently treated with a different formalism by Stapp.[3]  Just as there are four independent matrices necessary to specify the scattering matrix of nucleons having a two-dimensional spin space, there must be nine linearly independent matrices to describe the scattering of deuterons which have a three-dimensional spin space.  The application of parity and time-reversal restrictions reduces this number to five.  For the nucleons, the unit matrix and the three Pauli spin operators suffice, but for the deuteron there must be included in the scattering matrix not only terms linear in the spin operators, but second-rank tensor terms as well.

### A.  Formalism

A convenient set of operators given by Lakin includes the unit matrix, two linear combinations of spin operators, and three second-rank tensor products of spin operators, as well as the Hermitian adjoint of three of these.  The advantages of this particular representation are that the operators transform in spin space just as the spherical harmonics transform in coordinate

space, and further that the second-scattered intensity may be expressed in an especially simple manner.[a]

These matrices are:

$$T_{00} = 1$$

$$T_{11} = -\frac{\sqrt{3}}{2}(S_x + iS_y)$$

$$T_{10} = \sqrt{\frac{3}{2}}\, S_z$$

$$T_{22} = \frac{\sqrt{3}}{2}(S_x + iS_y)^2$$

$$T_{21} = -\frac{\sqrt{3}}{2}\left[(S_x + iS_y)S_z + S_z(S_x + iS_y)\right]$$

$$T_{20} = \frac{1}{\sqrt{2}}(3S_z^2 - 2)$$

$$T_{J,-M} = (-)^M T_M^{\dagger}$$

Choice of a particular coordinate system causes some of the $\langle T_{JM} \rangle$ resulting from a scattering process to equal zero. (This can be seen by considering an explicit form of M or MM$^{\dagger}$, as in Section C.) An especially useful system is that in which the y axis

---

[a] Like the spherical harmonics, the $T_{JM}$ are an irreducible set of tensor operators and hence have especially simple rotation transformations associated with them. (See Appendix B for fuller discussion.)

is normal to the scattering plane and the z axis is along the direction of motion of the once-scattered beam. (See Fig. 1.) For this situation the state of polarization of the scattered particles is completely described by the expectation values of four of the $T_{JM}$ operators as well as the normalization $\langle T_{00} \rangle$; further, all $\langle T_{2M} \rangle$ are real, while $\langle T_{11} \rangle$ is pure imaginary.

Lakin constructs a product of the scattered matrix and its adjoint $MM^{\dagger}$ which is invariant under space inversion and time reversal, and in the reference system defined above he obtains for the second-scattered intensity

$$I_p(\theta_2, \phi) = I_u(\theta_2) \left[ 1 + \langle T_{20} \rangle_1 \langle T_{20} \rangle_2 + 2 \left( \langle iT_{11} \rangle_1 \langle iT_{11} \rangle_2 \right. \right.$$

$$\left. \left. - \langle T_{21} \rangle_1 \langle T_{21} \rangle_2 \right) \cos \phi + 2 \langle T_{22} \rangle_1 \langle T_{22} \rangle_2 \cos 2\phi \right],$$

where $I_u$ is the cross section for scattering of an unpolarized beam; $\phi$ is the azimuthal angle between normals to the two scattering planes; [a] $\langle T_{JM} \rangle_1$ represents the expectation value of the tensor operator $T_{JM}$ after scattering of an unpolarized beam at an angle $\theta_1$ by Target 1; and $\langle T_{JM} \rangle_2$, the same for angle $\theta_2$ at Target 2. (The coordinate system used has its z axis along the direction of beam incident on the second target, but the $\langle T_{JM} \rangle$ for each of Targets 1 and 2 are defined with the z axis along the outgoing momentum because time reversal is used to obtain the $\langle T_{2M} \rangle_2$ of Target 2.)

The quantity $\langle iT_{11} \rangle$ is referred to as "vector polarization," as it is proportional to $\langle S_y \rangle$, the polarization normal to the scattering plane, while the $\langle T_{2M} \rangle$ are components of "tensor polarization" and represent a spin alignment rather than an orientation. The latter constitute a second-rank tensor, one of whose principal axes is along the direction of spin or parallel to $\langle iT_{11} \rangle$.

---

[a] defined by $\cos \phi = \bar{n}_1 \cdot \bar{n}_2$ or $\sin \phi = \bar{n}_1 \times \bar{n}_2 \cdot \bar{k}_{2i}$

(a)

(b)
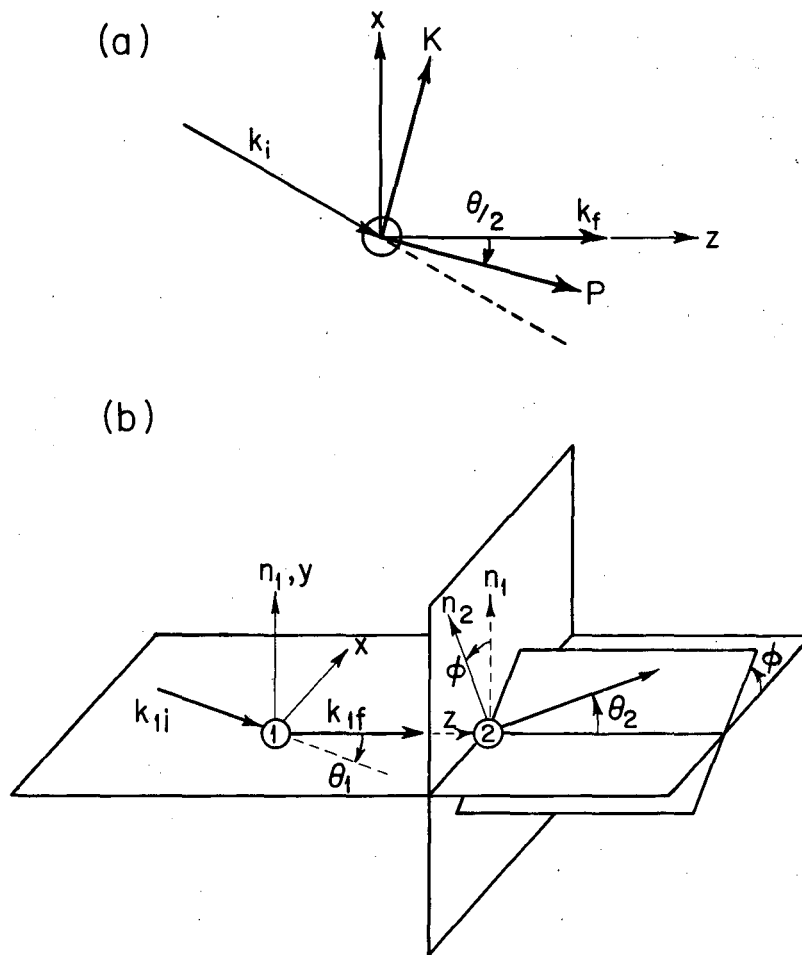
MU−17288

Fig. 1. (a) Coordinate system for single scattering as
seen in the plane of scattering.

(b) Geometry of double scattering.

This vector polarization is evidently not affected by a magnetic field normal to the plane of scattering, but such a field does cause rotation of the polarization tensor relative to the beam-defined coordinate system described above, and hence a mixing of the $\langle T_{2M} \rangle$ components.

## B. Description of State of Polarization

Description of the state of a particle following a scattering interaction may be given by the use of a scattering matrix M, which defines the final state in terms of the initial state,

$$\psi_f = M \, \psi_i.$$

The density matrix after scattering then takes the form

$$\rho_f = \sum_j \psi_f^j \, \psi_f^{j\dagger} = M\rho_i M^\dagger,$$

and this gives the expectation value of any spin operator $S^\mu$ after scattering,

$$\langle S^\mu \rangle = \frac{\mathrm{Tr}\,(\rho_f S^\mu)}{\mathrm{Tr}\,\rho_f} = \frac{\mathrm{Tr}\,M\rho_i M^\dagger S^\mu}{\mathrm{Tr}\,M\rho_i M^\dagger}.$$

The initial-density matrix may be expressed in terms of a complete set of these spin operators $R^\nu$, under the requirement $\mathrm{Tr}\,R^\alpha R^{\beta\dagger} = n_i \delta_{\alpha\beta}$, as

$$\rho_i = \frac{1}{n_i} \sum_\nu \langle R^\nu \rangle \, R^{\nu\dagger}$$

($n_i$ being the dimensionality of the initial spin space). Then the Wolfenstein-Ashkin relation[6] follows,

$$I \langle S^\mu \rangle_f = \frac{\mathrm{Tr}\rho_f}{\mathrm{Tr}\rho_i} \langle S^\mu \rangle_f = \frac{1}{n_i} \sum_\nu \langle R^\nu \rangle_i \, \mathrm{Tr}(M R^{\nu\dagger} M^\dagger S^\mu),$$

with $R^\nu$ and $S^\mu$ referring to the same set of spin operators for the description of initial and final states, respectively.

From this relation the cross section is found for second scattering,

$$I_2 = \frac{1}{n_i} \sum_\nu \langle R^\nu \rangle_i \, \mathrm{Tr}M^\dagger M R^\nu;$$

and polarizations or expectation values of spin operators after
single scattering are

$$I_u \left\langle S^\mu \right\rangle_f = \frac{1}{n_i} \cdot Tr \, (MM^\dagger S^\mu).$$

In the case of the deuteron, these spin operators $R^\nu$ and $S^\mu$ can of
course be defined as the $T_{JM}$ of Lakin.

Evidently, expressions either for $M^\dagger M$ and $MM^\dagger$ or for the
scattering matrix alone would be useful in describing the scattering
of a particle. Lakin chooses to define a general form for $MM^\dagger$ and
also for $M^\dagger M$ on the basis of invariance arguments;[a] he forms all
possible products of the above-described $T_{JM}$ and the spherical
harmonics $Y_{JM}$ (with arguments derived from $k_i$ and $k_f$, incident
and final momenta) that are invariant under space inversion by
using only those $Y_{JM}$ which are even in $k_i$ and $k_f$. He finds the
cross section for second scattering as a function of $\left\langle T_{JM} \right\rangle_1$,
$Y_{JM}$ $(\theta_2, \phi)$, and $\theta_2$- dependent coefficients of the $M^\dagger M$ terms by
substituting the $M^\dagger M$ expression into the $\left\langle S^\mu \right\rangle_f$ relation above and
taking $S^\mu$ equal to the unit matrix; he then notes that time reversal
requires $M^\dagger M$ to be equal to $MM^\dagger$ and finds the angle-dependent
coefficients in terms of the $\left\langle T_{JM} \right\rangle_2$ resulting from the scattering
of an unpolarized beam. (Subscripts refer to the geometries of
first and second scatterings.) The expression for second-scattering
cross section which he obtains is as given on page 9.

Stapp, on the other hand, prefers to define M alone as

$$M = A \, (\theta) + B_i \, (\theta) \, S_i + C_{ij} \, (\theta) \, S_{ij},$$

[a] $\overline{MM^\dagger} = J_0 + J_1 \sum_M Y_{2M} \, (\overline{k}_i) \, T^\dagger_{2M} + J_2 \sum_M \cdot Y_{2M} \, (\overline{k}_f) \, T^\dagger_{2M}$

$+ J_3 \sum_M Y_{2M} \, (\overline{k}_i, \overline{k}_f) \, T^\dagger_{2M} + J_4 \sum_M Y_{1M} \, (\overline{k}_i \times \overline{k}_f) \, T^\dagger_{1M}$, where

$Y_{2M} \, (\overline{k}_i, \overline{k}_f)$ is a second-degree harmonic, bilinear, and symmetrical
in $k_i$ and $k_f$.

with the $S_{ij}$ representing symmetrized products of spin operators. [a]
Invariance under space inversion and time reversal is again applied
to restrict the types of terms. As Wolfenstein and Ashkin have
shown, only the $S_i n_i$ term of the class of vector contractions is
invariant under space inversion and time reversal; similar arguments
show that of all the tensor products only $S_{ij} n_i n_j$, $S_{ij} P_i P_j$, and $S_{ij} K_i K_j$
terms are possible if $\bar{n}$ is the normal to the plane of scattering, $\bar{P}$
the sum of initial and final momenta, and $\bar{K}$ the difference of initial
and final momenta. (The $\bar{n}\bar{K}$ tensor changes sign under space inver-
sion; the $\bar{n}\bar{P}$ tensor, under both space inversion and time reversal;
and the $\bar{P}\bar{K}$ tensor, under time reversal.) Thus the most general
scattering matrix satisfying invariance requirements is

$$M = a\,(\theta) + b\,(\theta)\,S_i n_i + \left[ c\,(\theta)\,(n_i n_j - 1/3\,\delta_{ij}) \right.$$

$$\left. + d\,(\theta)\,(P_i P_j - K_i K_j) \right]\,S_{ij}\,.$$

Although this scattering matrix gives a rather complex expression
for cross section in second scattering, it is useful for evaluating
polarization components in terms of scattering-matrix elements,
which may be related to the scattering matrix for nucleon-nucleus
interaction.

### C. Cross Section for Second Scattering

Although Stapp's notation is more cumbersome than Lakin's,
his formalism gives a better understanding of the origin of the $\phi$-
dependence of terms in $I_2$. He defines the scattering matrix as
given above. The vectors entering into this matrix are represented
in Fig. 1a, their definitions being

$$\bar{n} = \text{unit vector along } \bar{k}_i \times \bar{k}_f,$$

$$\bar{P} = \text{unit vector along } \bar{k}_i + \bar{k}_f,$$

$$\bar{K} = \text{unit vector along } \bar{k}_f - \bar{k}_i.$$

---

[a] $S_{ij} \equiv 1/2\,(S_i S_j + S_j S_i) - 2/3\,I\,\delta_{ij}.$

In terms, then, of the xyz coordinates defined by the first scattering, as above, the vector components used in the scattering matrix for the second target may be represented as the following functions of $\theta$ and $\phi$,

$$n_{2x} = -\sin\phi, \qquad n_{2y} = \cos\phi, \qquad n_{2z} = 0;$$

$$K_{2x} = \sin\frac{\theta}{2}\cos\phi, \qquad K_{2y} = \sin\frac{\theta}{2}\sin\phi, \qquad K_{2z} = \cos\frac{\theta}{2};$$

$$P_{2x} = \cos\frac{\theta}{2}\cos\phi, \qquad P_{2y} = \cos\frac{\theta}{2}\sin\phi, \qquad P_{2z} = -\sin\frac{\theta}{2}.$$

If $I_2(\theta,\phi)$ is now determined by taking $I_2 = \mathrm{Tr}\, M_2 \rho_1 M_2^{\dagger}$, with $\rho_1$ the density matrix after first scattering, Stapp's form of the scattering matrix characterizing the interaction at Target 2 may be substituted to give

$$I_2 = \mathrm{Tr}\left\{\left[a + b\,\bar{S}\cdot\bar{n}_2 + c(n_i n_j - \delta_{ij}/3)_2 S_{ij}\right.\right.$$
$$+ d\,(P_i P_j - K_i K_j)_2\, S_{ij}\right] \cdot \rho_1 \left[a^* + b^*\bar{S}\cdot\bar{n}_2 + c^*(n_i n_j - \frac{\delta_{ij}}{3})_2 S_{ij}\right.$$
$$\left.\left. + d^*(P_i P_j - K_i K_j)_2\, S_{ij}\right]\right\} = a^2 + 2/3\, b^2 + 4/3\,\mathrm{Re}\,a^*b\,\mathrm{Tr}\,(\rho_1\bar{S}\cdot\bar{n}_2)\cdots$$

It is evident that the third term is proportional to $\langle S_y\rangle_1 \langle S_y\rangle_2 \cos\phi$[a] or to $\langle iT_{11}\rangle_1 \langle iT_{11}\rangle_2 \cos\phi$. Also there is a $\cos\phi$ term proportional to $\langle S_x S_z\rangle_1$ or to $\langle T_{21}\rangle_1$, which derives from

$$\mathrm{Tr}\left\{\rho_1 2\,\mathrm{Re}\,a^*d\,(P_x P_z - K_x K_z)\, S_{xz}\right\} \cong -\langle S_{xz}\rangle_1\, 2\,\mathrm{Re}\,a^*d\,\sin\frac{\theta}{2}\cos\frac{\theta}{2}\cos\phi.$$

Further, such terms as $\mathrm{Tr}\left\{\rho_1 d^2(P_x P_z - K_x K_z)^2 S_{xz}^2\right\}$ will reduce to the form $\cos^2\phi\langle S_y^2\rangle_1$, part of which is proportional to $\langle T_{22}\rangle_1$ $\cos 2\phi$; and $\mathrm{Tr}\left\{\rho_1 2\,\mathrm{Re}\,a^*d\,(P_z^2 - K_z^2) S_z^2\right\}$ will be of the form $(\cos^2\frac{\theta}{2} - \sin^2\frac{\theta}{2})\langle S_z^2\rangle_1$, or proportional to $a\langle T_{20}\rangle_1$ term independent of $\phi$.

---

[a]$\mathrm{Tr}\,(\rho_1 S_y)$ gives the expectation value $\langle S_y\rangle_1$ and its coefficient $\mathrm{Re}\,a^*b$ is proportional to the $\langle S_y\rangle_2$ that would result from scattering an unpolarized beam from the second target.

## D. Single Scattering

If the coordinate system considered has its y axis along the normal and its x and z axes in the plane of scattering, then $\langle S_y \rangle$ is the only component of spin polarization produced in the scattering of an unpolarized beam; i.e., $\langle S_x \rangle = \langle S_z \rangle = 0$. Further, it can be shown that the polarization tensor has one of its principal axes along the y axis, or that $\langle S_y S_x \rangle = \langle S_y S_z \rangle = 0$. This can be demonstrated formally by using either Stapp's or Lakin's expression for $MM^\dagger$.[a] The vanishing of these expectation values follows from the requirement that the terms in M be invariant under the parity operation.

In the coordinate system with the z axis parallel to the scattering normal, the requirements that $\langle S_x \rangle$ and $\langle S_y \rangle$ equal zero after the scattering of an unpolarized beam yield particular forms for the deuteron spin functions.[b] One solution is

$$\chi_A = \begin{bmatrix} \alpha e^{i\lambda} \\ \beta \\ -\alpha e^{-i\lambda} \end{bmatrix} e^{i\lambda_0^A} \qquad \text{and the other is} \qquad \chi_B = \begin{bmatrix} (\cos \delta/2)e^{i\lambda} \\ 0 \\ (\sin \delta/2)e^{-i\lambda} \end{bmatrix} e^{i\lambda_0^B},$$

where $\alpha$ and $\beta$ are real and $2\alpha^2 + \beta^2 = 1$. These wave functions are of interest in that the phases can be interpreted in terms of a magnetic field H applied along the z axis for a time t by solving the equation (with $\mu$ the magnetic moment of the deuteron)

$$-\mu S_z H_z \chi = i\hbar \dot\chi \qquad \text{to find} \qquad \lambda = \frac{\mu H_z}{\hbar} t.$$

---

[a] Formulae giving the reduction of spin-operator products are in Stapp's thesis,[3] p. 119.

[b] These $\chi_A$ and $\chi_B$ functions can, of course, be put in the same form as the Lakin or the Baldwin spin functions. (See Appendix B.)

Solution A may be interpreted as representing spin oriented in the plane of scattering with probability $\beta^2$ and spin oriented parallel or antiparallel to the normal with probability $\alpha^2$; the probability of finding an average spin orientation along the z-axis normal thus is zero. For Solution B, spin is oriented on the average at an angle to the normal, so that the probability of finding spin along the normal is cos $\delta$. For this case,

$$\langle S_{zz} \rangle = 1,$$

$$\langle S_{xx} \rangle = 1/2 \ (1 + \sin \delta \cos 2\lambda),$$

$$\langle S_{yy} \rangle = 1/2 \ (1 - \sin \delta \cos 2\lambda),$$

$$1/2 \ \left( \langle S_{xy} \rangle + \langle S_{yx} \rangle \right) = - \ 1/4 \sin \ \delta \sin 2 \ \lambda.$$

(These values, or their reciprocals, when plotted to give $\langle S^2 \rangle$ or $1/\langle S^2 \rangle$ in the x-y scattering plane, give an ellipse whose orientation relative to the direction of the motion of the deuterons is determined by the value of $\lambda$ or of $H_z t$ associated with the bending after scattering. See Fig. 2.)

·The polarization tensor is to be interpreted as the statistical distribution of deuteron spin; expectation values of $\langle S_{zz} \rangle$, $\langle S_{xx} \rangle$, and $\langle S_{yy} \rangle$ indicate the probability of finding spin aligned along the various axes. Hence, for Solution A above, $\overline{\langle S_{zz} \rangle} = 2\alpha^2$, although $\langle S_z \rangle$ is zero; for the second solution, $\langle S_{zz} \rangle = 1$, while $\langle S_{xx} \rangle$ and $\langle S_{yy} \rangle$ vary from 0 to 1 depending on the quantities sin $\delta$ and cos $2\phi$.

The $\langle T_{2M} \rangle$ tensor components have the following physical interpretations in the scattering of an unpolarized beam: $\langle T_{20} \rangle$ indicates the probability of finding spin aligned along the z axis; $\langle T_{22} \rangle$ , the preference for spin alignment along the x rather than the y axis; and $\langle T_{21} \rangle$ , the amount by which the orientation of the $\langle S_i S_j \rangle$ ellipse axes in the plane of scattering differs from that of the x-z scattering coordinates. These conclusions are based on the facts that $\langle T_{20} \rangle$ is dependent on $\langle S_z^2 \rangle$, $\langle T_{22} \rangle$ on $\langle S_x^2 \rangle - \langle S_y^2 \rangle$,

$z$

$\langle S_z \rangle = S \cos \delta$

spin S

$y$

$x$

(a)

$z$

$H$

$2 \sin \delta$

$y$

$\dfrac{d\lambda}{dt}$

$x$

(b)
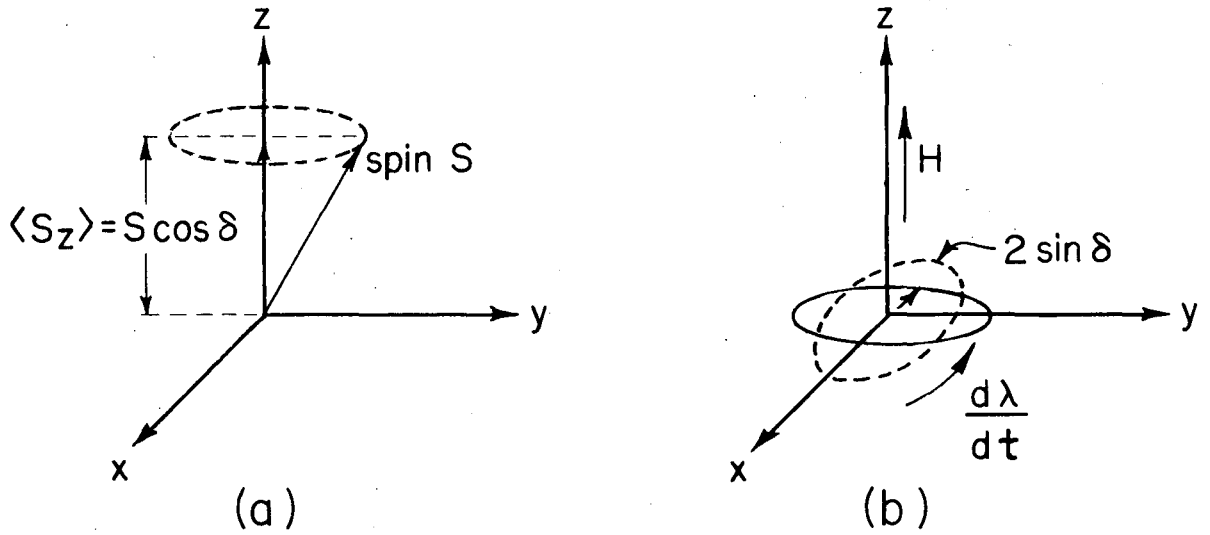
MU — 17289

Fig. 2. (a) Classical representation of a general type of wave function $(\chi_B)$ for spin-one particles.

(b) The projection of $\langle S^2 \rangle$ or $1/\langle S^2 \rangle$ in the x-v scattering plane.

and $\langle T_{21} \rangle$ on $\langle S_x S_z \rangle$ ; $\langle T_{20} \rangle$ has further significance in representing the extent by which the occupation of the $m_s = 0$ state for the z axis differs from the unpolarized value of one-third.

### E. Pure Polarization States

As is stated by Lakin and as can be shown by use of the spin operators and wave functions in Appendix B, the $\cos \phi$ term of the polarized cross section for $\theta_1 = \theta_2$ reaches a maximum of $3/2$ $\cos \phi$ if the first scattering puts all particles into the pure spin state $\chi_{+1}$ (or $\chi_{-1}$) along the normal (y axis). The limit of $3/2$ for e can also be obtained by noting that the unpolarized cross section ($I_u$) must be $1/3$ the polarized cross section at $\phi = 0$ ($I_0$) if the polarized beam contains only spin-up particles and these are all scattered left. Then

$$e = \frac{I_0 - I_{180}}{2 \, I_u} = \frac{I_0}{2/3 \, I_0} = 3/2.$$

The tensor components describing the once-scattered incident beam in this case have the values

$$\langle T_{10} \rangle = 0 \qquad \text{or} \qquad \langle S_z \rangle = 0,$$

$$\langle iT_{11} \rangle = \sqrt{3}/2 \qquad \text{or} \qquad \langle S_x \rangle = 0, \langle S_y \rangle = 1,$$

$$\langle T_{20} \rangle = -\frac{1}{2\sqrt{2}} \qquad \text{or} \qquad \langle S_z^2 \rangle = 1/2,$$

$$\langle T_{21} \rangle = 0 \qquad \text{or} \qquad \langle S_{xz} \rangle = -\langle S_{zx} \rangle ,$$

$$\langle T_{22} \rangle = -\sqrt{3}/4 \qquad \text{or} \qquad \langle S_x^2 \rangle - \langle S_y^2 \rangle = 1/2 - \langle S_y^2 \rangle = -1/2.$$

Thus all spins will be found in a cone along the +y axis; 1/4 of them will be along the +z or -z axis, but with average $S_z = 0$, and 1/4 along the +x or -x axis with average $S_x = 0$, while 1/2 will be aligned along the y axis. The $\hat{y}$ axis is a principal axis of the polarization tensor and indeed is the smallest of the three axes of the polarization ellipsoid representing this tensor. (See Appendix D.2.)

$$\left(\frac{1}{\langle S_y^2\rangle} < \frac{1}{\langle S_x^2\rangle} = \frac{1}{\langle S_z^2\rangle}.\right)$$ The ellipsoid has the form of an oblate

spheroid. Magnetic-field rotation of the tensor or ellipsoid about the y axis does not change the values of $\langle S_z^2\rangle$, $\langle S_x^2\rangle$, or $\langle S_y^2\rangle$, and hence leaves the $\langle T_{2M}\rangle$ unchanged.

The cross-section $\cos 2\phi$ term attains a maximum for the case of a pure $\chi_0^y$ state. $\langle S_y\rangle$ then $= 0$, as do also $\langle S_x\rangle$ and $\langle S_z\rangle$. The values of tensor components indicate that the spins of all particles lie in the plane of scattering, but are quite randomly aligned. Again the polarization ellipsoid is circularly symmetric about the y axis --i. e., $\langle S_{xz}\rangle + \langle S_{zx}\rangle = 0$--but it degenerates into a cylinder, as $1/\langle S_y^2\rangle$ is infinite.

### F. Tensor Rotation

Two effects enter into the transformation of the $\langle T_{JM}\rangle$. One of these is the rotation of the coordinate system resulting from deflection of the deuteron by the magnetic field; the other is the precession of spin axes in the plane perpendicular to the field direction. For relativistic particles, the latter must include the contribution of Thomas precession.[7] (See Fig. 3a) The deflection of the deuteron in the x-z plane is given by:

$$\omega_{cyclotron} t = 1/\gamma \frac{eH}{2m_p c} \quad t = 1/\gamma \quad \omega_{larmor} t = \eta.$$

The precession of the spin or magnetic moment is:

$$\omega_{precess} t = \left[\mu_d \omega_{larmor} + (1-\gamma)\omega_{cyclotron}\right] t,$$

where $\mu_d$ is the magnetic moment of the deuteron in terms of the nuclear magneton. Thus the angle through which the spin of the deuteron (or more exactly the axes of the polarization tensor, as the spin is on the average parallel to the field) is turned relative to the final direction of motion z' is:

$$\lambda = (\omega_{precess} - \omega_{cyclotron}) t = \gamma (\mu-1) \eta$$

$$= 1.22 (.8565 - 1) \eta \simeq -1/6 \eta.$$

(a)

(b)

MU−17290
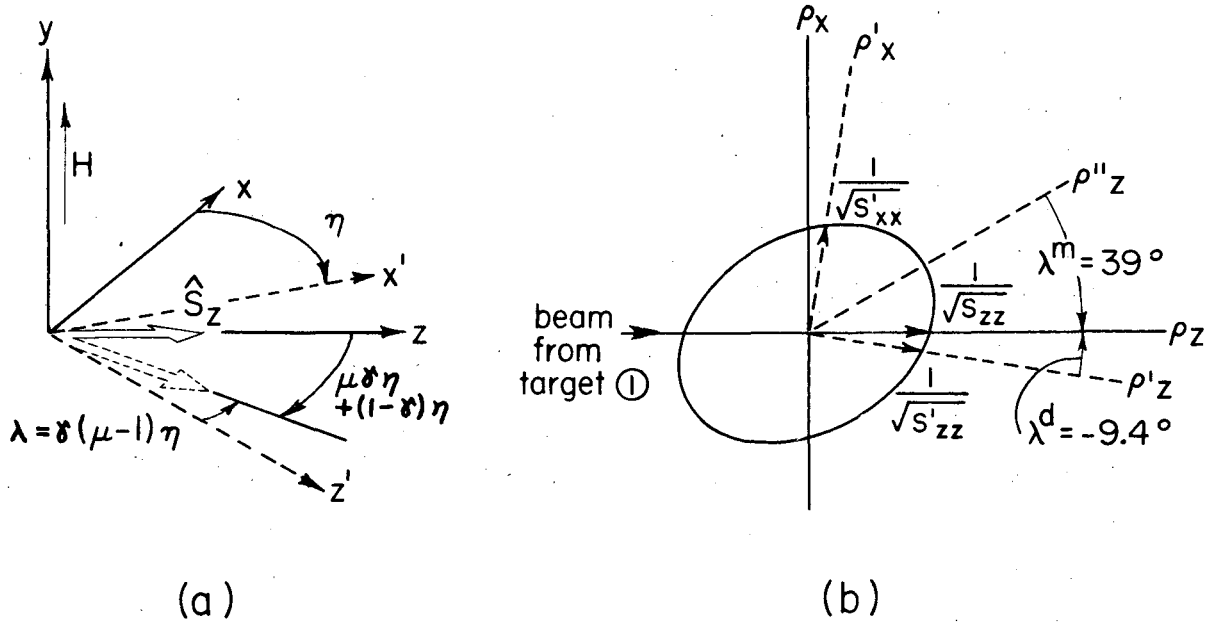
Fig. 3 (a) Rotation of deuteron spin under the action
of a magnetic field. Here z and z' are the initial
and final directions of motion of the deuteron.

(b) Section of polarization ellipsoid in x-z
plane of scattering, describing the state of polari-
zation after single scattering of an unpolarized
beam. The axis $\rho'_z$ is parallel to $k_{21}$ for the dee-
target beam; the axis $\rho''_z$ is parallel to $k_{2i}$ for
the meson-target beam. (See Fig. 1.)

The quantity $\eta$ is positive if deflection is clockwise along the negative y axis. (This is the case for deuterons scattered left in a field directed along the positive y axis.)

The equations expressing the rotated $\langle T_{2M} \rangle'$ quantities in terms of the original $\langle T_{2M} \rangle$ may be written

$$\langle T_{2M'} \rangle' = \sum_M a_{M'M} \langle T_{2M} \rangle ,$$

where the a's are trigonometric functions of the angle $\lambda$ or of the angle of deflection of the beam. Explicitly, the equations are

$$\langle T_{20} \rangle' = a_{00} \langle T_{20} \rangle + a_{01} \langle T_{21} \rangle + a_{02} \langle T_{22} \rangle$$

$$= (1 - 3/2 \sin^2\lambda) \langle T_{20} \rangle - (3/2)^{1/2} \sin 2\lambda \langle T_{21} \rangle$$

$$+ (3/2)^{1/2} \sin^2\lambda \langle T_{22} \rangle ,$$

$$\langle T_{21} \rangle' = 1/2 (3/2)^{1/2} \sin 2\lambda \langle T_{20} \rangle + \cos 2\lambda \langle T_{21} \rangle$$

$$- 1/2 \sin 2\lambda \langle T_{22} \rangle ,$$

$$\langle T_{22} \rangle' = 1/2 (3/2)^{1/2} \sin^2\lambda \langle T_{20} \rangle + 1/2 \sin 2\lambda \langle T_{21} \rangle$$

$$+ 1/2 (1 + \cos^2\lambda) \langle T_{22} \rangle .$$

(Note that the sign of each $\sin 2\lambda$ term is opposite to that given by Baldwin.[2,8]) Several methods may be used to derive these equations, the simplest being that of expressing an $S_i S_j$ tensor in terms of the complete set of $T_{JM}$ matrices and then transforming this tensor by rotation of the $\hat{S}_x$, $\hat{S}_y$, and $\hat{S}_z$ (or $\hat{x}$, $\hat{y}$, and $\hat{z}$) basis vectors about the y axis. (See discussion in Appendix D.1.)

To show that the transformation represented by the above equations is equivalent to the rotation of the polarization tensor or the ellipsoid representing this tensor (see Appendix D.2 and Fig. 3b), it is useful to consider the special case of a pure spin state $m_s = 0$

along the x axis; this situation gives zero values for $\langle iT_{11} \rangle$ and for e , but a maximum value for f when double scattering at the same angle is performed. As can be seen by simple calculations with the $\chi_0$ eigenfunction of $S_x$, the expectation values of spin products are

$$\langle S_x^2 \rangle = 0$$

$$\langle S_y^2 \rangle = 1$$

$$\langle S_z^2 \rangle = 1$$

$$\langle S_y S_x \rangle = \langle S_y S_z \rangle = \langle S_x S_z \rangle = \langle S_z S_x \rangle = 0.$$

The reciprocals of $\langle S_x^2 \rangle$, $\langle S_y^2 \rangle$, and $\langle S_z^2 \rangle$ give the ellipsoid axes and in this case produce a degenerate ellipsoid, namely, a cylinder of radius 1 extending to plus and minus infinity along the x axis.

If this cylinder is rotated through an angle $\lambda$ (change of spin direction relative to particle motion) equal to 90 deg, the new ellipsoid should be a cylinder of radius 1 extending to infinity along the z axis. Then the spin-product expectation values are

$$\langle S_x^2 \rangle = 1,$$

$$\langle S_y^2 \rangle = 1,$$

$$\langle S_z^2 \rangle = 0,$$ with expectation values of other products still zero. The tensor components $\langle T_{2M} \rangle$ may be expressed in terms of these:

$$\langle T_{20} \rangle = 1/\sqrt{2} \left( 3 \langle S_z^2 \rangle - 2 \right),$$

$$\langle T_{21} \rangle = -\sqrt{3}/2 \left( \langle S_{xz} \rangle + \langle S_{zx} \rangle + i \langle S_y S_z \rangle + i \langle S_z S_y \rangle \right),$$

$$\langle T_{22} \rangle = \sqrt{3}/2 \left( \langle S_x^2 \rangle - \langle S_y^2 \rangle \right).$$

The values of $\langle T_{2M} \rangle$ before magnetic-field rotation were

$$\langle T_{20} \rangle = 1/\sqrt{2} \ (3-2) = 1/\sqrt{2};$$

$$\langle T_{21} \rangle = 0;$$

$$\langle T_{22} \rangle = -\sqrt{3/2}.$$

The final value of $\langle S_z^2 \rangle'$ after rotation gives

$$\langle T_{20} \rangle' = 1/\sqrt{2} \ (0-2) = -\sqrt{2}.$$

This agrees exactly with the $\langle T_{20} \rangle'$ found from the first of the rotation equations above with $\lambda = 90^\circ$,

$$\langle T_{20} \rangle' = (1-3/2) \ \langle T_{20} \rangle + \sqrt{3/2} \ \langle T_{22} \rangle = -2/\sqrt{2};$$

and calculation of the other $\langle T_{2M} \rangle'$ values shows the two methods to be equivalent.

## G. Restrictions of Time-Reversal Invariance

Invariance under time reversal is satisfied for scattering processes if the scattering matrix as a function of the time-reversed momenta and spins is equal to the adjoint of the original scattering matrix,

$$M \ (-\bar{p}_2, -\bar{p}_1, -\bar{S}) = M^\dagger \ (\bar{p}_1, \bar{p}_2, \bar{S}).$$

Then it follows that

$$\text{Tr} \ M(\bar{p}, \bar{S}) \ M^\dagger(\bar{p}, \bar{S}) \ 0_i = \text{Tr} \ M^\dagger(-\bar{p}, -\bar{S}) \ M \ (-\bar{p}, -\bar{S}) \ 0_i,$$

where $0_i$ is any spin operator used in the description of scattering. A more general statement for scatterings complicated by the action of a magnetic field is the requirement that the transition probability for the forward process equal the transition probability for the time-reversed process[9]:

$$\text{Tr} \ M_2^\dagger \ M_2 \ e^{i\lambda S_y} M_1 M_1^\dagger \ e^{-i\lambda S}y = \text{Tr} \ M_1^\dagger \ M_1 \ e^{i\lambda S}y \ M_2 M_2^\dagger \ e^{-i\lambda S}y,$$

where $M_1$ is the scattering matrix associated with Target 1 and $M_2$ the scattering matrix associated with Target 2, while the rotation operator $e^{i\lambda S}y$ describes the action of the magnetic field between scatterings 1 and 2. Both of these conditions require that terms odd under time reversal, such as $S_{PK}$, not be included in the scattering matrix, and with parity conservation give the form of M presented by Stapp (or of $MM^\dagger$ discussed by Lakin).

Operators which are odd under the parity operation have expectation values after single scattering which are zero (Section II. D) if terms violating parity conservation and time-reversal invariance are not permitted in the scattering matrix M. The same sort of conclusion cannot be drawn for operators changing sign under time reversal. In the n-P-K coordinate system (defined in Section II. C), the scalar product $S_{ij}P_iK_j = (\bar{S}\cdot\bar{P})(\bar{S}\cdot\bar{K}) + (\bar{S}\cdot\bar{K})(\bar{S}\cdot\bar{P})$ or $S_{PK}$ is odd under time reversal. This means that it cannot appear in the scattering matrix M. However, permissible terms of M can combine in the product $MM^\dagger$ to give a nonzero expectation value for $S_{PK}$ after single scattering; i.e., the $S_nS_{KK}$ and $S_nS_{PP}$ terms of $MM^\dagger$ reduce to $S_{PK}$ and therefore give a quantity proportional to the Stapp coefficients $b(\theta) \times d(\theta)$ rather than zero for $\text{Tr } MM^\dagger S_{PK}$.

The orientation of the principal axes of the polarization ellipsoid in the plane of scattering would have been along the P and K directions, had $S_{PK}$ been required to be zero by time-reversal invariance; instead, the orientation should in general be at some angle to these directions. This angle can be only poorly estimated by the impulse-approximation evaluation of the coefficients in M; it was found experimentally to be about 40 deg (see Fig. 16).

## III. EXPERIMENT

### A. Introduction

A double scattering is necessary to determine the polarization components produced in scattering an unpolarized beam of particles. As has been shown in previous sections, the cross section for deuteron second scattering (without magnetic bending between targets) is

$$I_p (\theta_2, \phi) = I_u (\theta_2) \left[ 1 + \left\langle T_{20} \right\rangle_1 \left\langle T_{20} \right\rangle_2 + 2 \left( \left\langle iT_{11} \right\rangle_1 \left\langle iT_{11} \right\rangle_2 - \left\langle T_{21} \right\rangle_1 \left\langle T_{21} \right\rangle_2 \right) \cos\phi + 2 \left\langle T_{22} \right\rangle_1 \left\langle T_{22} \right\rangle_2 \cos 2\phi \right],$$

or, more simply,

$$I_p (\theta_2, \phi) = I_u (\theta_2) \left[ 1 + d + e \cos\phi + f \cos 2\phi \right],$$

where the parameters d, e, and f contain products of the polarization components which would be produced by scatterings of unpolarized beams at first and at second targets. Evidently there is, in addition to a left-right asymmetry arising from the $\cos\phi$ term, a vertical-horizontal asymmetry coming from the $\cos 2\phi$ contribution. Further, the polarized-beam cross section averaged over all $\phi$ is larger than the unpolarized beam cross section by the factor d. Measurements of the polarized cross section for at least three values of $\phi$ and of the unpolarized cross section are necessary to determine the quantities d, e, and f for a particular $\theta_2$.

The usual double scattering is not sufficient, however, to determine all tensor components, as it does not separate $\left\langle iT_{11} \right\rangle$ and $\left\langle T_{21} \right\rangle$, the vector and tensor polarization parts of the parameter e. To do this, it is necessary to perform a second scattering of two different polarized beams, one of which has been appreciably changed by the action of a large magnetic field between first and second scatterings. The $\left\langle T_{JM} \right\rangle_1$ in the above expression then become the "rotated" components discussed in Section II.

An essential part of the work reported here (the suggestion of Dr. Ronald Mermod) was the use of the magnetic field of the cyclotron to produce two external beams of differing polarization; there were utilized internally first a left-scattering target and then a right-scattering target, with the latter located some 230 deg back of the former so that scattered beams of the same momentum and magnitude of scattering angle passed through the exit channel to undergo a second scattering in the cave. (See Figs. 4 and 5) As has been shown, the rotation of the deuteron polarization tensor relative to the direction of motion is given by $\gamma$ ($\mu$-1) or about -1/6 times the angle of deflection; hence, bendings produced by the large magnetic field of the cyclotron (23,000 gauss) acting over considerably different distances were necessary to produce sufficiently different degrees of mixing of the tensor components and, through the comparison of the differing asymmetries, to permit reasonably good determination of $\left\langle T_{21} \right\rangle$.

One set of measurements was made with beryllium targets in which the internal scattering angles were 11 deg and the energy of the scattered beams was about 410 Mev. A later set was made with carbon targets, but with 10-deg scattering angles and higher energies of about 420 Mev. Second-scattering angles ranged from 6 to 18 deg and included the diffraction minimum (14.3 deg for beryllium and 13.0 deg for carbon). In both cases, the cross-section parameters d, e, and f were all found considerably different from zero; this was not so at the lower energies of 124 to 157 Mev, at which Baldwin et al. found only the quantity e different from zero and attributed this mostly to $\left\langle iT_{11} \right\rangle^2$.

It had been supposed that carbon might show different polarization effects from those obtained with beryllium, since it is a spin-zero nucleus while beryllium is not; however, the angular variations obtained were quite similar, with the patterns for carbon a little more compressed; e values for carbon were generally somewhat lower than for beryllium (see Fig. 14).
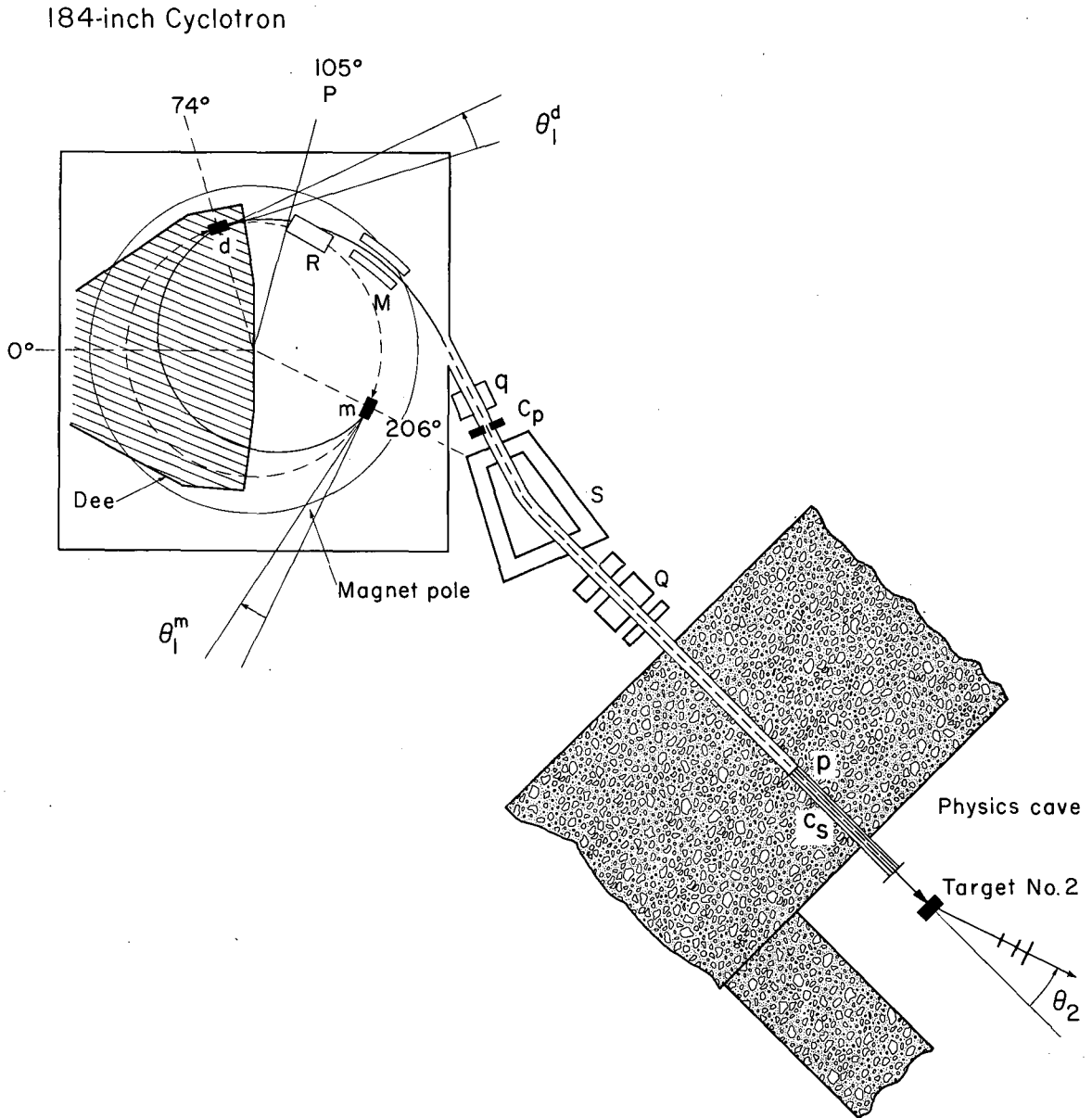
184-inch Cyclotron



MUB-277

Fig. 4.  View of cyclotron and paths of polarized beams.
Designated in the figure are:  d, dee target used
for first scattering; m, meson target used for
first scattering; R, regenerator; M, magnetic
channel; S, steering magnet; Q, 4-inch quadrupole;
$c_p$, premagnet collimator; and $c_s$, snout collimator.

## Dee target

## Meson target
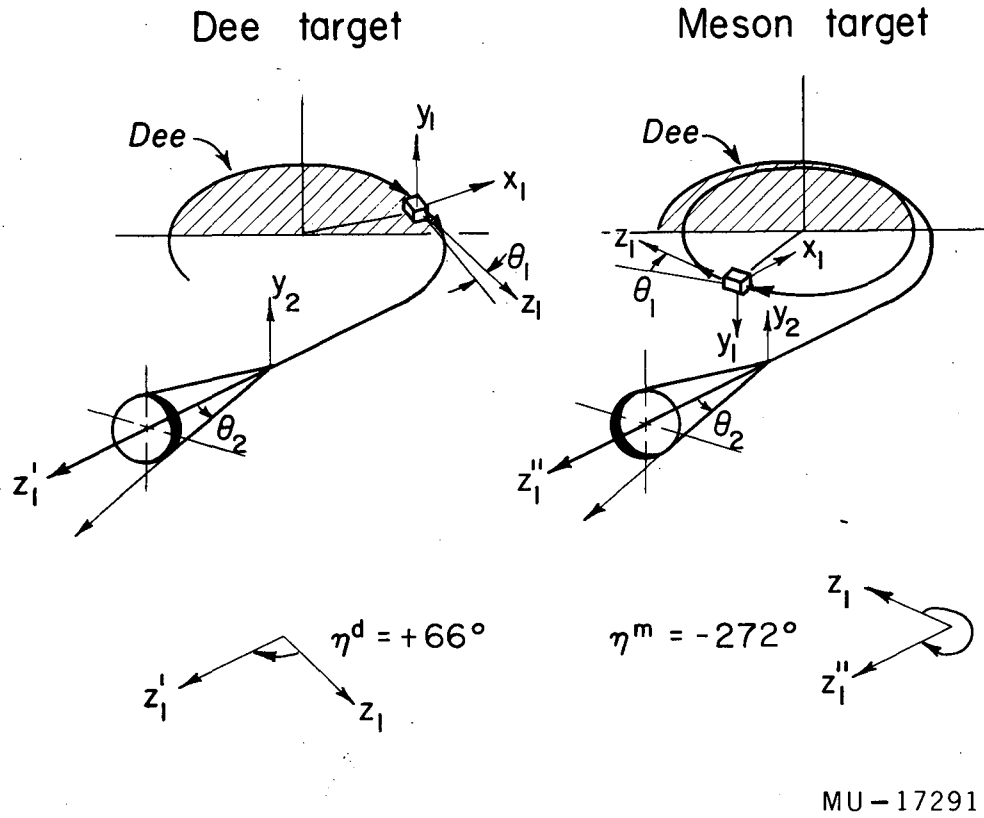
$$\eta^d = +66°$$

$$\eta^m = -272°$$

MU-17291

Fig. 5. Pictorial representation of dee- and meson-
target double scatterings. Cones represent
scattering of particles into angle $\theta_2$ at Target 2,
with the darker portions indicating greater in-
tensity of particles. The value of the deflection
angle $\eta$ is given in the $x_1 y_1 z_1$ system in each
figure.

An attempt was made to scatter a beam from a target in the
steering magnet (Fig. 4) in order to eliminate the effects of the
magnetic field and perhaps also some systematic errors. However,
this was found impractical because of an appreciable high-energy
tail and also considerable low-energy contamination. (The unwanted
particles appeared to derive from deuteron stripping; the method did
subsequently prove useful for polarizing full-energy or degraded
protons.)

## B. Geometry of Internal Scattering

The first target used, the so-called "dee target," was located
at an azimuthal position of 74 deg with respect to the center of the
dee and at a radius of 81 in. (Position d, Fig. 4). The target was
placed radially just inside the region where regeneration starts.
The strong regenerator field perturbation (centered at an azimuthal
angle of 116 deg and extending 8 deg in either direction) and also the
field variation in the magnetic channel leading to the exit pipe required
some careful orbit plotting for the determination of the desired target
position. (See Fig. 6.)

Since polarization theory and Baldwin's results indicated that
maximum polarization occurred at approximately the same value
of KR (with K the momentum transfer and R the nuclear radius) for
various energies and target nuclei, an estimate was made from
Baldwin's data that the scattering angle for maximum polarization
at some 400 Mev would be 10 or 11 deg. To avoid regenerator
action, but obtain maximum energy, 81 in. was chosen as the
greatest permissible radius. These choices of scattering angle and
radius then determined the target azimuthal position and the momen-
tum of the scattered beam; orbits showed that a beam of
$H\rho = 1.70 \times 10^6$ gauss-in. scattered at 11 deg from a target located
at 74 degrees azimuth passed through the magnetic channel into the
exit tube and through the beam-defining premagnet collimator.

Measurements inside the cyclotron tank indicated that the
dee target could be positioned to an accuracy of better than 1/2 in.
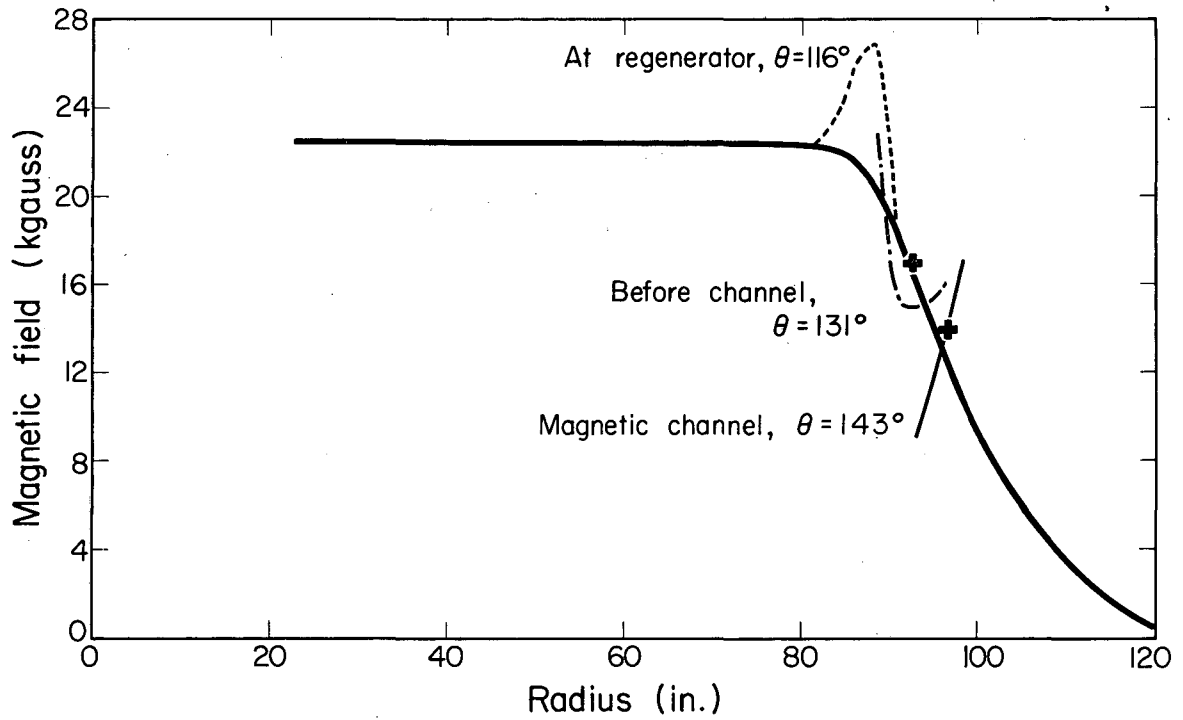
Fig. 6. Radial variation of cyclotron magnetic field.
(Measurements taken in October 1957.) The
crosses indicate the position of the scattered
beam at $\theta = 116$ and at $\theta = 143$ deg.

MU—17292

radially and azimuthally. The uncertainties in scattering angle arising from target radial and azimuthal positioning errors were 0.12 and 0.03 deg; the uncertainty due to a spread of perhaps $3 \times 10^3$ gauss-in. in momentum acceptance of a 2-in.-wide premagnet collimator was 0.50 deg; and the error due to radial oscillations was perhaps 0.13 deg. Thus there was an rms uncertainty of 0.53 deg in the internal scattering angle. The radial position of a copper collimator ("probe") put at 105 deg azimuth to stop regenerated beam served as an experimental check on the orbit of the scattered beam from the dee target.

The "meson target" (thus named because of its customary use for meson production) was located so as to scatter right through the same exit channel, again from a radius of 81 in. Several orbits at $1.71 \times 10^6$ gauss-in. momentum were extended back from the dee-target position to determine the azimuthal setting of the meson target necessary to send an 11-deg scattered beam through this dee position at 11 deg to the equilibrium orbit. (The azimuthal constancy of the cyclotron field between dee and meson targets assured an 11-deg meson-target scattering angle for an 11-deg beam angle at the dee-target position.) A variation of 4 deg in azimuthal setting of the meson target was found to give a 1-deg change in acceptable scattering angle.

In practice, the final position of the meson target was determined by maximizing beam intensity as a function of azimuthal position after setting the 105-deg probe as required by the dee-target beam; this differed slightly from the orbit-defined position in the case of beryllium, but the discrepancy could be well explained by a slightly lower momentum ($1.70 \times 10^6$ gauss-in.). The rms error in scattering angle was estimated to be perhaps 0.60 deg, only slightly greater than that of the dee-target beam because of the focusing action of the field.

The general character of the plotted orbits is shown in Fig. 4. The high field gradients of the regenerator and magnetic-channel

regions gave good momentum selection. To determine that the meson-target beam passed through the dee-target position, an attempt was made to clip the beam at that azimuth; however, the scattered beam from the clipper obscured the effect in meson-target beam. The position of the meson target, the beam momentum, and the probe position were considered sufficient confirmation of the orbit.

### C. Polarized Beams from Beryllium Targets

In the first phase of experimental work done with beryllium, the internal beam had a calculated energy of 447 Mev at 81 in. radius. Because of radial oscillations, the incident beam energy was perhaps 10 Mev lower; ionization loss in the 1-in. target was about 18 Mev and recoil loss 3.7 Mev. A range curve of the dee-target scattered beam (See Fig. 7a) showed it to have a mean energy of 410 Mev with a spread of ±2.5 Mev. The energy of the beam scattered from the meson target was 411 Mev with a spread of ±4.3 Mev. The degraded regenerated beam matched the dee-scattered beam almost exactly; its energy was 410 Mev with a spread of ±2.1 Mev (Fig. 7b).

In order to stop the regenerated circulating beam, which was perhaps fifteen times as large as the scattered beam, it was necessary to position a copper block on the main probe at 105-deg azimuth, the block having a 1.5-in.-diameter hole to pass the scattered beam. This probe reduced the regenerated beam by a factor of more than $1.6 \times 10^5$.

The procedure in obtaining the dee-target scattered beam was to optimize the steering-magnet current, to adjust the probe position for maximum beam intensity, and then to reoptimize the steering magnet. (See Figs. 8 and 9.) The meson-target beam required in addition considerable exploration of radial and azimuthal positions after the copper probe had been set as required by the dee target. (See Fig. 10.) Azimuthally the meson-target beam was especially well defined, with a half width of 3.0 deg, while the dee-target beam was much broader (with a peak found at 74 deg, as predicted by orbits). The 4-in. focusing quadrupole magnet in the exit channel
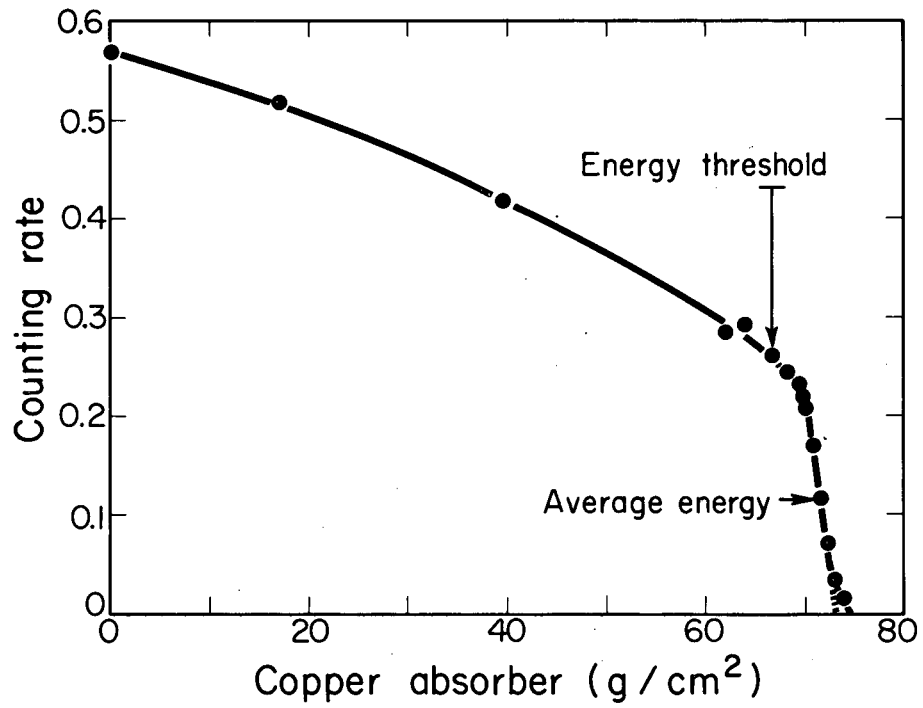
Fig. 7. (a) Range curve of beam scattered by dee
target (beryllium). The energy was found equal
to 410 ± 2.5 Mev, and the extrapolation factor
was 2.28. The energy threshold indicates the
amount of absorber (except for recoil correction)
used for scattering measurements.
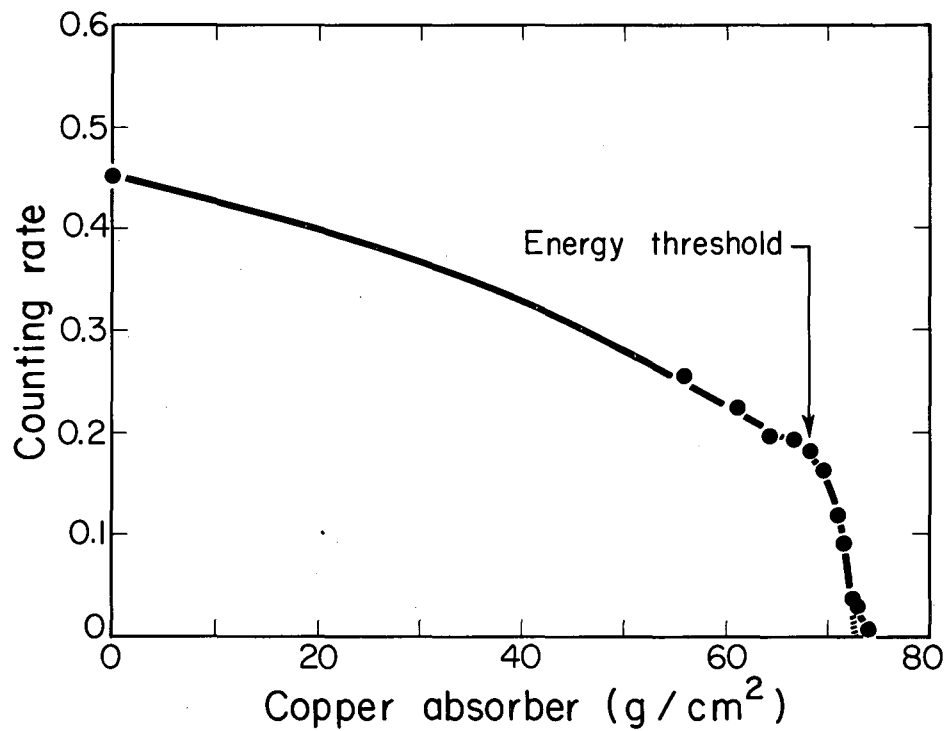
Fig. 7. (b) Range curve of degraded regenerated beam. The energy was found equal to 410 ± 2.1 Mev. This beam was used for beryllium scattering measurements.
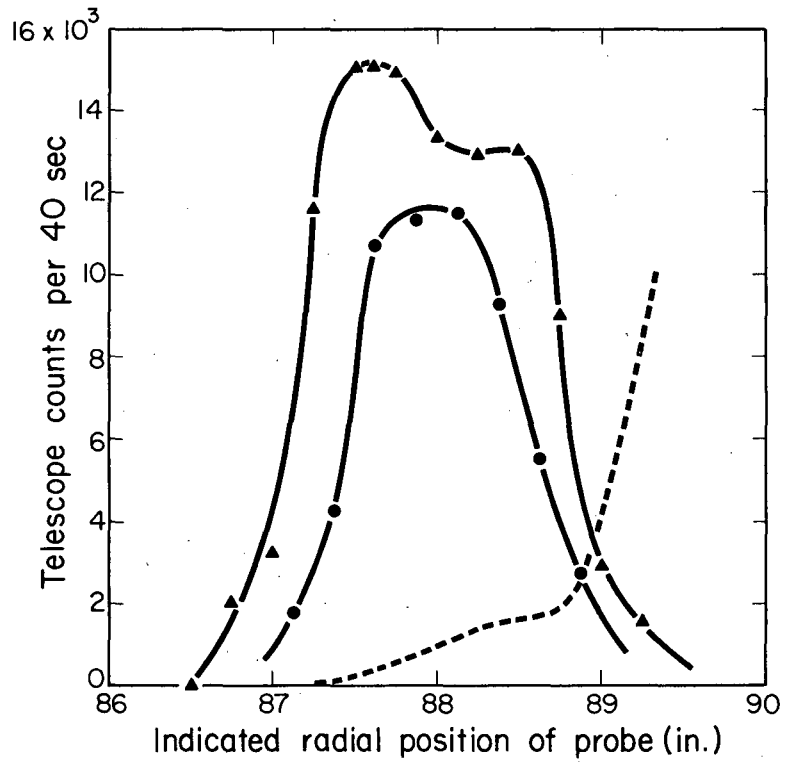
MU−17295

Fig. 8.  Variation of beam intensity with radial position
of copper probe.  The dotted curve represents
one-tenth the intensity of the regenerated beam
observed with dee and meson targets withdrawn.
Circles designate the dee-target beam; triangles,
the meson-target beam.  The position of the hole
in the probe was at a radius 5/8 in. greater than
the indicated reading; the edge clipping the re-
generated beam was at a radius of 5 in. less than
indicated.
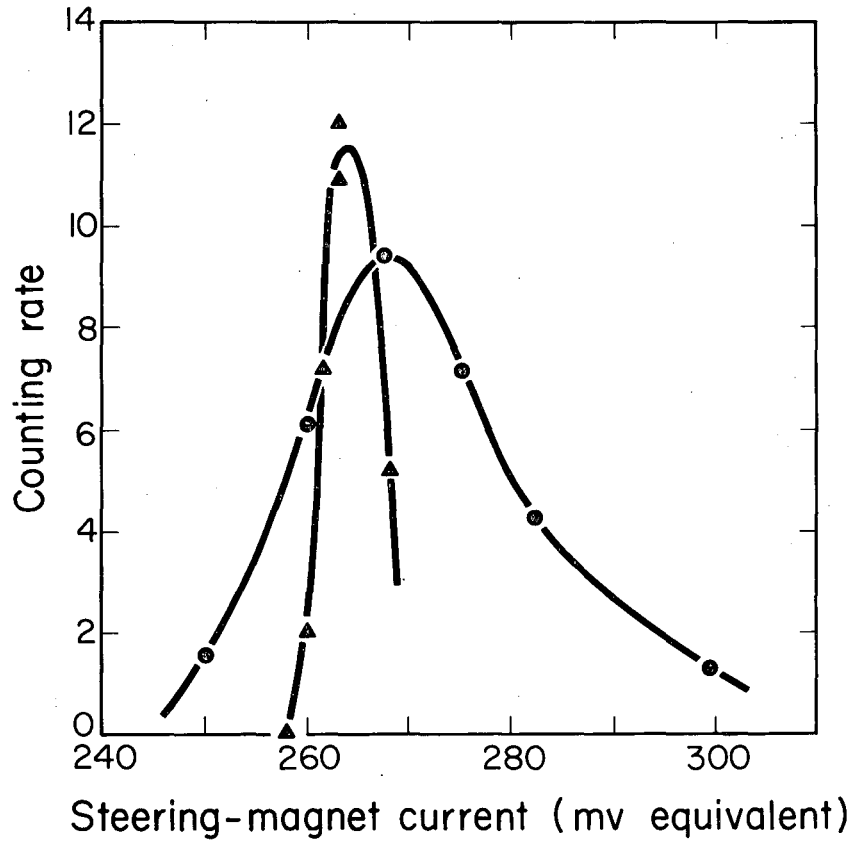
MU—17296

Fig. 9. Dependence of scattered-beam intensity on
steering-magnet current. Circles indicate the
dee-target beam; triangles, the meson-target
beam.
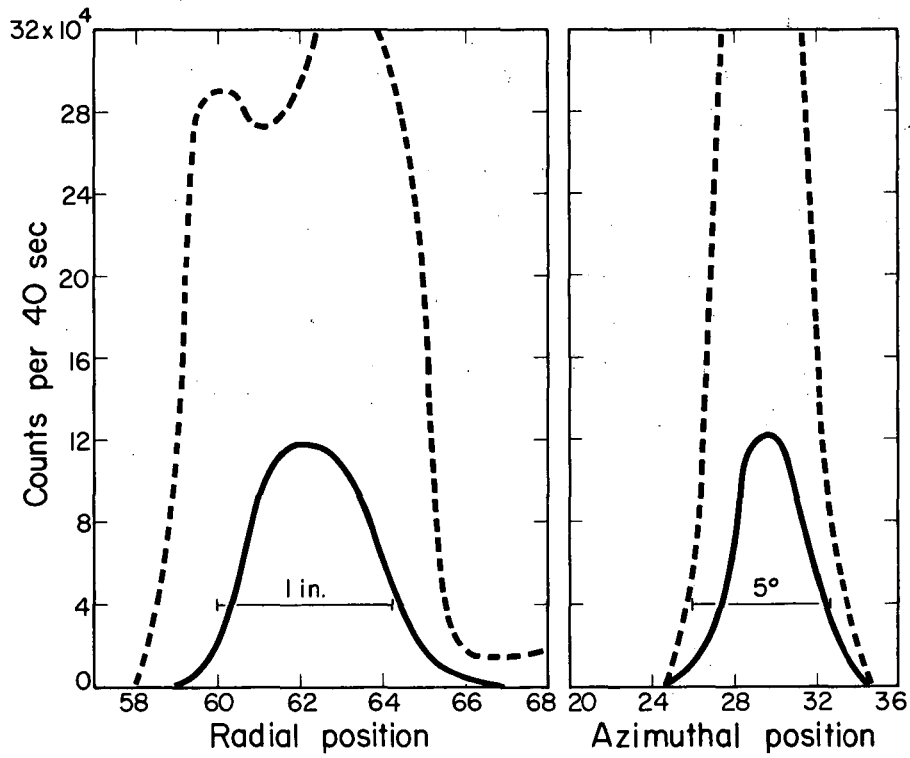
Fig. 10. Optimization of meson-target position. The
dotted curve represents beam intensity for all
energies; the solid curve represents only particles
of range greater than the energy threshold of Fig. 7a.

was set by maximizing the beam after choosing approximate currents calculated for a focus just beyond the point of entry into the cave.

Beryllium targets measuring 1 in. in the beam direction, 1 in. radially, and 1/2 in. vertically were used to obtain the polarized beams. The premagnet collimator (designated as $c_p$ in Fig. 4) had a 2x3-in. horizontal-vertical opening; and the snout collimator ($c_s$ in Fig. 4) was 1 in. in diameter and 46 in. long. Beam intensities obtained were

for dee target, $1.9 \times 10^5$/sec;

for meson target, $2.3 \times 10^5$/sec.[a]

For measurements of unpolarized cross sections, a regenerated beam of about $1.1 \times 10^6$/sec was used.

For characteristics of the various beams analyzed, see Table I.

---

[a]The fact that the meson-target beam intensity was greater than the dee-target intensity could perhaps be explained by a focusing action of the cyclotron field between meson-and dee-target positions and perhaps also by slightly greater circulating beam intensity near the meson-target location.

Table I.

| | | | |
|---|---|---|---|
| | | Beam characteristics | |

| | Dee-target scattered beam | Meson-target scattered beam | Degraded regenerated beam |
|---|---|---|---|
| **A. Beryllium targets** | | | |
| Position | $74^{\circ}$, 81.0" | $205.5^{\circ}$, 81.0" | |
| Scattering angle | $11.0 \pm 0.5^{\circ}$ | $11.0 \pm 0.6^{\circ}$ | |
| H$\rho$ (gauss-in.) | $1.70 \times 10^{6}$ | $1.70 \times 10^{6}$ | |
| Energy (Mev) | $410 \pm 2.5$ | $411 \pm 4.3$ | $410 \pm 2.1$ |
| Intensity ($10^{5}$/sec) | 1.9 | 2.3 | 11.0 |
| **B. Carbon targets** | | | |
| Position | $78^{\circ}$, 81.7" | $213^{\circ}$, 81.7" | |
| Scattering angle | $10.0 \pm 0.6^{\circ}$ | $10.0 \pm 0.7^{\circ}$ | |
| H$\rho$ (gauss-in.) | $1.75 \times 10^{6}$ | $1.75 \times 10^{6}$ | |
| Energy (Mev) | $416 \pm 2.7$ | $422 \pm 6$ | $425 \pm 2.1$ |
| Intensity ($10^{5}$/sec) | 0.65 | 0.93 | 15.0 |

## D. Polarized Beams from Carbon Targets

Extreme difficulty was encountered in extracting polarized beams for carbon measurements because of changes in the cyclotron magnetic field. After beryllium measurements were concluded, partial shorting of a coil in the main-field windings for the bottom pole face had necessitated shunting of the lower coils; main- and auxiliary-field values required for a good regenerated beam had changed. The regenerated beam was found to have increased in energy from 455 to 465 Mev. Changes in field gradients over the scattered-beam orbit could be only roughly estimated; with further shunting of the main field and careful tuning (phases and amplitudes of the reeds controlling the rf voltage), a meson target polarized beam of intensity almost comparable to the beryllium-scattered beam was obtained. The momentum having been determined for this beam, an orbit was plotted back from the exit channel through the experimentally determined probe and meson-target positions. The scattering angle at an 81-in. radius was found to be 10 deg rather than 11 deg, as a slightly higher-energy beam was selected by the magnetic channel than for beryllium. Corroboration of approximate orbits drawn with estimated field values was obtained when a beam was extracted from the dee target set at the position predicted for a 10-deg scattering. Energies of the polarized beams from the dee and meson targets were 416 and 422 Mev, respectively, with energy spreads comparable to those for the beams of earlier measurements. Other beam characteristics are given in Table I. The carbon dee target measured 5/8 in. radially, 3/4 in. vertically, and 2 in. azimuthally; the carbon meson target had the same radial and azimuthal measurements, but extended 2 in. vertically.

## E. Energy Degradation

In this experiment, polarized and unpolarized beams were not matched exactly in energy and energy spreads. Greater values of $d$ and $f$ required less concern over such techniques than in the experiment of Baldwin et al.[2] The maximum energy difference was

9 Mev and the maximum difference in spread (6.0 -2.1) Mev.

Degrading of the regenerated beam from 455 to 410 Mev for the beryllium experiment was accomplished by placing several inches of polyethylene absorber at the entrance to the snout collimator (Position p, Fig. 4). In one set of carbon measurements, degrading with copper absorber placed in the degrader box (Position q) was found to produce a beam undergoing greater attenuation than normal in the telescope absorber (probably because of protons originating from stripping in the degrader). Satisfactory unpolarized carbon cross sections were obtained by again degrading with polyethylene in the snout collimator from an energy of 465 to 425 Mev.

## F. Apparatus

The scattering table used was similar to that described in a report of earlier polarization work[10]; it permitted independent variation of the polar and azimuthal angles $\theta$ and $\phi$. Rigidity of the table was such that when the counter telescope was rotated through azimuthal angles from 0 to 360 deg, front and rear cross hairs were displaced by less than 1/64 in.; as the 0-deg line for the scattering arm was also closer than 1/64 in. to the line defined by the cross hairs, counter misalignment due to deformation of the scattering table during rotation should not have been more than 0.02 deg. Unlike the situation in nucleon scattering, the 0.1-deg error in the setting of the polar angle $\theta_2$ could produce errors in the deuteron cross-section parameters, since the ratio of polarized to unpolarized cross sections entered into the determination of each quantity.

To achieve the high azimuthal symmetry of incident beam especially necessary in deuteron measurements (done at four $\phi$ angles) and also to obtain good energy definition, a 1-in. snout collimator was used. The second target was generally 1/2 in. thick, with an additional 1/4 or 1/2 in. added to increase the intensity at larger angles of scattering.

The counter telescope consisted of three plastic scintillators

viewed by 1P21 photomultiplier tubes; the defining counter measured 1x6 in. and was placed 43.5 in. from the target. Sufficient copper absorber was put between Counters 1 and 2 (its position later being changed to that between Counters 2 and 3 in carbon measurements) to stop most of the inelastically scattered deuterons, the amount being varied slightly with scattering angle to compensate for changing recoil loss in the target. The scintillator of Counter 1 was 1/2 in. thick; Counters 2 and 3 were 3/8 in. in thickness. Counter 1 was centered on the scattering arm to within 1/64 in.

The various factors entering into the angular resolution of the counter telescope were well matched for scattering from the 1/2-in. target. The uncertainty in angle $\theta$ due to multiple scattering, to finite counter width, and to beam width were 0.38, 0.38, and 0.53 deg, respectively, for an rms uncertainty of 0.75 deg. (See formulae in Pettengill thesis.[11]) The resolution of the counter system without target was determined experimentally and checked very well with the theoretical estimate made:

$$\delta\theta_{1/2} = \frac{1.5}{\sqrt{12}} \frac{\sqrt{w_1^2 + w_2^2}}{62 \text{ in.}} = 0.57 \text{ deg.}$$

Here $w_1$ is the beam width at the collimator; $w_2$, the width of the defining counter; and 62 in., the distance from collimator to defining counter. For comparison, the half widths of the regenerated beam profiles given in Fig. 11 were found to be 0.52 and 0.62 deg. Resolution in the direction of $\phi$ variation was, of course, much poorer because of counter dimensions; however, the cross section varied much less rapidly with $\phi$ than with $\theta$.

## G. Experimental Procedure

After the optimizing of various internal parameters such as target position and steering-magnet current, the snout collimator was aligned by using x-ray film to obtain as homogeneous a beam as possible. As in previous polarization experiments, a transit was placed at the back of the experimental cave for the purpose of aligning the scattering table. Approximate alignment was

MU-17298

Fig. 11. Profiles of regenerated beam in horizontal plane (solid curve) and vertical plane (dotted curve); $\delta \theta_H$ and $\delta \theta_V$ are to be compared to an estimated resolution of 0.57 deg. Displacement of centerlines from 0 deg indicates the amount of realignment that was necessary.

accomplished by taking x-ray pictures of the beam at the front and back of the table, fixing the transit at the centers of the pictures, and moving the table to bring the cross hairs marking the axis of rotation into coincidence with the transit line. The front of the table was then assumed well aligned and the rear brought into more nearly exact alignment by equalizing counting rates both horizontally and vertically at small values of $\theta$; for homogeneous beams, this was done without a scattering target, while for a less uniform beam, the target was put in place and alignment made on multiply scattered particles. This beam profile was taken with telescope absorber of an amount used for small-angle scattering. The estimated accuracy of alignment was 0.06 deg with the x-ray pictures and 0.03 deg with counters; the latter was fairly consistent with observed differences in the 11-deg unpolarized cross-section measurements at various $\phi$ angles. (See Fig. 12.)

A range curve was taken at low beam with counters at zero deg by varying the amount of copper absorber in the telescope, and the "energy threshold" necessary to eliminate most of the inelastic-ally scattered particles was determined. (See Fig. 7.) The pro-cedure followed was to set the copper absorber at 2 $g/cm^2$ less than the knee of the range curve for the 11-deg scattering and then to add or subtract small amounts to compensate for recoil loss in the target.

As the geometry of scattering was such that most of the background, presumably from the snout collimator, could be ex-pected to pass through the target, an amount of absorber equivalent to the target should have been placed in the telescope for measure-ments with the target out. This was done for the set of scatterings with carbon targets and was found to have an effect of not more than a few percent in the cross section.

Two scintillation counters, 1 in. and 5/8 in. thick, were placed in the beam incident on the second target as monitors when low intensity was desired; this was the case when the counters were delayed and plateaued, the range curve was taken, or the table was
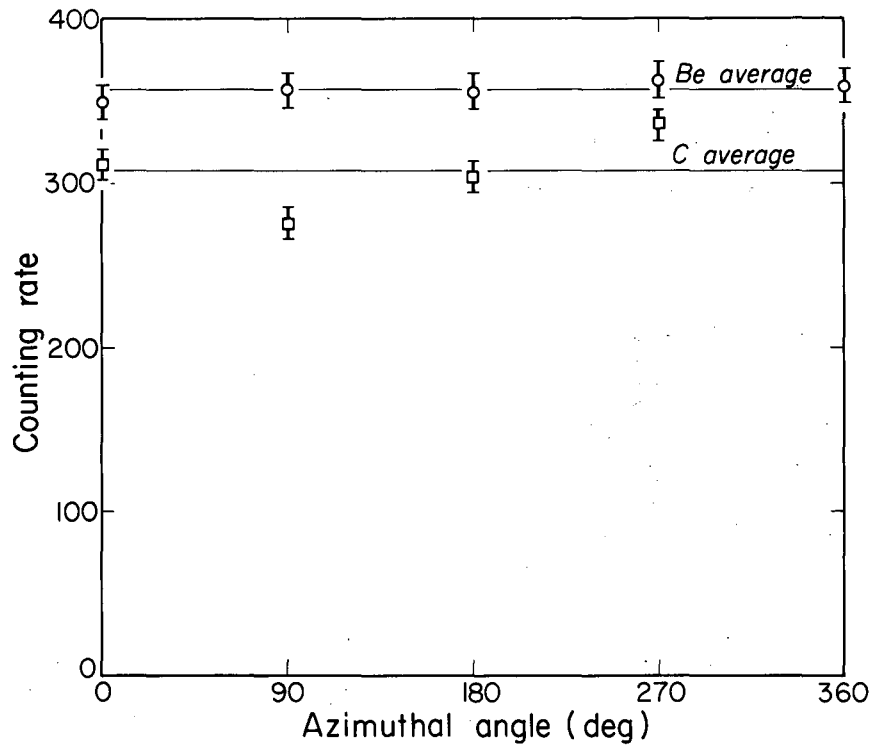
Fig. 12. Unpolarized cross section vs. azimuthal angle
φ at a scattering angle of 11 deg. Circles rep-
resent beryllium measurements; squares, the car-
bon values. No correction has been made for
absorber attenuation.

aligned. (For the first two situations, these monitors were unnecessary and were replaced by Counters 1 and 2 of the telescope when absorber was put between Counters 2 and 3, as was done for carbon measurements.) The usual intensity of incident beam used for these measurements was about 500 counts per second; this gave an inappreciable accidental rate, as there were 30,000 to 40,000 resolving times a second for the Garwin coincidence circuit used.

In scattering measurements, an argon-filled ion chamber was used as monitor; the multiplication factor for this chamber was calculated to be 1240 for 410-Mev deuterons on the basis of calibration information of earlier proton work.[12] With the scattered beams obtainable, this gave an electrometer charging rate of one full-scale deflection per 3.5 minutes, with full-scale being equivalent to 0.0104 $\mu$ coulomb of accumulated charge (designated loosely as an "integrated volt" or "I.V."). Corrections for ion-chamber drift were made, and amounted to as much as 3% of the actual beam rate for the scattered beams.

To eliminate low-energy particles scattered from the end of the snout collimator, 6in. of copper and lead shielding with a 2-in.-square hole for the beam was placed between the snout collimator and the target.

## H. Counting Procedure

The object of double scattering was to determine the cross-section parameters d, e, and f as functions of $\theta_2$. Measurements of the unpolarized-beam cross section were made first at a scattering angle of 11 deg with $\phi = 0$ deg (left), 90 deg (up), 180 deg (right), and 270 deg (down) to check scattering table alignment. (See Fig. 12.) With good alignment, as for beryllium unpolarized measurements, scattering measurements for only one $\phi$ were considered sufficient for the unpolarized cross section at other scattering angles $\theta_2$; for small-angle carbon scattering, the values of $i_u(\theta_2)$ used in calculations were averages obtained from measurements at all $\phi$. For the polarized beam, of course, measurements had to be

made at the four azimuthal angles for every $\theta_2$. Results for $\theta_2$ equal to $\theta_1$ were determined especially carefully, as the $\langle T_{JM} \rangle$ values obtained from these were to be used in finding $\langle T_{JM} \rangle (\theta)$ from measurements at other $\theta_2$.

Three counting rates were measured at each $(\theta, \phi)$ setting: "target in" with normal delay, "target in" with 76 nsec delay added to one counter,[a] and "target out." Accidentals were generally about 5% of the normal-delay measurements, while the background was about 10%. In the beryllium measurements, accidentals were improperly taken; the proton delay of 5.2 shakes was used and resulted in an almost negligible rate. Unpolarized-beam results obtained later as a check indicated that the accidentals should have been higher by about 11% of the effect for the unpolarized beam and 3% of the effect for the polarized beam. Corrections in d, e, and f were made accordingly.

## J. Results of Second Scattering

The subtraction of accidental and background counting rates from the "target in" measurement gave the actual rate of scattering by the target. Results for the polarized and unpolarized beams at the various $\phi$ angles were used to obtain the desired cross-section parameters at each angle $\theta_2$:

$$d = \bar{I}_p / I_u - 1 = \frac{I_0 + I_{90} + I_{180} + I_{270}}{4 I_u} - 1,$$

$$e = (I_0 - I_{180}) / 2 I_u,$$

$$f = (I_0 + I_{180} - I_{90} - I_{270}) / 4 I_u.$$

---

[a] 76 nsec is the time between two rf fine-structure pulses of deuterons. Accidentals were measured by delaying the first counter with respect to the adjacent second and third counters when the absorber was between Counters 1 and 2 and by delaying the rear counter with respect to Counters 1 and 2 when the absorber was placed after Counter 2.

The subscripts designate the angle $\phi$ or refer to polarized or un-
polarized measurements. (Note that the formulae given by Baldwin
for e and f, the latter being his quantity B, are incorrect, since
the first should contain $1+d+f$ and the second $1+d$ in the denominator;
he did, of course, find d and f to be zero within experimental
error.)

For the scattering of the polarized beam, a plot of the cross
section versus azimuthal angle at a scattering angle of 8 deg (Fig. 13)
shows a large left-right asymmetry; f, the $\cos 2\phi$ coefficient, on
the other hand, is given by the difference between the horizontal
and vertical averages and is rather small. The "left-right"
asymmetry $\dfrac{I_0 - I_{180}}{I_0 + I_{180}}$ used in nucleon scattering here is equal to

$e/(1+d+f)$, and the "horizontal-vertical" asymmetry $\dfrac{I_0 + I_{180} - I_{90} - I_{270}}{I_0 + I_{180} + I_{90} + I_{270}}$

equals $f/(1+d)$. These quantities are given with statistical errors
for beryllium and carbon scatterings in Table II.

Because each of the desired quantities d, e, and f contains
the ratio between polarized and unpolarized cross sections (which
appears in d in such a way as to make this particular quantity
very sensitive to any error), a serious problem arises. Careful
extrapolations to zero absorber to determine the actual elastic-
scattering cross sections (i.e., corrections for nuclear attenuation
in the telescope absorber) or some sort of normalization of un-
polarized to polarized cross sections must be made. The former is
ordinarily subject to considerable error; in the beryllium measure-
ments reported here, the extrapolation factors (ratio of counting
rate with zero absorber to that with absorber used in scattering
measurements) for polarized and unpolarized beams differed by about
10% and were found to produce a considerable effect in the quantity d.

The variation of extrapolation factors was investigated to
some extent. Displacement of the snout collimator by 1/8 in.
caused a 6% change in extrapolation factor; extreme changes in
counter geometry had no effect. That the alignment of the beam in
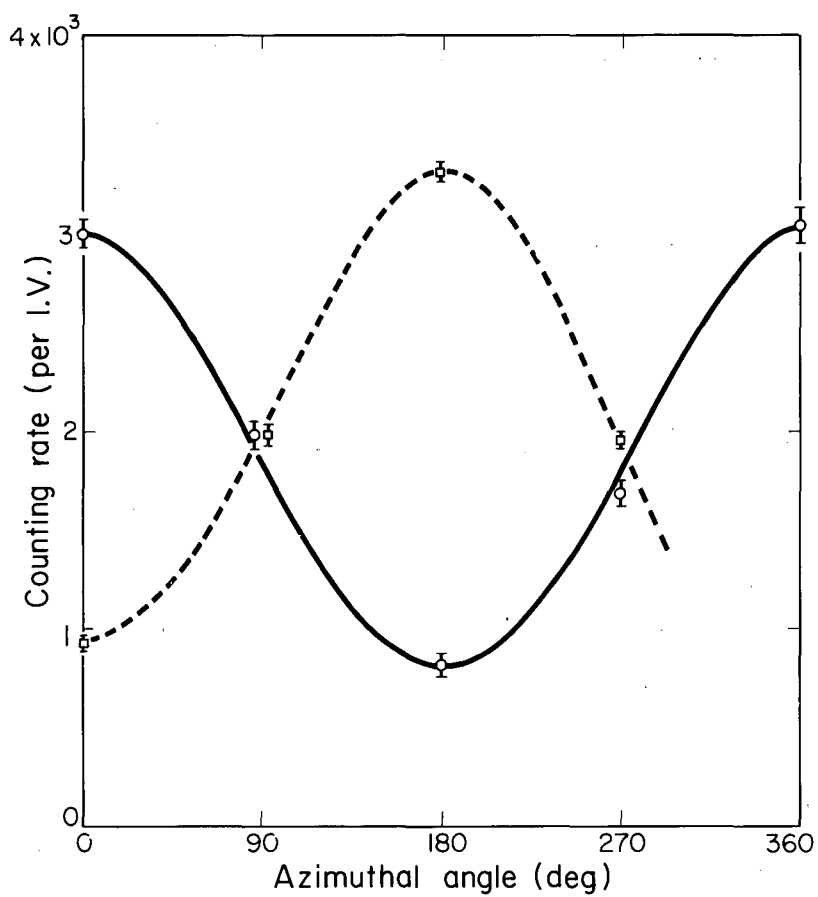
Fig. 13. Polarized cross section vs. azimuthal angle
for scattering from beryllium at an angle of 8 deg.
The solid line represents dee-target scattering;
the dotted line, meson-target scattering.

MU-17300

Table II.

Asymmetries in polarized-beam scattering
Here $e/(1+d+f)$ is the usual "left-right" asymmetry; $f/(1+d)$ is
"horizontal-vertical" asymmetry. Errors are statistical.

| $\theta_2$ | Dee target | | Meson target | |
|---|---|---|---|---|
| | $e/(1+d+f)$ | $f/(1+d)$ | $e/(1+d+f)$ | $f/(1+d)$ |
| **Beryllium** | | | | |
| $6^o$ | $0.411 \pm .016$ | $-0.003 \pm .012$ | $0.487 \pm .013$ | $0.050 \pm .008$ |
| $8^o$ | $0.555 \pm .014$ | $0.055 \pm .009$ | $0.562 \pm .011$ | $0.041 \pm .008$ |
| $10^o$ | $0.432 \pm .024$ | $0.070 \pm .021$ | $0.488 \pm .016$ | $0.078 \pm .012$ |
| $11^o$ | $0.322 \pm .016$ | $0.069 \pm .012$ | $0.448 \pm .010$ | $0.065 \pm .010$ |
| $12^o$ | $0.294 \pm .034$ | $0.073 \pm .025$ | $0.312 \pm .022$ | $0.085 \pm .017$ |
| $14^o$ | $0.213 \pm .032$ | $0.105 \pm .024$ | $0.185 \pm .026$ | $0.087 \pm .020$ |
| $16^o$ | $\cdots$ | $\cdots$ | $0.206 \pm .030$ | $0.101 \pm .024$ |
| **Carbon** | | | | |
| $6^o$ | $0.320 \pm .013$ | $0.040 \pm .010$ | $0.444 \pm .010$ | $0.035 \pm .009$ |
| $8^o$ | $0.402 \pm .021$ | $0.096 \pm .024$ | $\cdots$ | $\cdots$ |
| $9^o$ | $0.329 \pm .023$ | $0.125 \pm .019$ | $0.458 \pm .023$ | $0.054 \pm .017$ |
| $11^o$ | $0.167 \pm .030$ | $0.095 \pm .025$ | $0.258 \pm .026$ | $0.098 \pm .021$ |
| $13^o$ | $0.114 \pm .047$ | $0.022 \pm .035$ | $0.201 \pm .033$ | $0.069 \pm .025$ |
| $16^o$ | $0.170 \pm .084$ | $0.089 \pm .075$ | $0.212 \pm .040$ | $0.065 \pm .030$ |
| $18^o$ | $\cdots$ | $\cdots$ | $0.182 \pm .042$ | $0.105 \pm .035$ |

the snout collimator was important was further indicated by the fact that extrapolation factors for scattered beams centered about one value and for regenerated beams centered about another value slightly higher.

Thus the use of absolute cross sections to find d, e, and f seemed rather questionable. As a better alternative, the assumption was made that the polarized and unpolarized cross sections at 6 deg should be equal,[a] and the unpolarized cross section was normalized to the polarized for all $\theta$. Figure 14 shows the angular dependences of the quantities d, e, and f which were obtained through normalization and also extrapolation of cross sections; the differences in $(1+d)$, e, and f values for the two methods were about 2.5% for beryllium and 3.5% for carbon. Had d been taken as small and positive instead of zero at 6 deg, f would also have been increased, since $f/(1+d)$ depends only on $I_p (\theta_2, \phi)$ and is unaffected by normalization of $I_u$ to $\bar{I}_p$; a behavior closer to $\sin^2 \theta$ for $\langle T_{20} \rangle$ and $\langle T_{22} \rangle$ then could have been obtained.

The unpolarized cross sections as functions of scattering angle are given in Fig. 15. These were obtained by substituting for the integrated-volt monitor unit (I.V.) the equivalent incident intensity of $5.24 \times 10^7$ particles. The unpolarized cross section for scattering by beryllium in a later run agreed with the values given in Fig. 15 to within 3.0% at 8 deg and 12% at 11 deg; better agreement could probably not be expected in view of the uncertainties discussed above.

### K.  Energy Asymmetry,  Beam Contamination

Comparison of the range curves taken of the dee-target beam at $\theta = 0$ and $\theta = 10$ deg left indicated that the beam was low in energy

---

[a]This assumption was based on the fact that in first Born approximation, $\langle T_{20} \rangle$ is proportional to terms in $\sin^2 \theta$ (Stapp,[3] pp. 77 and 99), but is probably a little extreme.
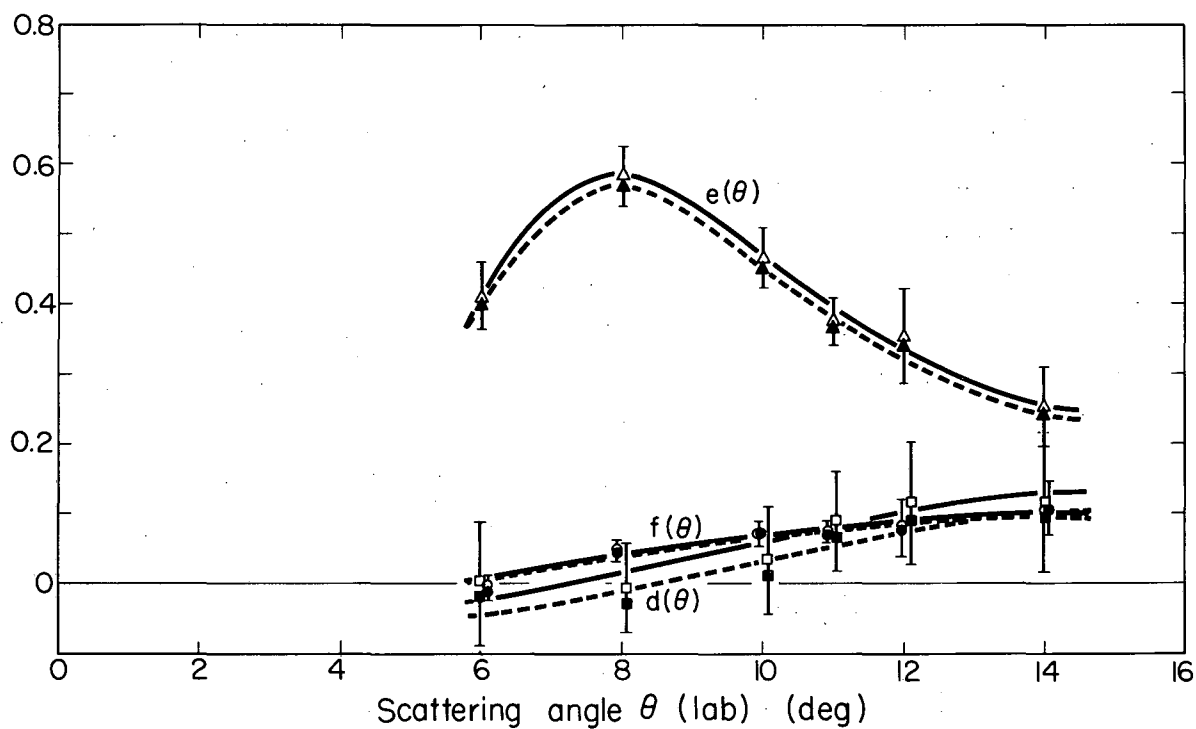
Fig. 14. (a) Cross-section parameters vs. scattering
angle, with total errors, for the beryllium dee-
target scattering. Solid lines refer to values
obtained by normalization; dotted lines, to values
from extrapolation of cross-section measurements.
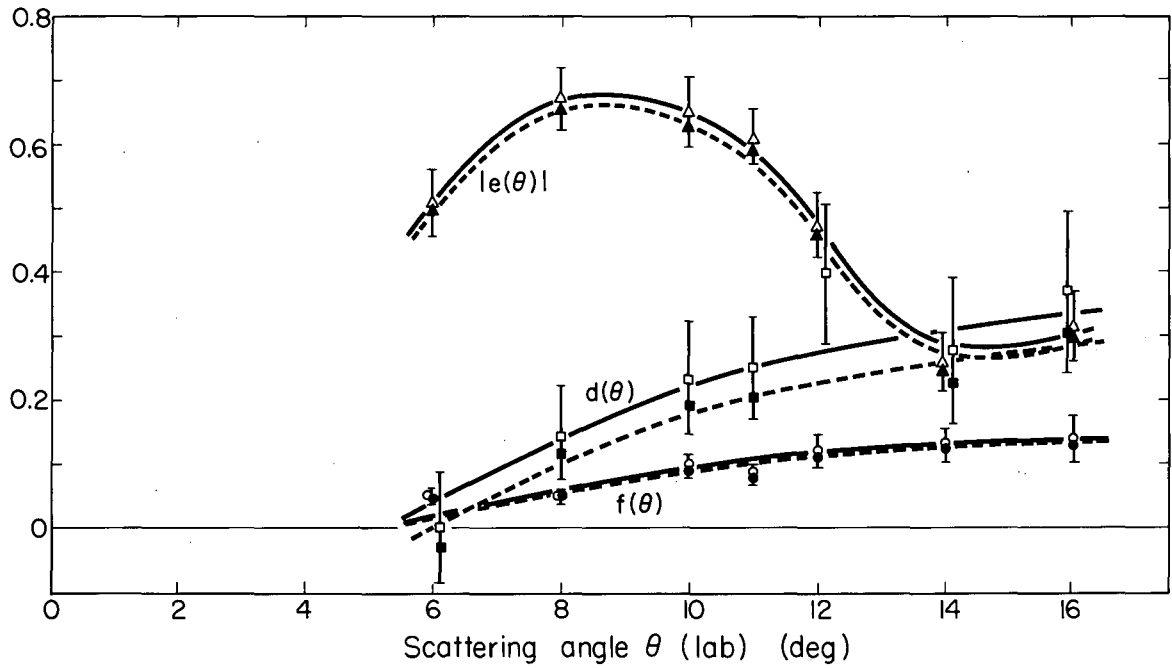
MU-17322

Fig. 14. (b) Cross-section parameters vs. scattering
angle, with total errors, for the beryllium meson-
target scattering. Solid lines refer to results
from normalized data; dotted lines, to those from
extrapolated data.
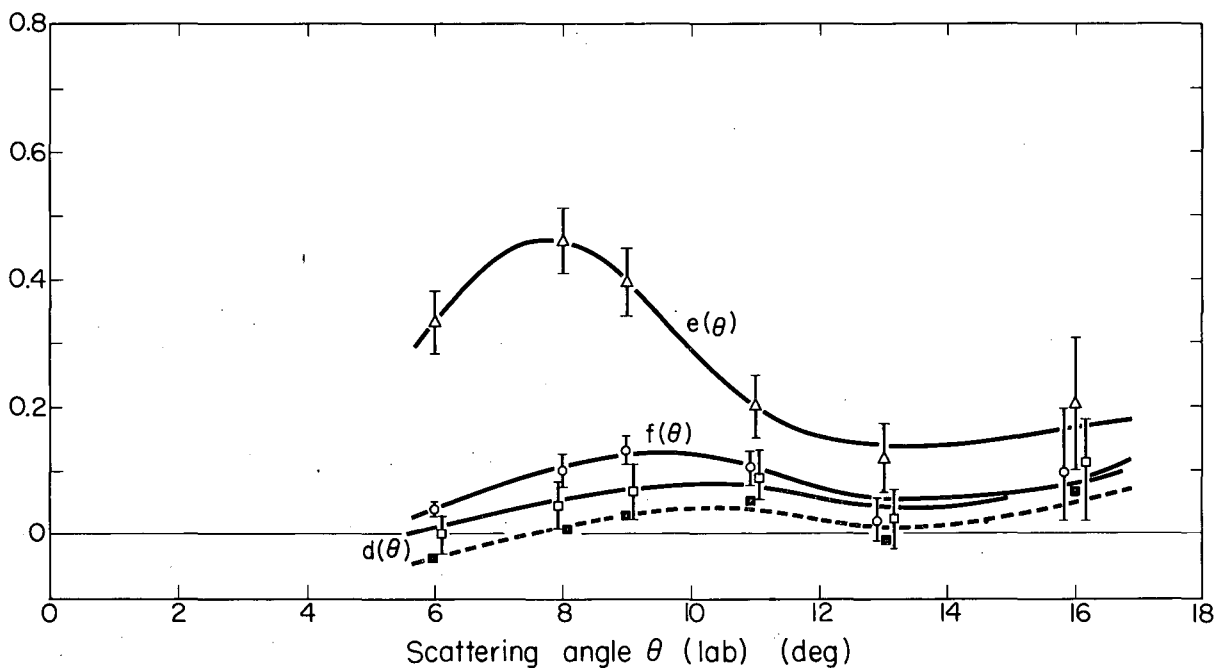
Fig. 14. (c) Cross-section parameters vs. scattering angle, with total errors, for the carbon dee-target scattering. The dotted curve represents results from extrapolation rather than normalization.

0.8

0.6

$|e(\theta)|$

0.4

$d(\theta)$

0.2

$f(\theta)$

0

0    2    4    6    8    10    12    14    16    18

Scattering angle $\theta$ (lab) (deg)
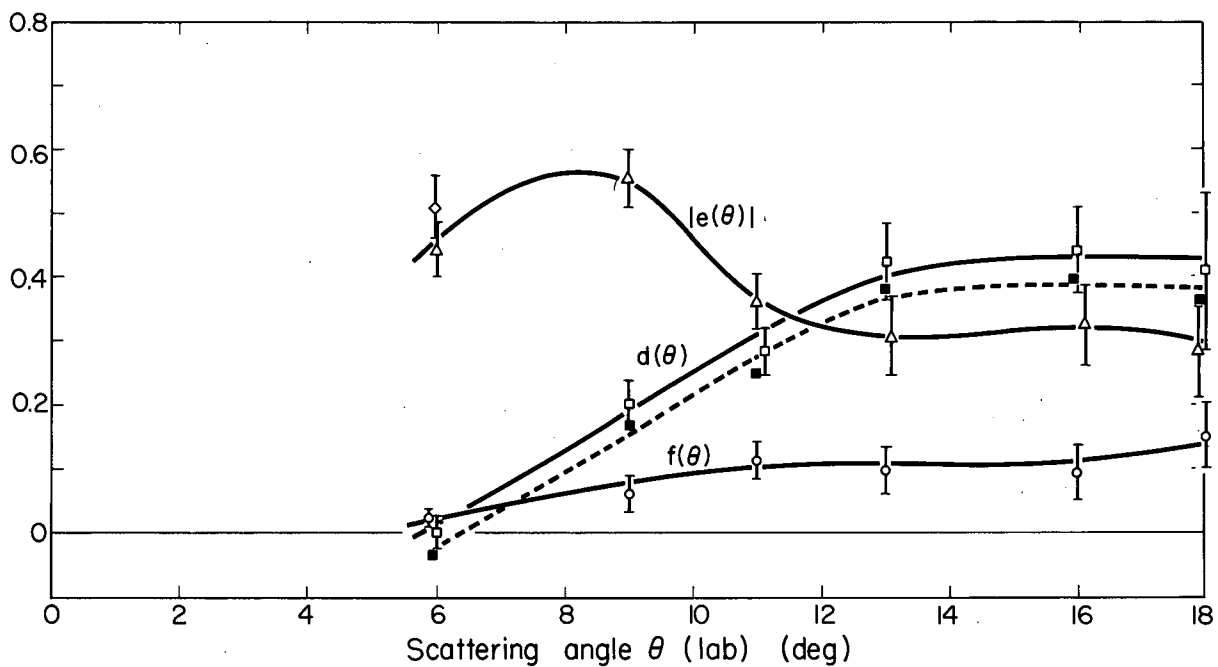
MU-17302

Fig. 14. (d) Cross-section parameters vs. scattering
angle, with total errors, for the carbon meson-
target scattering. The dotted curve represents
results from extrapolation rather than normalization.
The diamond at 6 deg indicates the e value  obtained
from cross-section measurements at 45, 135, 225,
and 315 deg azimuth.
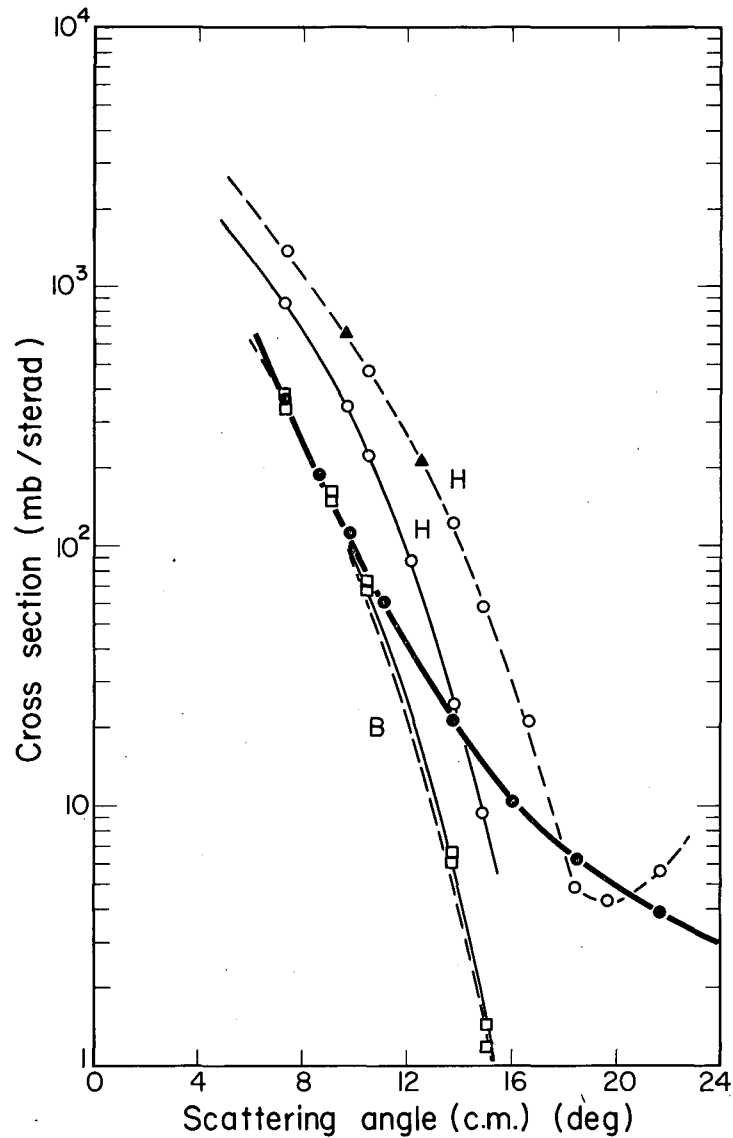
MU—17303

Fig. 15. (a) Cross section for the scattering of un-
polarized deuterons by beryllium at 410 Mev. The
heavy curve represents experimental results, for
which errors were less than the size of the points
plotted. The H designates calculations done in the
impulse approximation with Hafner proton ampli-
tudes, the solid curve including the effect of
simultaneous scattering. The B indicates impulse-
approximation results obtained with Bjorklund
amplitudes for proton scattering (solid curve) and
neutron scattering (dotted curve); both include
simultaneous scattering. Triangles show the
negligible effect of including the deuteron D state
in the Hafner calculations.
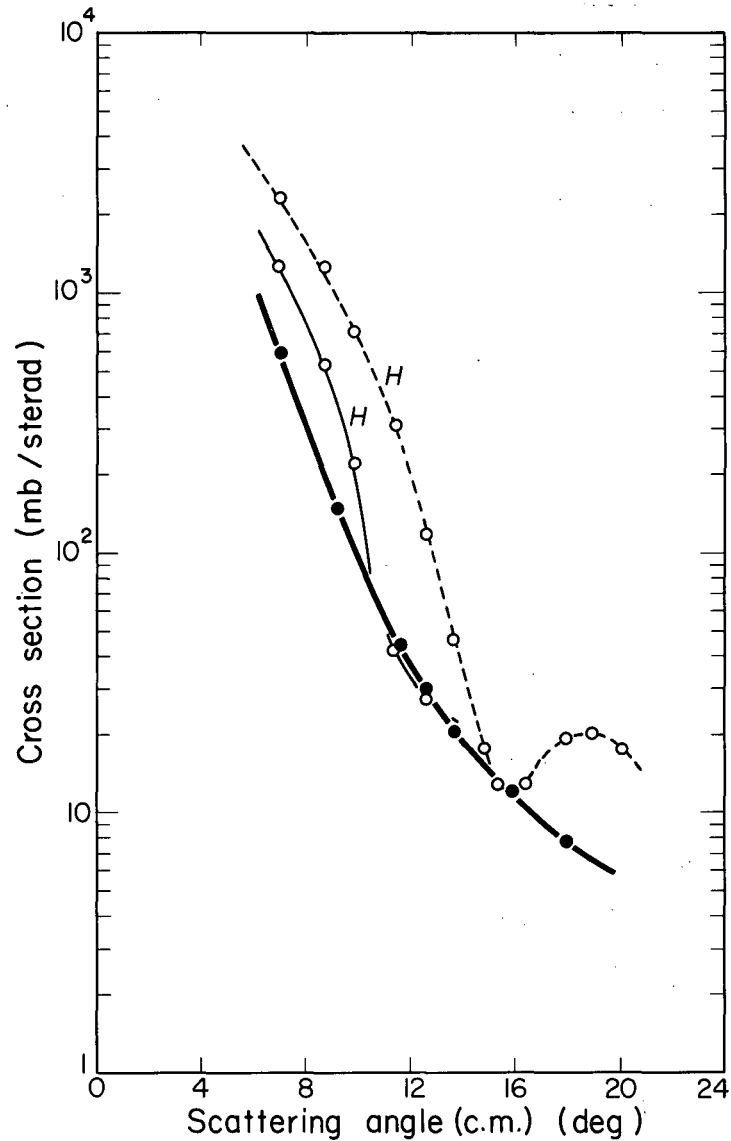
Fig. 15 (b) Cross section for scattering of unpolarized
deuterons by carbon at 425 Mev. Experimental
results are indicated by the heavy line. The H
designates calculational results from the impulse
approximation with Hafner proton amplitudes,
the solid curve including the effect of simulaneous
scattering.

on the left or $\phi = 0$ side. The decrease in average range (corrected for recoil loss at 10 deg)showed that $I_0 - I_{180}$ or the quantity e required a 4% correction for this effect.

The ratios of counting rate at the energy threshold to that at the average energy were compared for $\theta = 0$ and 10 deg left. The amount by which they differed indicated that, for 10 deg, there was an 8% inelastic contamination of the beam above the energy threshold. However, on the basis of Tripp's determination of the negligible effect of inelastic contamination on asymmetry results with nucleons,[1] it was concluded that the inelastic part of the deuteron beam probably had little effect on measurements except perhaps in the region of the diffraction minimum.

## L.  Errors

Errors in d, e, and f derived chiefly from three sources: statistics of counting, comparison of polarized and unpolarized beams, and misalignment of the scattering apparatus. Systematic errors as well as statistical are given with values of d, e, and f in Table III. Expressions for evaluating errors from the three sources mentioned are given in Appendix E.

In the normalization of the unpolarized cross section to the polarized, error was introduced by the statistical uncertainties of the 6-deg cross-section measurements. Relative error in $I_u$ and hence (1+d), e, and f due to normalization amounted to 6% for beryllium and 2.2% for carbon results.

The expected misalignment of the scattering table in polarized-beam measurements could be estimated by observing the horizontal and the vertical misalignments evident in unpolarized-beam cross sections. For beryllium measurements, misalignment observed at $\theta = 11$ deg was only 0.012 deg, while for carbon, it was at least 0.06 deg. Misalignment of the snout collimator also produced asymmetric effects in scattering which were included in these estimates; and the misalignment error indicated was perhaps an over-estimate for the polarized beams.

Table III. A.

## Cross-section parameters with total errors for scattering from beryllium at 410 Mev

### Dee-target scattering

| $\theta_2$ | Error in $d^d$ statistics | normalization | misalignment | $d + \Delta d_{rms}$ | Error in $e^d$ statistics | normalization | misalignment | $e + \Delta e_{rms}$ | Error in $f^d$ statistics | normalization | misalignment | $f + \Delta f_{rms}$ |
|---|---|---|---|---|---|---|---|---|---|---|---|---|
| $6^o$ | 0.0629 | 0.0615 | 0.0016 | $0.00 \pm .088$ | 0.0305 | 0.0253 | 0.0252 | $0.411 \pm .047$ | 0.0127 | 0.0002 | 0.0016 | $-0.003 \pm .013$ |
| $8^o$ | 0.0204 | 0.0611 | 0.0070 | $-0.006 \pm .065$ | 0.0146 | 0.0359 | 0.0186 | $0.583 \pm .043$ | 0.0099 | 0.0031 | 0.0070 | $0.050 \pm .013$ |
| $10^o$ | 0.0437 | 0.0636 | 0.0048 | $0.034 \pm .077$ | 0.0279 | 0.0287 | 0.0163 | $0.467 \pm .043$ | 0.0156 | 0.0044 | 0.0048 | $0.072 \pm .017$ |
| $11^o$ | 0.0208 | 0.0670 | 0.0029 | $0.090 \pm .070$ | 0.0194 | 0.0231 | 0.0130 | $0.376 \pm .033$ | 0.0131 | 0.0046 | 0.0029 | $0.075 \pm .014$ |
| $12^o$ | 0.0527 | 0.0687 | 0.0029 | $0.117 \pm .087$ | 0.0636 | 0.0217 | 0.0132 | $0.354 \pm .068$ | 0.0411 | 0.0050 | 0.0029 | $0.081 \pm .041$ |
| $14^o$ | 0.0731 | 0.0687 | 0.0013 | $0.117 \pm .100$ | 0.0543 | 0.0156 | 0.0083 | $0.254 \pm .057$ | 0.0371 | 0.0067 | 0.0013 | $0.109 \pm .038$ |

### Meson-target scattering

| $\theta_2$ | Error in $d^m$ statistics | normalization | misalignment | $d + \Delta d_{rms}$ | Error in $e^m$ statistics | normalization | misalignment | $e + \Delta e_{rms}$ | Error in $f^m$ statistics | normalization | misalignment | $f + \Delta f_{rms}$ |
|---|---|---|---|---|---|---|---|---|---|---|---|---|
| $6^o$ | 0.0620 | 0.0615 | 0.0027 | $0.00 \pm .087$ | 0.0336 | 0.0314 | 0.0267 | $-0.510 \pm .053$ | 0.0083 | 0.0030 | 0.0027 | $0.050 \pm .009$ |
| $8^o$ | 0.0152 | 0.0707 | 0.0068 | $0.149 \pm .073$ | 0.0149 | 0.0413 | 0.0214 | $-0.671 \pm .049$ | 0.0092 | 0.0029 | 0.0068 | $0.047 \pm .012$ |
| $10^o$ | 0.0470 | 0.0759 | 0.0055 | $0.234 \pm .089$ | 0.0326 | 0.0399 | 0.0200 | $-0.650 \pm .055$ | 0.0151 | 0.0059 | 0.0055 | $0.096 \pm .017$ |
| $11^o$ | 0.0208 | 0.0769 | 0.0047 | $0.250 \pm .080$ | 0.0177 | 0.0374 | 0.0174 | $-0.609 \pm .045$ | 0.0119 | 0.0051 | 0.0047 | $0.083 \pm .014$ |
| $12^o$ | 0.0660 | 0.0860 | 0.0043 | $0.398 \pm .109$ | 0.0390 | 0.0291 | 0.0153 | $-0.473 \pm .051$ | 0.0240 | 0.0073 | 0.0043 | $0.119 \pm .025$ |
| $14^o$ | 0.0826 | 0.0785 | 0.0020 | $0.277 \pm .114$ | 0.0406 | 0.0159 | 0.0109 | $-0.259 \pm .045$ | 0.0263 | 0.0079 | 0.0020 | $0.128 \pm .027$ |
| $16^o$ | 0.0959 | 0.0841 | 0.0011 | $0.367 \pm .128$ | 0.0492 | 0.0192 | 0.0078 | $-0.312 \pm .053$ | 0.0341 | 0.0085 | 0.0011 | $0.137 \pm .035$ |

Table III. B.

**Cross-section parameters with total errors for scattering from carbon at 420 Mev**

Dee-target scattering

| $\theta_2$ | Error in $d^d$ | | | | Error in $e^d$ | | | | Error in $f^d$ | | | |
|---|---|---|---|---|---|---|---|---|---|---|---|---|
| | statistics | normal-ization | misalign-ment | $d+\Delta d_{rms}$ | statistics | normal-ization | misalign-ment | $e+\Delta e_{rms}$ | statistics | normal-ization | misalign-ment | $f+\Delta f_{rms}$ |
| 6° | 0.0214 | 0.0214 | 0.0054 | 0.00±.031 | 0.0162 | 0.0071 | 0.0452 | 0.333±.049 | 0.0098 | 0.0009 | 0.0054 | 0.040±.011 |
| 8° | 0.0290 | 0.0224 | 0.0088 | 0.046±.038 | 0.0297 | 0.0099 | 0.0406 | 0.461±.051 | 0.0241 | 0.0022 | 0.0088 | 0.101±.026 |
| 9° | 0.0352 | 0.0229 | 0.0098 | 0.068±.043 | 0.0342 | 0.0085 | 0.0409 | 0.396±.054 | 0.0210 | 0.0028 | 0.0098 | 0.133±.023 |
| 11° | 0.0321 | 0.0234 | 0.0050 | 0.094±.040 | 0.0367 | 0.0043 | 0.0317 | 0.201±.049 | 0.0266 | 0.0022 | 0.0050 | 0.104±.027 |
| 13° | 0.0441 | 0.0219 | 0.0019 | 0.023±.049 | 0.0495 | 0.0026 | 0.0196 | 0.119±.053 | 0.0352 | 0.0005 | 0.0019 | 0.023±.035 |
| 16° | 0.0858 | 0.0237 | 0.0002 | 0.109±.089 | 0.1016 | 0.0044 | 0.0104 | 0.205±.102 | 0.0797 | 0.0021 | 0.0002 | 0.099±.080 |

Meson-target scattering

| $\theta_2$ | Error in $d^m$ | | | | Error in $e^m$ | | | | Error in $f^m$ | | | |
|---|---|---|---|---|---|---|---|---|---|---|---|---|
| | statistics | normal-ization | misalign-ment | $d+\Delta d_{rms}$ | statistics | normal-ization | misalign-ment | $e+\Delta e_{rms}$ | statistics | normal-ization | misalign-ment | $f+\Delta f_{rms}$ |
| 6° | 0.0165 | 0.0165 | 0.0078 | 0.00±.025 | 0.0151 | 0.0071 | 0.0370 | -0.442±.041 | 0.0094 | 0.0007 | 0.0077 | 0.024±.012 |
| 9° | 0.0309 | 0.0200 | 0.0083 | 0.200±.038 | 0.0366 | 0.0091 | 0.0252 | -0.555±.045 | 0.0273 | 0.0010 | 0.0080 | 0.061±.028 |
| 11° | 0.0285 | 0.0215 | 0.0035 | 0.284±.036 | 0.0378 | 0.0060 | 0.0182 | -0.363±.042 | 0.0287 | 0.0019 | 0.0035 | 0.113±.029 |
| 13° | 0.0519 | 0.0308 | 0.0037 | 0.424±.060 | 0.0527 | 0.0066 | 0.0274 | -0.306±.060 | 0.0357 | 0.0021 | 0.0037 | 0.098±.036 |
| 16° | 0.0597 | 0.0311 | 0.0013 | 0.440±.067 | 0.0646 | 0.0070 | 0.0109 | -0.326±.066 | 0.0430 | 0.0020 | 0.0013 | 0.093±.043 |
| 18° | 0.1188 | 0.0304 | 0.0008 | 0.407±.123 | 0.0722 | 0.0061 | 0.0031 | -0.281±.072 | 0.0499 | 0.0032 | 0.0008 | 0.149±.050 |

One other source of systematic error not included in Table II was that resulting from the uncertainty in internal scattering angle. For the quantity $\langle iT_{11} \rangle$, which changed by 13% and 14% per deg for carbon and beryllium, respectively, this amounted to about a 7% error in the dee-target and a 12% error in the meson-target scattering.

Incorrect quadrupole focusing or snout-collimator misalignment was observed to produce a slightly elliptical deformation of the normally round beam pattern incident on Target 2; the possibility of error from this was investigated. For an intensity pattern having a "quadrupole moment" with separation of 1/32 in., it was found that any vertical-horizontal difference was negligible and corresponded to a misalignment for the scattering table of $5 \times 10^{-5}$ deg.

Also, if the center of gravity of the beam were as much as 1/64 in. displaced from the cross hairs at the front and at the rear of the scattering apparatus, the error in angle was only 0.08 deg, and correction of rear-end alignment with the use of counter measurements as described above generally reduced this by a factor of at least two.

One notable deviation from expected results was a difference between 90- and 270-deg measurements for the polarized beam. This was observed first in scattering from the beryllium dee target, for which 90-270 deg differences were four to seven standard deviations for angles of scattering ranging from 6 to 14 deg. Relative differences appeared essentially independent of angle; after subtraction of the known error due to misalignment, vertical asymmetries for beryllium were found to average about 7±4%. Within experimental error, no differences were observable in meson-target measurements. In carbon scatterings, there again were found 90-270 deg differences for the dee-target beam and practically no differences for the meson-target beam. The asymmetries after subtraction of misalignment errors were found to average about 2.5%.

The possibility that the spin (1/2) of the beryllium nucleus

might cause these deviations from expected cross-section behavior can be ruled out on theoretical grounds. Thus it would appear that there was some systematic error inherent in dee-target scattering and perhaps associated with vertical misalignment of the fixed entrance end of the snout collimator;[a] such effects might be expected to differ for beryllium and carbon scatterings because of slightly different conditions, such as source size and position and orientation of beam in the exit channel. Since errors in the 90- and 270-deg measurements cancelled approximately when they were summed for d and f evaluations, no attempt was made at further investigation of the differences.

In summary, many possible sources for experimental error were investigated. These included counter and cross-hair alignment relative to the scattering apparatus, counter geometry, internal target positions, accidental counting rate, beam attenuation of the telescope absorber (extrapolation factor), and beam-energy asymmetry. Extreme changes in counter geometry produced no effect in the range curve; that accidentals were correctly subtracted was verified by obtaining the same cross-section values at several beam levels. Measurements at $\phi$ angles of 45, 135, 225, and 315 deg agreed very well with those at the usual angles. Double scatterings using a beryllium internal target and carbon second target gave consistent results with the separate sets of measurements for each element. (Section IV. K)

---

[a] If the nonconservation of parity should be possible in strong interactions, a reasonable explanation of dee-target vertical asymmetries and meson-target vertical symmetries would be the production of a small component of polarization in the plane of scattering (violating parity restrictions) such that the difference in relative spin rotation angle $\lambda$, equal to 60 deg, would cause this component of polarization to have a near-maximum value for dee-target scattering and a near-minimum value for meson-target scattering.

# IV. ANALYSIS OF RESULTS

## A. Cross-Section Parameters

Measurements of cross sections for each of the two polarized beams gave values of

$$d = \langle T_{20} \rangle_1' \langle T_{20} \rangle_2',$$

$$e = 2\left[ \langle iT_{11} \rangle_1 \langle iT_{11} \rangle_2 - \langle T_{21} \rangle_1' \langle T_{21} \rangle_2' \right],$$

$$f = 2 \langle T_{22} \rangle_1' \langle T_{22} \rangle_2,$$

where the subscripts 1 and 2 refer to internal scattering at angle $\theta_1$ and external scattering at angle $\theta_2$ and primes indicate transformation of the original tensor polarization components by action of the cyclotron field. The beam from the dee target was scattered left and underwent a deflection of about 66 deg before second scattering; the beam from the meson target was scattered right and was deflected through an angle of about 272 deg. (See Fig. 5.) At the second target, more particles were scattered left than right for the dee-target beam (positive asymmetry), and more scattered right than left for the meson-target beam (negative asymmetry), as viewed in the usual coordinate system with the y axis parallel to the dee-target scattering normal.

Since the normal to the plane of scattering at the meson target was opposite to that at the dee target, the coordinate system for the former was obtained by rotation about the z axis of the dee-target system and had its y axis directed downward. Thus if the angle of deflection $\eta$ was defined as positive for the usual left scattering in the cyclotron field, it was then negative for a right scattering; $\lambda$, the angle of spin rotation relative to particle direction, was negative for the left scattering and positive for the right scattering. Values of $\lambda$ were -9.4 and +39 deg for the dee and meson targets, respectively.

The effect of the cyclotron field then was to mix the $\left\langle T_{2M} \right\rangle$ tensor components of polarization produced by the first scattering. With the above values of $\lambda$ used to calculate coefficients, the "rotated" components characterizing the beam at the point of second scattering could be expressed in terms of the $\left\langle T_{2M} \right\rangle$ for angle $\theta_1$ from the equations give in Section II. F.

An alternate method of finding the rotated $\left\langle T_{2M} \right\rangle$ is the use of the x-z plane ellipse (Fig. 16 and Appendix D). $\left\langle T_{20} \right\rangle$ is dependent on $\left\langle S_z^2 \right\rangle$, $\left\langle T_{22} \right\rangle$ on $\left\langle S_x^2 \right\rangle$, and $\left\langle T_{21} \right\rangle$ on $\left\langle S_x S_z \right\rangle$; thus their behavior may be easily determined by taking the inverse squares of the rotated $\rho_z'$ and $\rho_x'$ intercepts for evaluations of $\left\langle T_{20}' \right\rangle$ and $\left\langle T_{22}' \right\rangle$, respectively, and by substituting some associated $\rho_z$ and $\rho_x$ into the equation of the ellipse for $\left\langle T_{21}' \right\rangle$.

As an example of the use of the ellipse, consider the carbon, Case B value of $\left\langle T_{20} \right\rangle$ without magnetic field rotation; it is $-.405$ and gives a $\rho_z$ intercept of

$$1 \bigg/ \sqrt{S_z^2} \quad = \quad \frac{1}{\sqrt{0.476}} \quad = 1.45,$$

since

$$\left\langle T_{20} \right\rangle \quad = \quad 1 \bigg/ \sqrt{2} \; \left( 3 \left\langle S_z^2 \right\rangle - 2 \right).$$

Rotation of 39 deg corresponding to meson-target scattering brings the $\rho_z'$ axis into approximate coincidence with the major axis of the ellipse:

$$1 \bigg/ \sqrt{S_z^2} \quad = \quad 1.58$$

and

$$\left\langle T_{20} \right\rangle \quad = \quad 1 \bigg/ \sqrt{2} \; ( 3 \times .400 - 2 ) = -0.565.$$

(This increase in the magnitude of $\left\langle T_{20} \right\rangle$ compared to the unrotated value is reasonable, as $\left\langle T_{20} \right\rangle$ or $d$ is observed experimentally to be greater for meson-target than for dee-target scattering.)
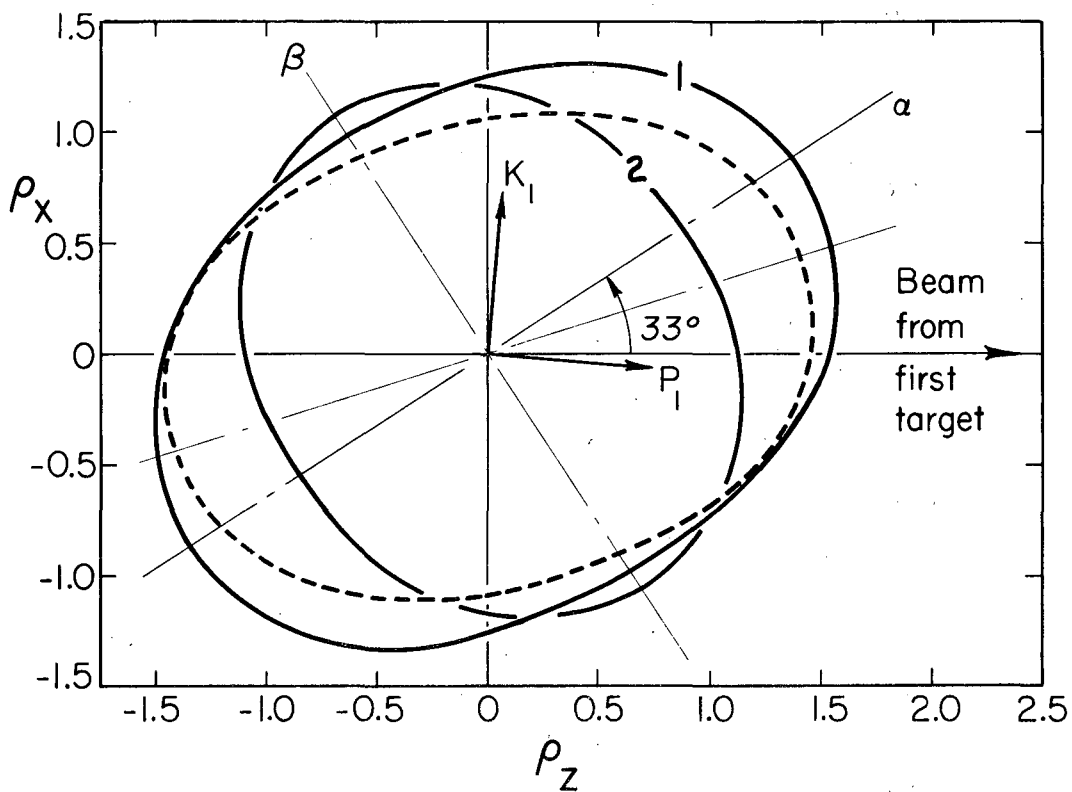
MU — 17305

Fig. 16. Polarization ellipse in the plane of scattering.
This was determined with tensor components from
carbon measurements with systematic errors.
Solid curves represent Case B solutions for negative
$\langle T_{20} \rangle$ (curve 1) and positive $\langle T_{20} \rangle$ (curve 2); the
dotted curve represents Case A with negative $\langle T_{20} \rangle$.
The principal axes of the Case B ellipses are desig-
nated by $\alpha$ and $\beta$.

The same answer is found by substitution in the formulae given above:

$$\langle T_{20} \rangle ' = 0.158 \,(-.405) - 1.22 \times .255 + 0.687 \,(-.235) = -0.536$$

As viewed in the coordinate system of meson-target scattering,

$$\frac{|e^m|}{2} = \langle iT_{11} \rangle_1 \langle iT_{11} \rangle_2 - \langle T_{21} \rangle '_1 \langle T_{21} \rangle '_2 \,,$$

where $\langle T_{21} \rangle '$ is calculated with positive $\lambda$. (No sign correction has to be made in the $d^m$ and $f^m$ expressions, as $\langle T_{20} \rangle '$ and $\langle T_{22} \rangle '$ are even under rotation about the z axis. To eliminate $\langle iT_{11} \rangle$ products from the e parameters obtained from experiment, the expression for $e^d$ was subtracted from that for $\left| e^m \right|$ for each value $\theta_2$:

$$\frac{\left| e^m \right| - e^d}{2} = \left( \langle T_{21} \rangle '^d_1 - \langle T_{21} \rangle '^m_1 \right) \langle T_{21} \rangle_2 \,.$$

The difference between $\left| e^m \right|$ and $e^d$ was in general sufficiently great to yield a fairly precise value for $\langle T_{21} \rangle$.

B. <u>Solution of Equations for</u> $\theta_2 = \theta_1$

Double scattering with the two different internal targets gave six measured quantities at each angle $\theta_2$; the values at $\theta_2 = \theta_1$ (11 deg for beryllium and 10 deg for carbon measurements) then yielded six quadratic equations in the four unknowns $\langle iT_{11} \rangle$, $\langle T_{20} \rangle$, $\langle T_{21} \rangle$, and $\langle T_{22} \rangle$. Reduced to five equations in three unknowns, these were:

$$d^m = \left( 0.158 \, \langle T_{20} \rangle - 1.22 \, \langle T_{21} \rangle + 0.687 \, \langle T_{22} \rangle \right) \langle T_{20} \rangle \,,$$

$$f^m / 2 = \left( 0.344 \, \langle T_{20} \rangle + 0.496 \, \langle T_{21} \rangle + 0.720 \, \langle T_{22} \rangle \right) \langle T_{22} \rangle \,,$$

$$\left( \left| e^m \right| - e^d \right) / 2 = \left( -0.855 \, \langle T_{20} \rangle + 1.04 \, \langle T_{21} \rangle + 0.698 \, \langle T_{22} \rangle \right) \langle T_{21} \rangle \,,$$

$$d^d = \left( 0.936 \, \langle T_{20} \rangle + 0.494 \, \langle T_{21} \rangle + 0.052 \, \langle T_{22} \rangle \right) \langle T_{20} \rangle \,,$$

$$f^d / 2 = \left( 0.026 \, \langle T_{20} \rangle - 0.202 \, \langle T_{21} \rangle + 0.979 \, \langle T_{22} \rangle \right) \langle T_{22} \rangle \,,$$

where the m and d superscripts designate meson- and dee-target values and the coefficients pertain to the scatterings done with carbon.

The ($|e^m|$ - $e^d$)/2 equation contains the difference between dee-target and meson-target rotated $\langle T_{21}\rangle'$ components as indicated above. Substitution of the numerical values for the $\langle T_{JM}\rangle$ of carbon obtained from the given system of equations shows that it was possible for the $|e^m|$ and $e^d$ quantities to differ appreciably in magnitude:

$$\frac{|e^m| - e^d}{2} = \left[0.285 - (-160)\right] \times 0.255 = 0.114.$$

Experimentally determined values for $e^m/2$ and $e^d/2$ were -0.235±.040 and 0.140±.035.

The $d^d$ and $d^m$ quantities were subject to considerable error, especially because of the difficulty in matching range curves of polarized and regenerated beams (Section III. J). Thus there was to be expected considerable error in $\langle T_{20}\rangle$. However, IBM calculations showed that these uncertainties in d and d' affected inappreciably the results obtained from the search program. In other words, the more accurate determinations of e and f were dominant in the analysis and served to determine $\langle T_{20}\rangle$ even if the d measurements were ignored.

As the system of equations for the $\langle T_{2M}\rangle$ at the angle $\theta_1$ was overdetermined, different procedures for solution were found to give slightly different results. Three methods were utilized: simultaneous solutions of pairs of equations; use of direct expressions for $\langle T_{JM}\rangle$ involving $d^d/d^m$ and $f^d/f^m$ ("$\beta \gamma \delta$ -formulae" given in Appendix F); and the application of a $\chi^2$ search program. The second method, although most direct, gave a rather biased set of results because of the large errors in the d and f ratios.

The best method of solution appeared to be the $\chi^2$ fit, similar to the Fermi phase-shift determination in pion-nucleon scattering;[13] applied to the problem here considered, it required the determination

of that combination of $\langle T_{2M} \rangle$ values for which

$$M = \sum_i \left( \frac{x^i_{exp} - x^i_{calc}}{\Delta x^i_{exp}} \right)^2 \quad ( = \chi^2 )$$

was a minimum. Here $x^i$ represents each of the five d, e, and f quantities given above, $x^i_{exp}$ and $\Delta x^i_{exp}$ being experimental measurement and error and $x^i_{calc}$ the corresponding calculated quantity for a particular set of $\langle T_{2M} \rangle$ values.

To find first an approximate set of solutions, $\langle T_{21} \rangle$ was plotted as a function of $\langle T_{20} \rangle$ for each of the five quadratic equations in $\langle T_{2M} \rangle$ given by the measured parameters and with several values assumed for $\langle T_{22} \rangle$ ; i.e., two-dimensional cuts perpendicular to the $\langle T_{22} \rangle$ axis were taken in the three-dimensional $\langle T_{2M} \rangle$ surfaces representing the five given equations. (See Fig. 17.) This preliminary use of a graphical method of solution was found helpful in making systematic errors evident. For example, the sensitivity of d and d' values to normalization of cross sections was reflected to some degree in the divergence of the associated curves from those of other experimental quantities.

Some calculations to minimize M were done by hand (Fig. 18), but final solutions were obtained with slightly greater accuracy by setting up an IBM search program. All IBM work was done with the d, e, and f quantities at $\theta_2 = \theta_1$ obtained by normalizing to give equality of polarized and unpolarized cross sections at 6 deg. Effects of normalization are indicated in the curves used in the graphical analyses of beryllium data, only the d and d' values showing appreciable differences with and without normalization. IBM fits to data at $\theta_1$ were made with statistical errors and with systematic plus statistical errors, where the systematic included normalization and misalignment errors as given in Table III.

Best-fit $\langle T_{JM} \rangle$ values and their rms errors for the various cases considered in IBM calculations are shown in Table IV. The Case A IBM solutions were quite comparable to the "simultaneous-
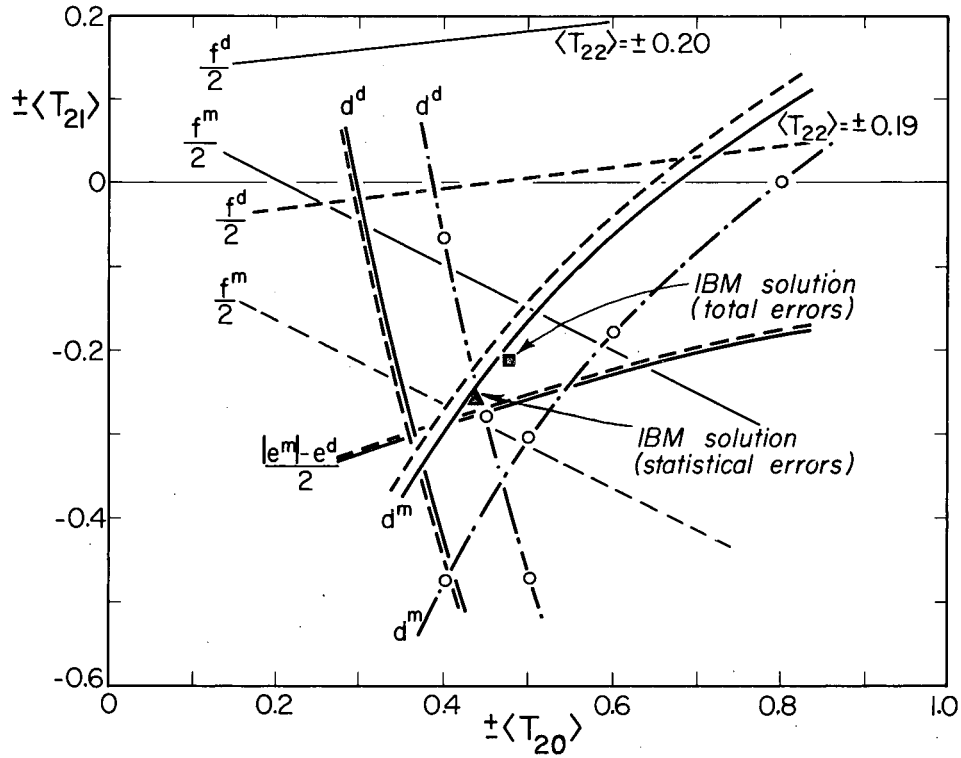
MU-17306

Fig. 17. (a) Plots of $\langle T_{21}\rangle$ vs. $\langle T_{20}\rangle$ representing cross-section parameters for beryllium scattering at angles $\theta_1 = \theta_2 = 11$ deg. Signs are those of Case B. Normalized data were used except for the points designated by circles, which were obtained with nonextrapolated, unnormalized data. (Appreciable differences were observed only for the d quantities.) The solid (and the unnormalized) curves were obtained with $\langle T_{22}\rangle = \pm 0.20$; the dotted curves, with $\langle T_{22}\rangle = \pm 0.25$. (Values do not agree exactly with final results because the relativistic Thomas precession was not included in calculation of the $\langle T_{JM}\rangle$.)
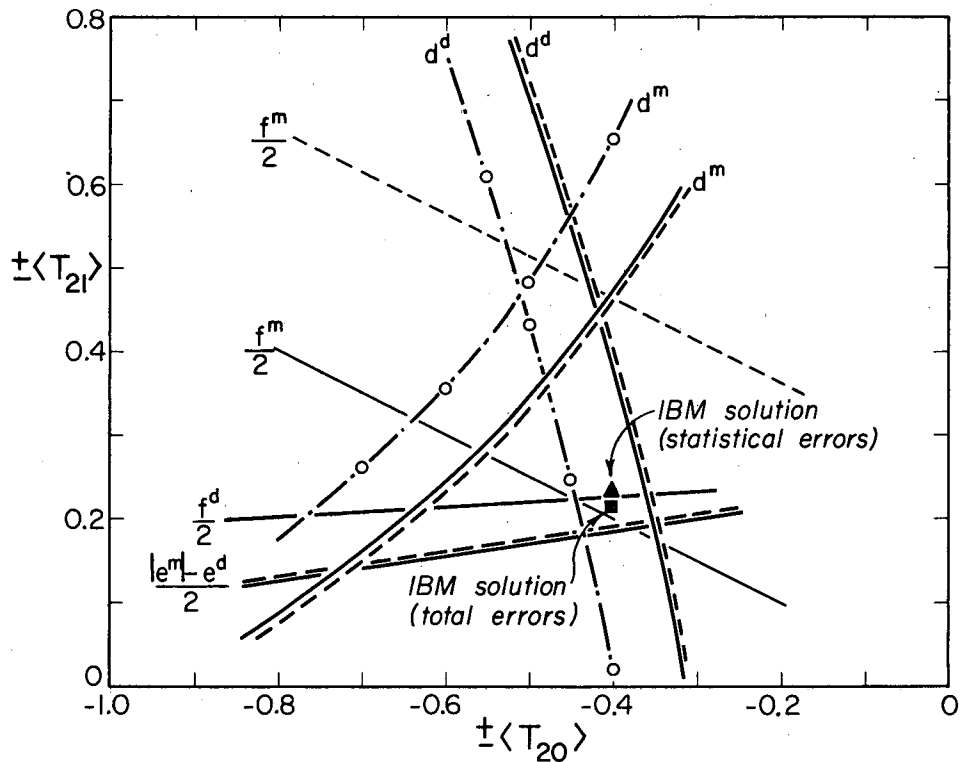
MU-17307

Fig. 17. (b) Plots representing cross-section parameters
for beryllium scattering at angles $\theta_1 = \theta_2 = 11$ deg.
Signs are those of case A. Normalized data were
used except for the points designated by circles.
The solid (and unnormalized) curves were obtained
with $\langle T_{22} \rangle = \pm 0.225$, the dotted curves, with
$\langle T_{22} \rangle = \pm 0.20$.
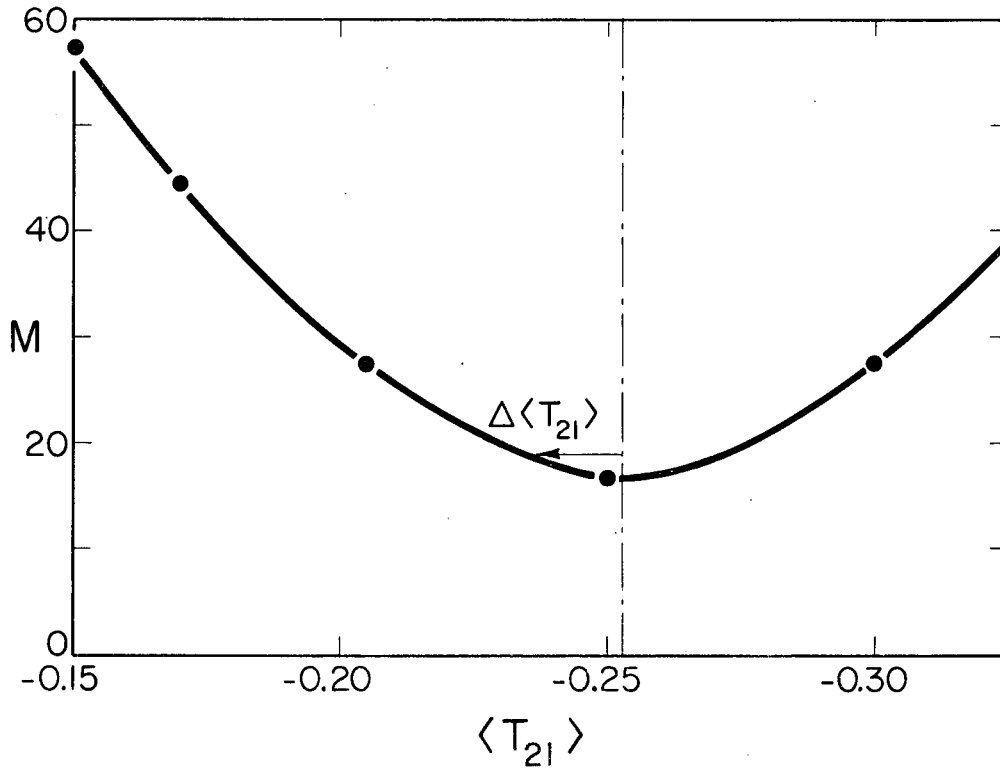
MU-17308

Fig. 18. Variation of M with the tensor component $\langle T_{21} \rangle$ in fitting beryllium unnormalized data (with statistical errors) at 11 deg. Values of $\langle T_{20} \rangle$ = 0.495, $\langle T_{22} \rangle$ = 0.22, and $\langle iT_{11} \rangle$ = ± 0.52 were used.

Table IV.

Best-fit $\langle T_{JM} \rangle$ values and associated M values for $\theta_1 = \theta_2$, determined with cross-section parameters calculated from normalized measurements. (Solutions with the same magnitudes but opposite signs for the $\langle T_{2M} \rangle$ components are also possible.)

| | Beryllium ($\theta = 11^{\circ}$) | | Carbon ($\theta = 10^{\circ}$) | |
|---|---|---|---|---|
| | Case A | Case B | Case A | Case B |
| **With systematic and statistical errors in d, e, and f** | | | | |
| $\langle T_{20} \rangle$ | $-0.305 \pm .070$ | $-0.446 \pm .050$ | $-0.420 \pm .090$ | $-0.405 \pm .030$ |
| $\langle T_{21} \rangle$ | $+0.210 \pm .025$ | $+0.215 \pm .035$ | $+0.230 \pm .030$ | $+0.255 \pm .026$ |
| $\langle T_{22} \rangle$ | $+0.230 \pm .012$ | $-0.185 \pm .015$ | $+0.260 \pm .025$ | $-0.235 \pm .014$ |
| $\langle iT_{11} \rangle$ | $\pm 0.494 \pm .012$ | $\pm 0.502 \pm .010$ | $\pm 0.425 \pm .024$ | $\pm 0.465 \pm .020$ |
| M | 7.61 | 3.43 | 31.3 | 1.80 |
| Q($>$M) | 0.02 | 0.18 | ~0 | 0.41 |
| **With statistical error in d, e, and f[a]** | | | | |
| $\langle T_{20} \rangle$ | $-0.402 \pm .022$ | $-0.438 \pm .007$ | $-0.450 \pm .038$ | $-0.405 \pm .015$ |
| $\langle T_{21} \rangle$ | $+0.233 \pm .013$ | $+0.257 \pm .018$ | $+0.226 \pm .026$ | $+0.270 \pm .026$ |
| $\langle T_{22} \rangle$ | $+0.206 \pm .010$ | $-0.196 \pm .009$ | $+0.244 \pm .021$ | $-0.240 \pm .011$ |
| $\langle iT_{11} \rangle$ | $\pm 0.498 \pm .007$ | $\pm 0.515 \pm .007$ | $\pm 0.430 \pm .014$ | $\pm 0.465 \pm .014$ |
| M | 38.4 | 14.3 | 27.3 | 2.01 |
| Q($>$M) | 0 | .003 | 0 | .36 |

[a] These results differ more from the systematic fits than they should because the relativistic Thomas precession effect was not included in calculating the rotated tensor components.

equation" and the "$\beta\gamma\delta$-formulae" solutions; but the Case B combination of signs also appeared acceptable and indeed proved to be the better choice, as indicated by the M values of Table IV.

## C. Search Program

For normally distributed errors in experimental measurements, the probability that M lies between M and M+dM is approximately

$$P_{M_0} (M) \, dM = \frac{1}{2^{M_0/2} \, \Gamma (M_0/2)} \, e^{-M/2} \, M^{(M_0-2)/2} \, dM,$$
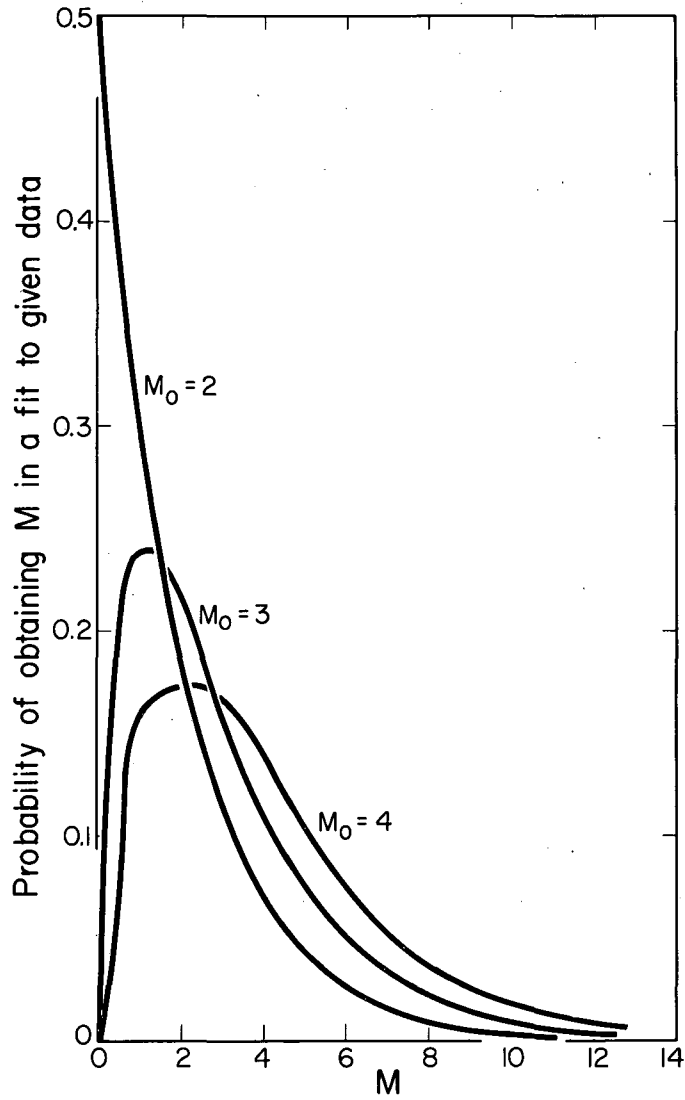
if $M_0$ is the number of degrees of freedom or the number of observations minus the number of determined quantities.[14] (See Fig. 19.) The average value of M obtained for many sets of measurements is $M_0$; the probability that M is greater than a certain value M' is

$$Q (>M') = \int_{M'}^{\infty} P_{M_0} (M) \, dM$$

and for $M_0 = 2$ is given in Table IV for the M values found for each set of $\langle T_{JM} \rangle$ solutions.

Large M values indicated that actual errors were considerably greater than statistical; but with some systematic errors included, the M values were close to 2 for a few cases considered. The values found for $Q(>M')$ showed that the Case B solution was definitely preferred to Case A for carbon and at least as good as Case A for beryllium.

The $\langle T_{JM} \rangle$ values found by the IBM search program did not differ greatly with the inclusion of systematic errors from values found with statistical errors alone. Solutions are indicated on the $\langle T_{21} \rangle$ vs. $\langle T_{20} \rangle$ plots of Fig. 17. To ascertain that the IBM solutions were not appreciably affected by the large uncertainties in $d^d$ and $d^m$, these quantities were removed from calculations and the search program used to satisfy the remaining three equations. There was found only a negligible effect on $\langle T_{20} \rangle$ and none on $\langle T_{21} \rangle$

Fig. 19. M distribution. $M_0$ is the number of degrees of freedom, or the number of observations minus the number of determined quantities.

or $\langle T_{22} \rangle$ :

|  | $\langle T_{20} \rangle$ | $\langle T_{21} \rangle$ | $\langle T_{22} \rangle$ |
|---|---|---|---|
| with $d^d$, $d^m$ | -0.405 | 0.255 | -0.235 |
| without $d^d$, $d^m$ | -0.405 | 0.255 | -0.230 |

(Values obtained are for the carbon, Case B solution with systematic errors.)

Also, to determine that the four cases (two sets of Case A solutions with opposite absolute signs and two sets of Case B solutions with opposite signs) represented all possible solutions to the data, the $f^d/2$ equation (which has a negligible $\langle T_{20} \rangle \langle T_{22} \rangle$ term) was used to plot a $\langle T_{22} \rangle$ vs. $\langle T_{21} \rangle$ curve on which any solution had to lie for an arbitrary value of $\langle T_{20} \rangle$. Then M was computed by IBM program for successive points along the curve between limits $\langle T_{21} \rangle = \pm\sqrt{3}$. Only one minimum M was found, for negative or for positive $\langle T_{20} \rangle$, on each of the two curves representing the two roots of $\langle T_{22} \rangle$ obtained from $f^d/2$. Calculations with and without $d^d$ and $d^m$ gave identical solutions. All cases were computed without $d^d$ and $d^m$. The four minima found corresponded very closely to the four Case A and Case B solutions.

## D. Error

After a best fit has been obtained for experimental data giving a minimum M, an "error matrix" $G_{rs}$ can be defined[15] such that for variations $\epsilon_r$ and $\epsilon_s$ in the determined quantities (here the $\langle T_{2M} \rangle$) designated by r and s, M becomes

$$M = M_{min} + \sum_{r,s} \epsilon_r \epsilon_s G_{rs} .$$

The inverse of the error matrix is given by

$$(G^{-1})_{rs} = \langle \epsilon_r \epsilon_s \rangle = \frac{\int d\epsilon_1 d\epsilon_2 \cdots d\epsilon_n \, e^{-M/2} \epsilon_r \epsilon_s}{\int d\epsilon_1 d\epsilon_2 \cdots d\epsilon_n \, e^{-M/2}} ,$$

and its diagonal elements are the mean-square errors of the quantities determined by minimizing M.

An IBM program was set up to compute from the $G^{-1}$ expression above the statistical and total errors in the $\langle T_{2M} \rangle$ found by the search program. As is shown in Table III, the largest is about 20%.

## E. Restriction of Solutions

By choosing a particular coordinate system, namely, that with the z axis normal to the plane of scattering, Lakin obtains a simple form for the density matrix in terms of just three of the $\langle T_{JM} \rangle$ components. By considering the limitations on the possible statistical weights of the pure states of polarization, he is able to impose a restriction on the $\langle T_{JM} \rangle$ components resulting from single scattering such that any possible state must fall within a truncated cone defined in Lakin's $\langle T_{10} \rangle - \langle T_{20} \rangle$ $\langle T_{22} \rangle$ space. (Appendix C.) The inequality to be satisfied is

$$\langle T_{10} \rangle^2 + \left[ \sqrt{2} \langle T_{22} \rangle \right]^2 \leq 1/3 \left[ \langle T_{20} \rangle + \sqrt{2} \right]^2.$$

In order to apply this to the solutions obtained above, one expresses the $T_{JM}$ of Lakin's system in terms of $S_x$, $S_y$, and $S_z$. (These are $-S_x$, $S_z$, and $S_y$, respectively, in the usual scattering coordinate system with the $S_x$ and $S_z$ taken along the principal axes of the polarization ellipse in the plane of scattering to give a real quantity for $\langle T_{22} \rangle$)

To this end, it is convenient to construct the section of the $\langle S_i S_j \rangle$ ellipsoid in the plane of scattering. (See Appendix D. 2 and Fig. 3.) Substitution of the Case B solutions for $\langle T_{JM} \rangle$ in the equation for the tensor ellipsoid x-z section (usual coordinate system),

$$1 = \langle S_x^2 \rangle \rho_x^2 + \langle S_z^2 \rangle \rho_z^2 + \left( \langle S_x S_z \rangle + \langle S_z S_x \rangle \right) \rho_x \rho_z ,$$

gives the curve of Fig. 16. The principal axes of the ellipse, $\alpha$ and $\beta$, correspond to Lakin's x and y axes, and the inverse squares of the intercepts are his $\langle S_x^2 \rangle$ and $\langle S_y^2 \rangle$. As indicated in the

figure, the major and minor axes of the ellipse are interchanged by a reversal in sign of all the $\langle T_{2M} \rangle$ .

For Case B solutions (IBM best fit), the $\langle T_{JM} \rangle$ of Lakin's system assume the following values for scattering at 10 deg by carbon:

| | B Solution with negative $\langle T_{20} \rangle$ | B Solution with positive $\langle T_{20} \rangle$ (in usual system) |
|---|---|---|
| $\langle T_{10} \rangle =$ | 0.649 | 0.649 (in Lakin's system) |
| $\sqrt{2} \; \langle T_{22} \rangle =$ | 0.392 | -0.472 |
| $\langle T_{20} \rangle =$ | 0.490 | -0.489 |

For Case B solutions, the inequality is definitely not satisfied for positive $\langle T_{20} \rangle$ , but is a very reasonable relation for negative $\langle T_{20} \rangle$ . For Case A, the inequality is not satisfied for negative $\langle T_{20} \rangle$ ; but its restriction is just barely met by the solution for positive $\langle T_{20} \rangle$ . Conclusions are the same for both beryllium and carbon scatterings. Quantities appearing in the inequality are tabulated for all possible solutions to beryllium and carbon data in Table V.

### F. Born-Approximation Predictions of Tensor Components

It has been shown that an inequality of Lakin may be applied to determine the absolute signs of tensor components. This prediction of sign and further the prediction of behavior at small angles are possible also through use of the impulse approximation.

The thesis of Henry Stapp treats the impulse approximation (see Section V) in the first Born approximation, the first Born approximation with the D state of the deuteron included, and the second Born approximation; a Gaussian nuclear form factor and an integral form of the deuteron wave function are used to estimate parameters of the scattering matrix.[3] The first Born approximation (with simultaneous scattering included) using deuteron-scattering amplitudes obtained directly from proton and neutron amplitudes is sufficient to fit cross sections at low energies[a] and also vector

---

[a]See introduction of article by Stapp[3].

Table V.

Quantities characterizing $\langle T_{JM} \rangle$ fits.

| Relative $\langle T_{2M} \rangle$ signs | Absolute $\langle T_{20} \rangle$ sign | Terms of Lakin inequality | | | Occupation of $m_s = 0$ spin state |
|---|---|---|---|---|---|
| | | $\langle T_{10} \rangle^2$ | $\left( \sqrt{2} \langle T_{22} \rangle \right)^2$ | $\left( \langle T_{20} \rangle + \sqrt{2} \right)^2 / 3$ | $1/3 - N(0)/N$ |
| Beryllium | | | | | |
| Case A | + | 0.488 | 0.291 | 0.797 | +0.061 |
| | - | 0.488 | 0.254 | 0.550 | -0.061 |
| Case B | + | 0.503 | 0.168 | 0.311 | -0.212 |
| | - | 0.503 | 0.158 | 1.16 | +0.212 |
| Carbon | | | | | |
| Case A | + | 0.361 | 0.406 | 0.773 | +0.051 |
| | - | 0.361 | 0.327 | 0.570 | -0.051 |
| Case B | + | 0.420 | 0.222 | 0.285 | -0.231 |
| | - | 0.420 | 0.154 | 1.21 | +0.231 |

polarization at high energies; it appears that inclusion of D state
in the deuteron wave function is unnecessary, but that use of the
second Born approximation is probably required to bring predictions
of $\langle T_{20} \rangle$ and $\langle T_{22} \rangle$ into better agreement with experiment.

In the first Born approximation, the scattering matrix is the
usual expression proportional to the matrix element of the central
plus spin-orbit potentials taken between initial and final states.
It is necessary to include the D state to obtain tensor terms c $(\theta)$
and d $(\theta)$ of the scattering matrix,

$$M_{sc} = a\,(\theta) + b\,(\theta)\,\overline{S}\cdot\overline{n} + \left[ c\,(\theta)\left(N_i N_j - \frac{\delta_{ij}}{3}\right) + d\,(\boldsymbol{\theta})\,(P_i P_j - K_i K_j)\right] S_{ij}.$$

In this approximation, c $(\theta)$ is found equal to d $(\theta)$, but very small
in comparison with a $(\theta)$ and b $(\theta)$.

The second Born approximation is the evaluation of the matrix
element

$$H = H_{fi} + \frac{H_{fm}\,H_{mi}}{E - E_m + i\epsilon}$$

between initial and final states; it indicates that at small angles
there is dominant a particular tensor term, such that c $(\theta)$ equals
-d $(\theta)$.

In the first Born approximation, Stapp found

$$c\,(\theta) = d\,(\theta) = 1/6\ k^2 r_0^2\ a\,(\theta)\,\sin^2\frac{\theta}{2},$$

where k is the incident momentum of the deuteron and $r_0 = 1.4 \times 10^{-13}$ cm.
For 410-Mev deuterons, this is $9.0\ a\,(\theta)\,\sin^2\frac{\theta}{2}$; and with the approxi-
mate expression[a] for b $(\theta)$ of $10\lambda_c^2\ k^2\ a\ \sin\theta$, $\langle T_{20} \rangle$ and $\langle T_{22} \rangle$ may
be calculated from Eqs. (25) and (28) of the Stapp article:

---

[a] In first Born approximation, $b(\theta) = i\lambda_c^2\ k^2\ a\,(\theta)\,\sin\theta\ \dfrac{\left|V_s\right|_{r=0}}{\left|V_c\right|_{r=0}}$,

$$t(\theta) = \sqrt{2} \left\langle T_{20} \right\rangle (\theta) = (1/I_u) \left\{ 2 \cos \theta \, \text{Re} \left[ d(a+c/3 + ib \tan \theta)^* \right] \right.$$

$$\left. -2/3 \, \text{Re} \left[ c(a+c/3)^* \right] - 1/3 \, dd^* - 1/3 \, bb^* + 1/3 \, cc^* \right\} ,$$

$$w(\theta) = 2\sqrt{3} \left\langle T_{22} \right\rangle (\theta) = (1/I_u) \left\{ -2 \cos \theta \, \text{Re} \left[ d(a+c/3 + ib \tan \theta)^* \right] \right.$$

$$\left. -2 \, \text{Re} \left[ c(a+c/3)^* \right] - dd^* - bb^* + cc^* \right\} .$$

At small angles, these expressions become

$$\left\langle T_{20} \right\rangle (\theta) = (1/I_u)(-32 \, a^2 \theta^2),$$

$$\left\langle T_{22} \right\rangle (\theta) = (1/I_u)(-44 \, a^2 \theta^2);$$

in scattering from beryllium, they yield the values

$$\left\langle T_{20} \right\rangle \simeq -0.16 \text{ and } \left\langle T_{22} \right\rangle \simeq -0.22 \text{ for } \theta = 4^\circ \text{ lab, and}$$

$$\left\langle T_{20} \right\rangle \simeq -0.27 \text{ and } \left\langle T_{22} \right\rangle \simeq -0.38 \text{ for } \theta = 11^\circ \text{ lab.}$$

Comparison with experimental results shows that Stapp's first Born-approximation estimates of $\left\langle T_{20} \right\rangle$ and $\left\langle T_{22} \right\rangle$ are too large at small angles and for $\left\langle T_{20} \right\rangle$ too small at larger angles. However, this approximation definitely substantiates the choice of one of the Case B solutions as preferable to Case A.

The second Born approximation should not appreciably change the estimate of the $\left\langle T_{22} \right\rangle$ polarization component at small angles; this results from the fact that $c(\theta)$ and $d(\theta)$ are found to have similar magnitudes, but opposite signs, so that the first two terms of the $\left\langle T_{22} \right\rangle$ expression above should cancel; and these are the chief tensor contributions at small angles. $\left\langle T_{20} \right\rangle$ will, however, be affected by second Born-approximation contributions to its first two terms. At larger angles, $\left\langle T_{22} \right\rangle$ will not become so large negatively as in the first Born approximation because the positive contribution of $cc^*$ becomes large as $\text{Im}(a)$ goes to zero. (The behavior of deuteron amplitudes is assumed similar to that of proton amplitudes. See Fig. 20 for plots of proton-carbon scattering amplitudes.[16])

In conclusion, it can be said that the first Born approximation predicts a $\sin^2 \theta$ dependence for both $\left\langle T_{20} \right\rangle$ and $\left\langle T_{22} \right\rangle$ at small angles; the second Born approximation predicts the same $\left\langle T_{22} \right\rangle$, but a more complex behavior of $\left\langle T_{20} \right\rangle$, approaching a $\sin^2 \theta$ dependence only for moderately large angles.
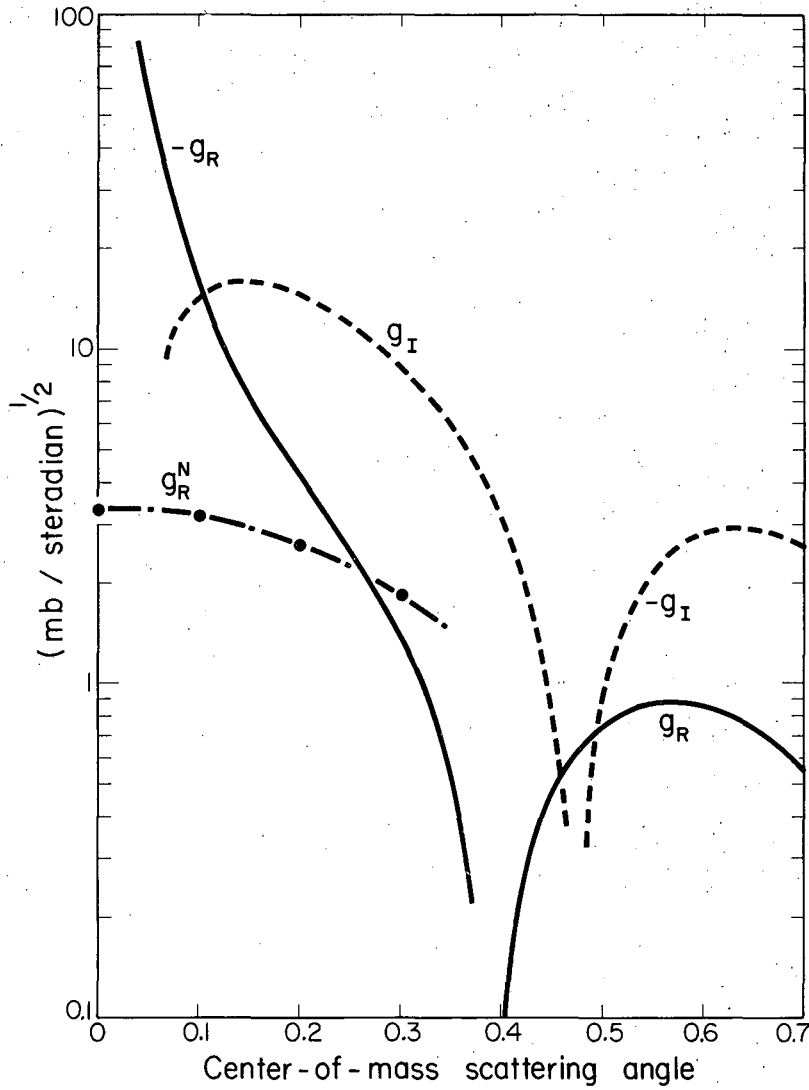
Fig. 20. (a) Spin-independent proton-carbon scat-
tering amplitudes at 220 Mev. These were
obtained by Hafner through fitting a Woods-
Saxon potential to his experimental data with a
WKB analysis. There is indicated also $g_R$ for
neutron scattering, the amplitude differing most
from that for proton scattering.
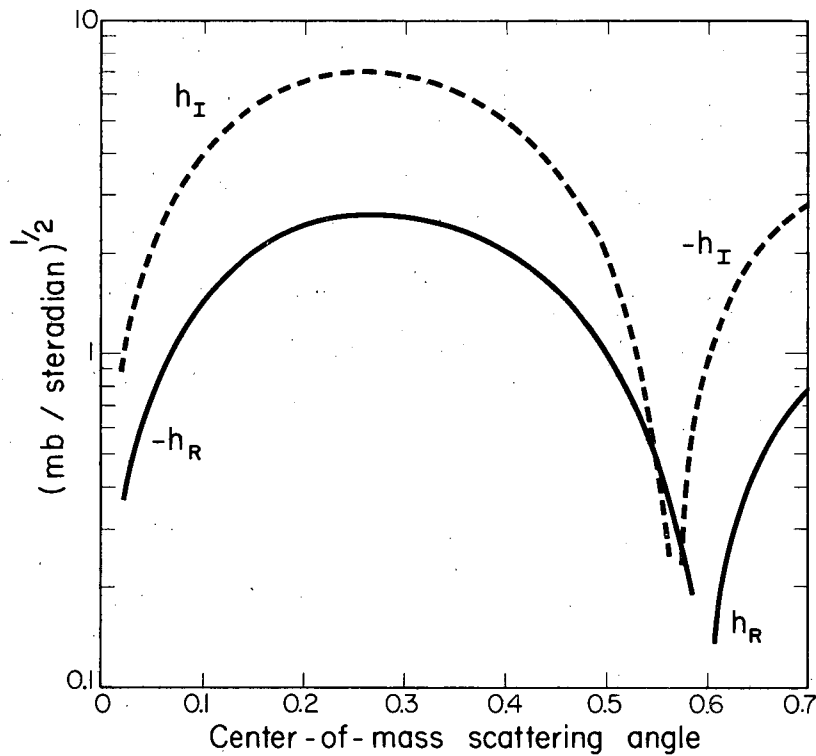
MU—17311

Fig. 20. (b) Spin-dependent proton-carbon amplitudes
obtained by Hafner at 220 Mev.

## G. Physical Interpretation

An examination of the physics of the scattering process may help further to select a unique set of $\langle T_{JM} \rangle$ signs. Such an argument has been appealed to before in choosing the sign of $\langle iT_{11} \rangle$ to be positive on the basis of the type of interaction observed in shell-model spin-orbit coupling.[4,17] Here certain conclusions may be drawn upon consideration of the occupation of quantum-mechanical states and the behavior of the cross-section parameter d with increasing scattering angle.

Some indication of the proper $\langle T_{JM} \rangle$ signs is given by the values of $\langle T_{20} \rangle$ and $\langle T_{22} \rangle$ under the assumption that there are possible only the three pure spin states associated with the normal to the scattering plane. The occupation of the $m_s = 0$ spin state associated with the y axis in the usual coordinate system can be shown to differ from the unpolarized value of 1/3 by an amount

$$1/3 - N(0)/N = 1/3 \left( 3 \left\langle s_y^2 \right\rangle - 2 \right)$$

or

$$1/3 - N(0)/N = \frac{1}{\sqrt{3}} \left\langle T_{22} \right\rangle - \frac{1}{3\sqrt{2}} \left\langle T_{20} \right\rangle .$$

For the sign combination Case A, $N(0)/N$ is very close to 1/3, while for Case B, it is 0.55 or 0.10 for the two choices of absolute sign. (See Table V.) As is further confirmed by estimating the occupation of the +1 and -1 spin states through the combining of the measured $\langle iT_{11} \rangle$ with N(0) values, neither set of signs for Case A seems to give unreasonable results, but for Case B only the negative $\langle T_{20} \rangle$ – negative $\langle T_{22} \rangle$ solution appears acceptable, the fractional occupations being

$$\frac{N(+)}{N} : \frac{N(-)}{N} : \frac{N(0)}{N} = 0.70 : 0.20 : 0.10.$$

It has been shown through analysis of experimental data that the major and minor axes of the polarization tensor ellipse in the x-z scattering plane differ appreciably and for some sign choices

indicate a predominant spin alignment along the x or z axis. It
seems possible to relate the direction of predominant spin align-
ment to the behavior of the cross-section quantity d (or of $\langle T_{20} \rangle$ )
with variation in scattering angle; d is observed to increase from
practically zero, or perhaps slightly negative values, to appreciable
positive ones as $\theta$ increases. To explain this increase in polarized
over unpolarized cross section, there should be a predominant spin
alignment transverse to the direction of motion, giving a greater
effective geometrical cross section than for the unpolarized beam.
(This assumes single scattering or the usual impulse approximation.
Stapp says that simultaneous scattering predominates at large angles,[3]
but calculations indicate this to be less important than his formulae
suggest.)

The deuteron is a prolate spheroid with its long axis coinci-
dent with the axis of spin, the length being 1.14 times the average
radius of the deuteron; in a simple picture, one can think of the
loosely bound nucleons as being placed one after the other along the
spin axis. Then it is evident that with this axis preferentially trans-
verse to the direction of motion, there is greater probability for pol-
arized than unpolarized scattering and hence a positive value for d.[a]

The above argument does not support the positive $\langle T_{20} \rangle$ signs
of Case A, as $\langle S_z^2 \rangle / \langle S_x^2 \rangle$ is 0.86/0.71. For the negative $\langle T_{20} \rangle$ –
negative $\langle T_{22} \rangle$ set of Case B solutions favored by the IBM fit and
Lakin inequality, it can be seen from the polarization ellipsoid
section in the plane of scattering that there is some preference for
alignment along the x axis in that plane; also, there is predominant
an alignment normal to the plane. ( $\langle S_x^2 \rangle$ = 0.63 and $\langle S_y^2 \rangle$ = 0.90,
while $\langle S_z^2 \rangle$ = 0.48.) Thus, for this set of solutions, the polarized
should be greater than the unpolarized cross section, as observed in
experiment.

---

[a] $\langle T_{20} \rangle \equiv \frac{1}{\sqrt{2}} (3 \langle S_z^2 \rangle - 2)$, which indicates z-axis alignment, would
tend toward a maximum negative value with increasing d.

## H. Choice of Signs

It has been shown that experimental results determine the relative but not the absolute signs of the $\langle T_{2M} \rangle$ polarization components. In fact, even the relative signs were not definitely determined, and two possible sign combinations were found, because of the small magnitude of cross terms in the e-d-f quadratic equations. Thus it has been necessary to discuss theoretical and physical interpretations of the various sets of experimentally possible solutions.

In conclusion, there have been a number of considerations mentioned that should permit a definite statement as to the absolute signs of the tensor components. These support predominantly Case B relative signs with $\langle T_{20} \rangle$ and $\langle T_{22} \rangle$ both negative and $\langle T_{21} \rangle$ positive. Only the $\beta \gamma \delta$ formulae, which involve considerable error, tend to favor the positive $\langle T_{20} \rangle$ signs. The negative $\langle T_{20} \rangle$ —Case B solution must be chosen on the basis of

    (a) minimization of M,

    (b) application of Lakin inequality,

    (c) predictions of Stapp's Born approximation,

    (d) physical interpretation of spin alignment,

    (e) results of impulse approximation with the use
        of nucleon-nucleus scattering amplitudes
        (Section V)

## J. Determination of $\langle T_{JM} \rangle (\theta)$

The experimentally determined functions of second scattering angle, d, f, and $\left| e^{mes} \right| - e^{dee}$, contain products of the various $\langle T_{2M} \rangle (\theta_2)$ and the rotated $\langle T_{2M} \rangle ' (\theta_1)$. For the beryllium measurements,

$$d(\theta_2) = \langle T_{20} \rangle ' (11^\circ) \langle T_{20} \rangle (\theta_2),$$

$$f(\theta_2) = 2 \langle T_{22} \rangle ' (11^\circ) \langle T_{22} \rangle (\theta_2),$$

$$\left| e^{mes}(\theta_2) \right| - e^{dee}(\theta_2) = 2 \left[ \langle T_{21} \rangle '^d (11^\circ) - \langle T_{21} \rangle '^m (11^\circ) \right] \langle T_{21} \rangle (\theta_2).$$

Also,

$$e(\theta_2) = 2\left[ -\langle T_{21}\rangle'(11^\circ)\ \langle T_{21}\rangle\ (\theta_2) + \langle iT_{11}\rangle(11^\circ)\ \langle iT_{11}\rangle\ (\theta_2)\ .\right]$$

The rotated $\langle T_{2M}\rangle'(\theta_1)$ quantities can be obtained either from the x-z ellipse or from their expressions in terms of the untransformed $\langle T_{2M}\rangle$ and functions of the tensor rotation angle $\lambda$; another method, simply the division of parameters obtained at $\theta_2 = \theta_1$ by the $\langle T_{JM}\rangle$ $(\theta_2)$ obtained from the search program, was thought preferable in perhaps minimizing systematic error. $\langle T_{JM}\rangle$ $(\theta)$ values were then calculated from the d, e. and f values for various $\theta_2$; and averages of dee- and meson-target results were plotted with the total errors of Table III. (Fig. 21 and 22.)

## K. Consistency of Results

The sets of measurements for beryllium and for carbon were made at different times and under somewhat different cyclotron field conditions; orbits had been known quite exactly for the beryllium measurements, but were less dependable for carbon because of lack of exact field information following the change. Thus it seemed of considerable importance to compare beryllium and carbon results.

This was done by determining cross-section parameters for a beryllium-carbon double scattering (beryllium as first target and carbon as second target) at three different values of $\theta_2$; two of these measurements were taken in the carbon run and one in the beryllium run. Tensor components giving internal consistency for beryllium-beryllium and for carbon-carbon results were used to calculate the beryllium-carbon parameters; and these were found in good agreement with measured values. (See Table VI.)
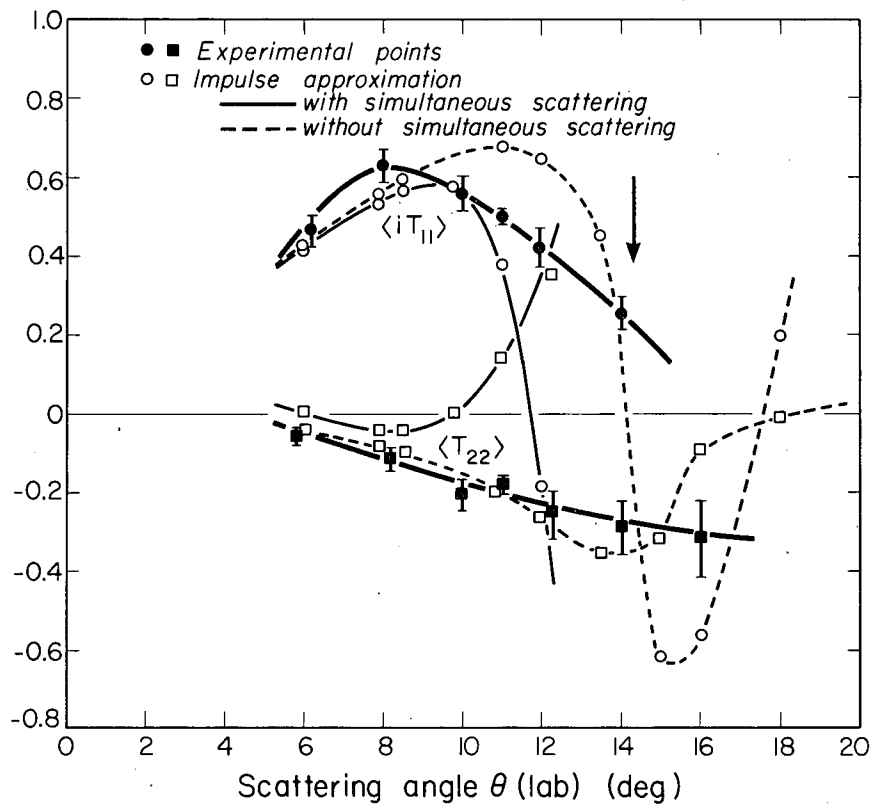
MU−17312

Fig. 21. (a) Polarization components for 410-Mev
deuterons scattered by beryllium. Errors on
experimental points include statistical and
systematic effects. Impulse-approximation
calculations were done with Hafner proton amplitudes.
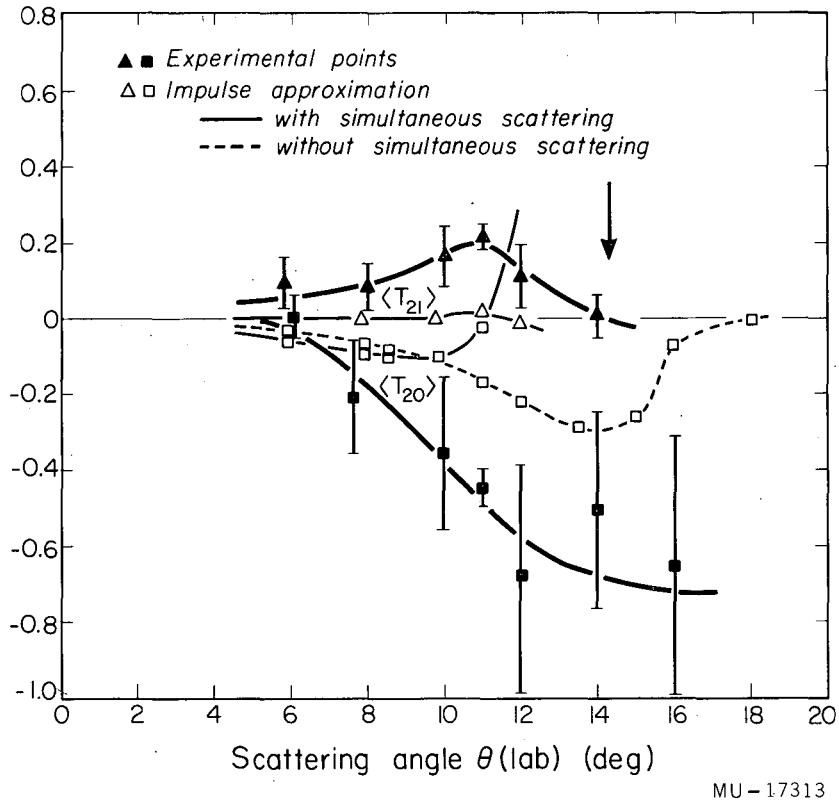The vertical arrow indicates the position of the
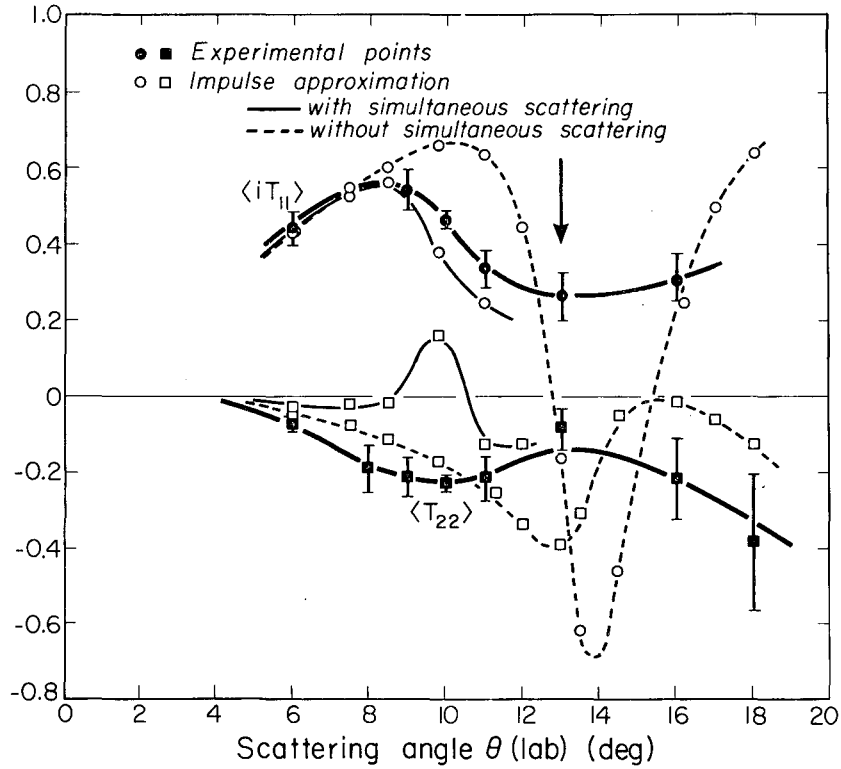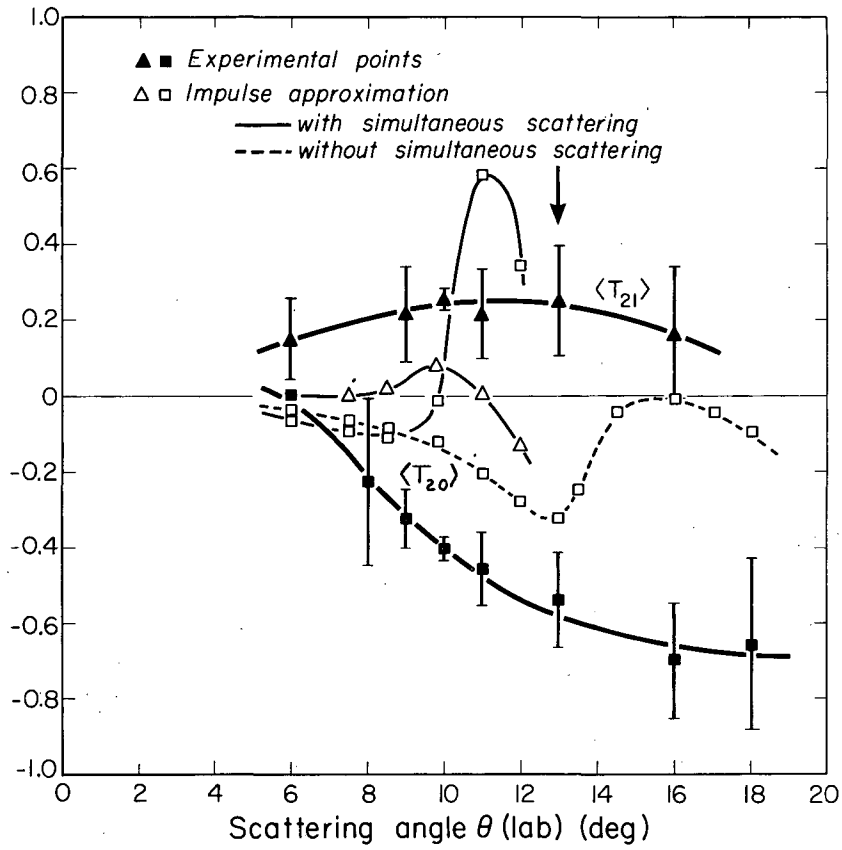diffraction minimum.

Fig. 21. (b) Polarization components for 410-Mev
deuterons scattered by beryllium. Errors on
experimental points include statistical and
systematic effects. Impulse-approximation cal-
culations were done with Hafner proton amplitudes.
The vertical arrow indicates the position of the dif-
fraction minimum. $\langle T_{21} \rangle$ is zero in the usual
impulse approximation.

MU-17314

Fig. 22. (a) Polarization components for 420-Mev
deuterons scattered by carbon, with impulse-
approximation predictions from Hafner proton
amplitudes. Total errors are indicated. The
arrow designates the diffraction minimum.

Fig. 22. (b) Polarization components for 420-Mev
deuterons scattered by carbon, with impulse-
approximation predictions from Hafner proton
amplitudes. Total errors are indicated. The
arrow designates the diffraction minimum.

Table VI.

| Beryllium-carbon double-scattering results |
|---|

| Cross-section parameters | | Scattering angle, $\theta_{lab}$ (deg) | | |
|---|---|---|---|---|
| | | 6 | 11 | 14 |
| d | measured | $0 \pm .022$ | $0.142 \pm .032$ | |
| | calculated | 0 | 0.197 | |
| e | measured | $0.572 \pm .017$ | $0.354 \pm .039$ | |
| | calculated | 0.552 | 0.520 | |
| f | measured | $0.041 \pm .011$ | $0.060 \pm .026$ | |
| | calculated | 0.026 | 0.075 | |
| $\dfrac{e}{1+d+f}$ | measured | | | $0.199 \pm .034$ |
| | calculated | | | 0.177 |
| $\dfrac{f}{1+d}$ | measured | | | $0.088 \pm .027$ |
| | calculated | | | 0.058 |

Errors indicated are statistical only.

## V. IMPULSE APPROXIMATION

### A. Born Approximation in Scattering of Nucleons

A complex spin-dependent potential is necessary to account for the observed polarization of nucleons scattered by nuclei. The general form representing a scattering interaction may be written[18] as

$$V(r) = V_c(r) - \overline{\sigma} \cdot \overline{\nabla} \rho \times \overline{p} \left( \frac{\lambda_c^2}{\hbar} \right) ,$$

where $V_c(r)$ is a complex central potential,

$\overline{\nabla} \rho$ represents the gradient of nuclear density,

$\overline{\sigma}$ and $\overline{p}$ are the spin and momentum of the incident nucleon,

$\lambda_c$ is the proton Compton wave length.

Expressed in its more usual form, with $V_s(r)$ as the spin-orbit interaction, the potential is

$$V(r) = V_c(r) - 1/r \frac{dV_s(r)}{dr} \overline{\sigma} \cdot \overline{1} \left( \frac{\lambda_c^2}{\hbar} \right) .$$

The $V_c(r)$ must have real and imaginary parts to account for scattering and absorption processes; further, an imaginary part is necessary to produce the interference with the spin-dependent term which is manifested in polarization phenomena. Extensive optical-model studies have been made to determine the general form and magnitude of the central potential.[1]

The existence of a spin-orbit term is suggested by the observance of spin-orbit coupling in bound nuclear systems and by the presence of the Thomas term in atomic interactions; also, it can be shown by optical-model considerations[19] that the term is a necessary consequence of the spin dependence of nucleon-nucleon interactions. The spin-orbit potential was first proposed by Fermi as giving rise to polarization phenomena, and its form has since been determined by many authors through analysis of scattering data.

The Born approximation, which is valid for energies greater than 300 Mev, for forward scattering angles, and for light nuclei, permits the determination of the scattering matrix from the interaction potential:

$$f(\theta) = M_{sc} = \left(-\frac{m}{2\pi\hbar^2}\right) \int \psi_f \, V \, \psi_i \, d\tau,$$

with $m$ the nucleon mass and $\psi_f$ and $\psi_i$ the final and initial wave functions. If the scattering matrix $M_{sc}$ is defined as

$$M_{sc} = g(K) + h(K) \, \bar{\sigma} \cdot \bar{n},$$

and if there is made the usual assumption that $V_c(r)$ and $V_s(r)$ have the same radial dependence, the quantities $g(K)$ and $h(K)$ are seen to take the forms

$$g = \left(-\frac{m}{2\pi\hbar^2}\right) \int e^{-i\bar{k}_f \cdot \bar{r}} \, V_c(r) \, e^{i\bar{k}_i \cdot \bar{r}} \, d\bar{r}$$

$$\bar{\sigma} \cdot \bar{n} \, h = \left(\frac{m}{2\pi\hbar^2}\right) \, \lambda_c^2 \int e^{-i\bar{K} \cdot \bar{r}} \, (\bar{\sigma} \cdot \bar{\nabla} \, V_s \times \bar{k}_i) \, d\bar{r}$$

$$= i \left(-\frac{m}{2\pi\hbar^2}\right) \, \lambda_c^2 \int e^{-i\bar{K} \cdot \bar{r}} \, V_s \, (\bar{\sigma} \cdot \bar{K} \times \bar{k}_i) \, d\bar{r}$$

$$= i \left(-\frac{m}{2\pi\hbar^2}\right) \, \lambda_c^2 \quad \bar{\sigma} \cdot \bar{k}_i \times \bar{k}_f \int e^{-i\bar{K} \cdot \bar{r}} V_s \, d\bar{r}.$$

Thus there results

$$g(K) = \left(-\frac{m}{2\pi\hbar^2}\right) \int e^{-i\bar{K} \cdot \bar{r}} \, V_c(r) \, d\bar{r}$$

$$h(K) = -i\lambda_c^2 \, k^2 \, \sin\theta \, g(K) \frac{\left|V_s\right|_{r=0}}{\left|V_c\right|_{r=0}}$$

(Stapp chooses to define the spin-orbit potential as $V_s = G \, Re \, V_c$, and finds that $G$ is approximately 20 for fits to proton data at 300 Mev and about 24 for deuteron data at 165 Mev. The 410-Mev deuteron measurements reported here give a $G$ value of about 19.)

### B. Born Approximation in Scattering of Deuterons

The impulse approximation can be applied to deuteron scattering by assuming charge independence and a Hamiltonian of the form

$$\mathcal{H} = T_1 + T_2 + U_d \, (r_{12}) + V_1 \, (r_1, p_1, \sigma_1) + V_2 \, (r_2, p_2, \sigma_2),$$

or

$$\mathcal{H} = \mathcal{H}_0 + \mathcal{H}_1$$

with

$$\mathcal{H}_0 = T_1 + T_2 + U_d \quad \text{and} \quad \mathcal{H}_1 = V_1 + V_2 \, ,$$

where the 1 refers to Nucleon 1 and the 2 to Nucleon 2 of the deuteron; $U_d$ represents the interaction between the two nucleons, and V, the interaction between the nucleon and the nucleus. The idea of the impulse approximation is contained in $\mathcal{H}_1$, whose form indicates that an impulse given by the nucleus to either Nucleon 1 or 2 produces scattering of the whole deuteron (unless dissociation occurs), but has no direct effect on the partner nucleon.

As a first approximation, the internal wave function $\chi \, (r_{12})$ is assumed to represent just the deuteron S state. Then, with the assumption that $V_1$ is equal to $V_2$ and that the nucleon potential has the form given above, the scattering matrix in Born approximation becomes

$$M_d = \left( -\frac{m_d}{2 \pi \hbar^2} \right) \int dr_1 \, dr_2 \, \chi^* \, (r_{12}) \, e^{-i \overline{k}_f \cdot (1/2) (\overline{r}_1 + \overline{r}_2)}$$

$$\cdot \left[ V(r_1) + V(r_2) \right] \, \chi \, (r_{12}) \cdot e^{i \overline{k}_i \cdot (1/2) (\overline{r}_1 + \overline{r}_2)}$$

$$= \left( -\frac{m_d}{2 \pi \hbar^2} \right) \int dr_{12} \, \chi^2 \, (r_{12}) \, e^{i \frac{\overline{K}}{2} \cdot \overline{r}_{12}} \int dr \, e^{-i \overline{k}_f \cdot \overline{r}}$$

$$\cdot \left[ 2 V_c (r) - \overline{S} \cdot \overline{\nabla} V_s \times \overline{p} \right] \, ,$$

or

$$M_d = f^{1/2} (K) \left[ 2 g_d(K) + h_d (K, k) \overline{S} \cdot \overline{n} \right] \, .$$

(This corresponds to Stapp's $M = a + b \overline{S} \cdot \overline{n}$.) The sticking factor $f(K)$, whose square root is the Fourier transform of the square of the deuteron ground-state wave function,[20] represents the probability of the deuteron's staying intact during the scattering process.

Evidently the $g_d(K)$ and $h_d(K)$ of the deuteron scattering matrix can be expressed in terms of the nucleon scattering amplitudes:

$$g_d(K) = \left( \frac{m_d}{m_n} \right) g_n \; (K)$$

$$h_d(K, \, k_d) = \left( \frac{k_d}{k_n} \right)^2 \frac{\sin \theta_d}{\sin \theta_n} \left( \frac{m_d}{m_n} \right) h_n \; (K, k_n).$$

Thus the values for $g_d$ and $h_d$ (hence those for $I_u$ and the polarization components) may be predicted from known values for $g_n$ and $h_n$; the nucleon data used should be for nucleons of momentum about half that of the deuteron and scattering angle twice as large, so that the momentum per nucleon and the total momentum transfer are the same in both nucleon and deuteron scatterings.

By using the above expression for $M_{sc}$ and the expression for $T_{JM}$ expectation values,

$$I_u \left\langle T_{JM} \right\rangle = (1/3) \; \text{Tr} \; (MM^\dagger T_{JM}),$$

it can be shown[2] that in first Born approximation,

$$I_u^d = (1/3) \; \text{Tr} \; M^\dagger M = f(K) \left[ 4 \, g_d^2 + (2/3) \, h_d^2 \right] \, ,$$

$$I_u \left\langle i T_{11} \right\rangle = f(K) \, (2/\sqrt{3}) \, 2 \, \text{Re} \, g_d^* \, h_d = (\sqrt{3}/2) \, I_u \left\langle S_y \right\rangle \, ,$$

$$I_u \left\langle T_{20} \right\rangle = -f(K) \, (1/3\sqrt{2}) \left| h_d \right|^2 \, ,$$

$$I_u \left\langle T_{21} \right\rangle = 0,$$

$$I_u \left\langle T_{22} \right\rangle = -f (K) \ (1/2\sqrt{3}) \left| h_d \right|^2 .$$

## C. Determination of $g_d$ and $h_d$ in First Born Approximation

Cross-section and polarization data from the scattering of
nucleons can be used to determine the values of nucleon and deuteron
scattering amplitudes if there is some means of estimating the
relative phase of the spin-independent and spin-dependent nucleon
amplitudes. Alternatively, nucleon scattering amplitudes may be
obtained directly from phase shifts determined through the fitting of
a potential to scattering data.

Various methods were used to estimate the phases of the
amplitudes for nucleon scattering by beryllium and carbon at 220
Mev: comparison of potentials from Riesenfeld-Watson calculations,
Hafner experimental data,[16] and the Ferbach-Serber-Taylor model.[21]
The average phase difference between spin-dependent and spin-
independent amplitudes at small angles was about 20 deg.

Calculations for deuteron cross sections and polarization com-
ponents were carried out for the complete range of experimental
angles with nucleon scattering amplitudes obtained from Hafner at
Rochester (Fig. 20) and Bjorklund at Livermore. (See Figs. 21, 22,
and 23.) Both used a Woods-Saxon potential to fit experimental data,
but with somewhat differing parameters:
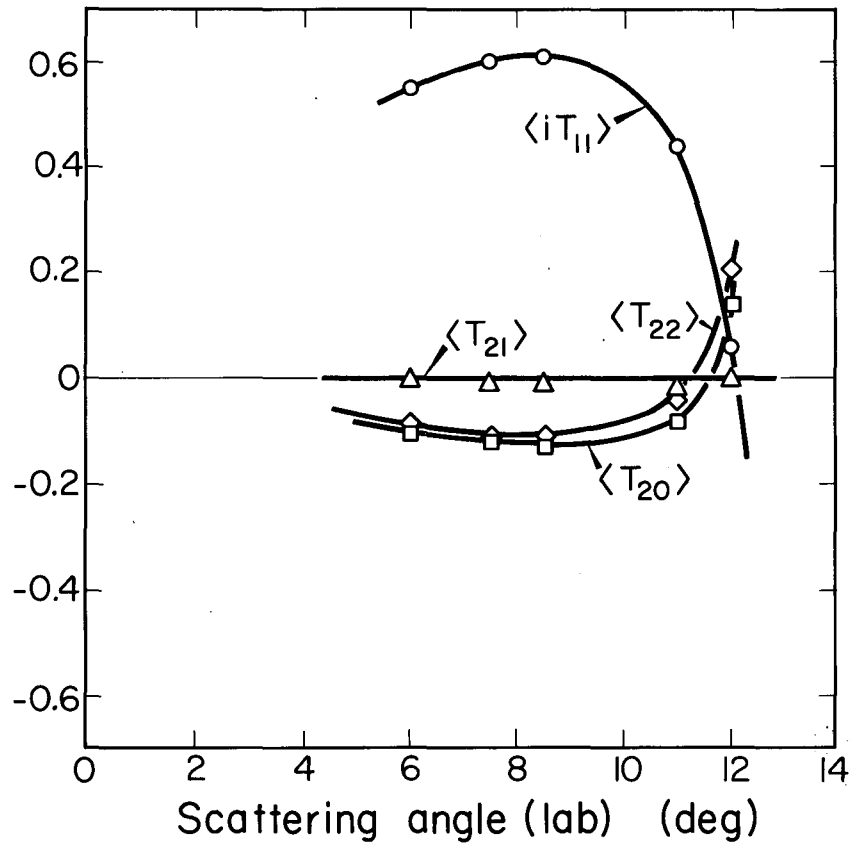
MU-17316

Fig. 23. (a) Calculated polarization components for
410-Mev deuterons scattered by beryllium.
Bjorklund amplitudes for proton scattering were
used in the impulse approximation with simultaneous
scattering included.
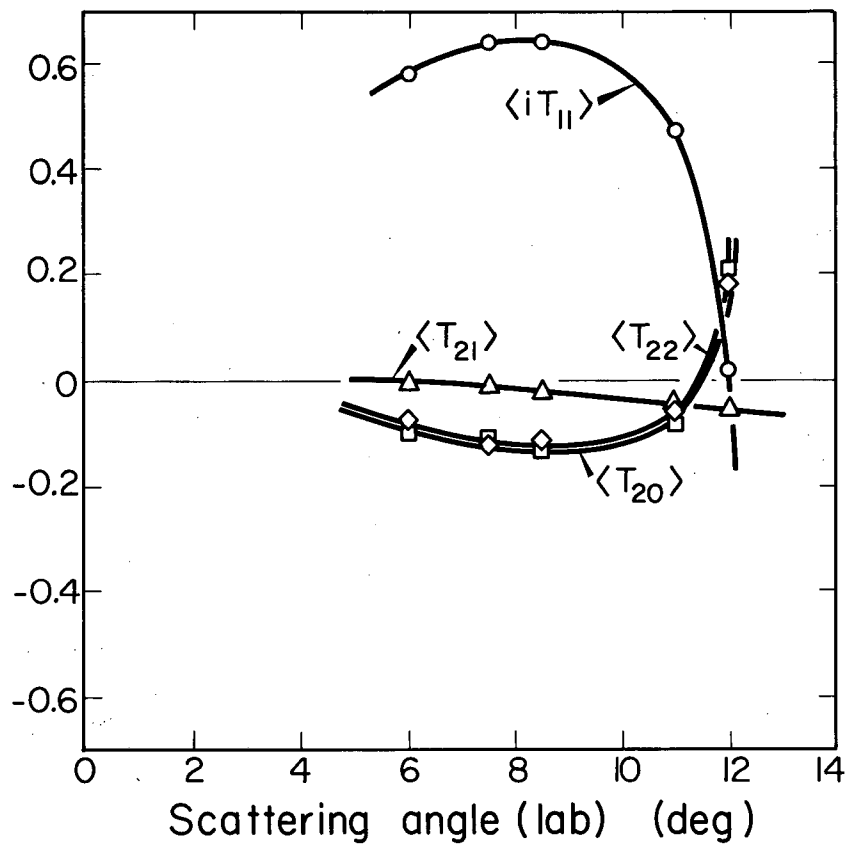
MU-17317

Fig. 23. (b) Calculated polarization components for
410-Mev deuterons scattered by beryllium.
Bjorklund amplitudes for neutron scattering were
used in the impulse approximation with simultaneous
scattering included.

|        | Hafner | Bjorklund | Riesenfeld-Watson |
|--------|--------|-----------|-------------------|
| Re $V_c$ | 10 Mev | 3 Mev | 3.5 Mev |
| Im $V_c$ | 25 | 16 | 13 |
| Re $V_s$ | 225 | 450 | 45 |
| Im $V_s$ | 0 | -240 | -61 |
| $r_0$ [a] | $(1.09 A^{1/3} - a)$ f, | $1.0 A^{1/3}$ f | |
| a | 0.1 f | 0.5 f | |

Riesenfeld-Watson potential wells determined by superposition of nucleon-nucleon amplitudes are indicated for comparison. The Hafner amplitudes gave a considerably better fit to the Rochester nucleon-nucleus cross sections than did the Bjorklund amplitudes, which were too small at all angles; the former also gave a somewhat better fit to nucleon polarization.

Calculations to determine the characteristics of deuteron scattering were done first in the simplest approximation with only the S-state deuteron wave function and without the inclusion of simultaneous scattering effects. These results are indicated in Figs. 18a and 18b. The deuteron cross section as calculated with Hafner amplitudes was larger than experimental measurements by a factor of five or six at small angles in the simplest approximation for both beryllium and carbon scatterings.

Deuteron cross-section results for beryllium using Bjorklund amplitudes dropped much too rapidly with angle. However, cross-section and polarization calculations with Bjorklund proton and neutron amplitudes did indicate that charge independence could be approximately

---

[a] Note that the value of $r_0$ used is small. Hafner found it to give a low absorption cross section and suggested that his choice of Im $V_s$ as zero had perhaps required a small $r_0$ to fit cross section and polarization. Bjorklund, however, also found a small $r_0$ necessary even with a nonzero Im $V_s$.

assumed, even though Coulomb interference was effective out to
rather large angles. The real part of the spin-independent amplitude
was found to go negative (at angles below the diffraction minimum) and
the real part of the spin-dependent amplitude somewhat reduced for
proton in comparison with neutron scattering; but real amplitudes
were much less than the unchanged imaginary parts of the amplitudes
at all angles except very small ones. Thus Coulomb interference had
very little effect on polarization, where it entered into the product of
two small terms, and no appreciable effect on cross section. In
other words, the Coulomb effect was inappreciable because the phases
of the scattering amplitudes were close to 90 deg.

The magnitude of $\langle iT_{11} \rangle$ was well predicted by the impulse
approximation at small angles. $\langle T_{22} \rangle$ was given reasonably well,
and the sign and general behavior, if not the magnitude, of $\langle T_{20} \rangle$
were corroborated (again indicating Case B signs to be preferable
to those of Case A). $\langle T_{21} \rangle$ was zero without simultaneous scat-
tering.

### D. Higher-Order Approximations

Tensor terms in the scattering matrix resulting in appreciable
tensor polarization components arise either from a higher-order
Born approximation or from the inclusion of the D state in the deu-
teron wave function used in the first Born approximation. In the
latter case, the scattering matrix takes the particularly simple form

$$M_{sc} = a\,(\theta) + b\,(\theta)\,S_i\,n_i + c\,(\theta)\,S_{ij}\,K_i\,K_j ,$$

with a $(\theta)$ and b $(\theta)$ as given above in terms of the $g_d(\theta)$ and $h_d(\theta)$
amplitudes. (K represents the unit vector in the direction of momentum
transfer.) The sticking factor becomes much more complex[3] and
includes various orders of Bessel functions taken between S- and
D-state wave functions.

Calculations utilizing the D-state wave function were done for
two angles of scattering and gave results for cross section and polari-
zation components differing inappreciably from those for the S-state

wave function alone.

Tensor terms of the scattering matrix arise also from simultaneous scattering of both particles in the deuteron with a contribution to the transition matrix element proportional to $V_1 V_2$ in addition to the linear combination of $V_1$ and $V_2$ describing scattering in the usual impulse approximation. Stapp treated this effect in some detail with the use of time-dependent perturbation theory and found expressions for the additional elements of the scattering amplitude; he determined simultaneous scattering to be the dominant effect at large angles and was able to obtain good agreement with experimental cross section at low energies (near 150 Mev) only with the inclusion of this effect, which increased the large-angle and decreased the small-angle estimate of scattering.[3]

Stapp's formulae were used to calculate the contributions of simultaneous scattering to the amplitudes for deuteron scattering from carbon and beryllium at 420 and 410 Mev, respectively. Results obtained for cross section and polarization components, as calculated with the Hafner proton data and with the Bjorklund proton and neutron data, are given in Figs. 15 and 21 through 23. Calculations with the impulse approximation including simultaneous scattering are not given beyond the diffraction minimum, as unreasonable results were obtained--probably because the assumptions made by Stapp that the amplitudes for nucleon scattering did not change phase rapidly with angle were not good in the region of the diffraction minimum.

Inclusion of simultaneous scattering effects reduced beryllium and carbon cross sections to within a factor of 2.5 to 3 of experiment at small angles and brought agreement at moderate angles. However, the inclusion of simultaneous scattering effects gave rather poor results for tensor components of polarization. $\langle T_{21} \rangle$ values predicted were much smaller than experimental results.

# VI. CONCLUSIONS

## A. Values of Tensor Components

The vector polarization $\langle iT_{11} \rangle$, proportional to the probability of finding deuteron spin normal to the plane of scattering, reaches a maximum at 8 deg, with behavior similar to that of the quantity e ; its value indicates that the maximum $\langle S_y \rangle$ polarization is 73% for beryllium and 62% for carbon. Although scattering could not be done at angles smaller than 6 deg, measurements suggested that $\langle iT_{11} \rangle$ probably rises rather rapidly with angle, as in Baldwin's experiment at lower energies. $\langle iT_{11} \rangle$ for the various energies of scattering on beryllium and carbon is plotted as a function of angle in Fig. 24. Figure 25 gives its dependence on the quantity $KA^{1/3}$ (proportional to momentum transfer times nuclear radius); this graph shows that at the higher energies, $\langle iT_{11} \rangle$ is displaced from the function of $KA^{1/3}$ obtained at the lower energies[8] and is perhaps less uniform for different scatterers.

For deuterons of about 100 to 150 Mev, $\langle T_{21} \rangle$ was estimated by Stapp as less than 15% of the quantity $\langle iT_{11} \rangle$ and was assumed equal to zero by Baldwin and Tripp for purpose of calculations. Here it is evidently a considerable fraction of the vector polarization, as much as 30 to 40% at moderate angles of scattering. The tensor components $\langle T_{20} \rangle$ and $\langle T_{22} \rangle$ also assume values appreciably different from zero; they increase uniformly with scattering angle, $\langle T_{20} \rangle$ approaching 70% and $\langle T_{22} \rangle$ going to approximately 30% at 16 deg.

## B. Utilization of Results

Complete knowledge of the tensor components in deuteron polarization provides a useful tool for the determination of transition amplitudes in the reaction

$$p + p \rightarrow \pi^+ + d.$$
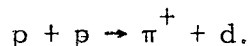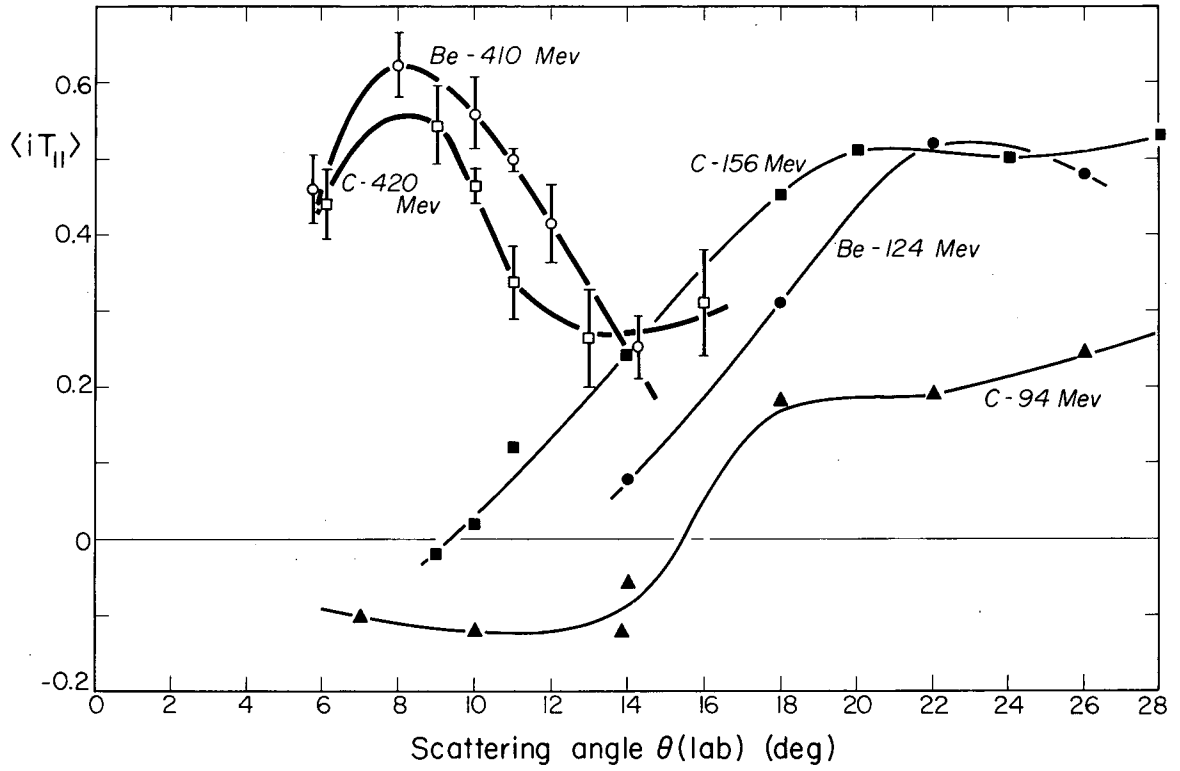
Fig. 24. Vector polarization $\langle iT_{11} \rangle$ vs. scattering angle for various energies and target materials.
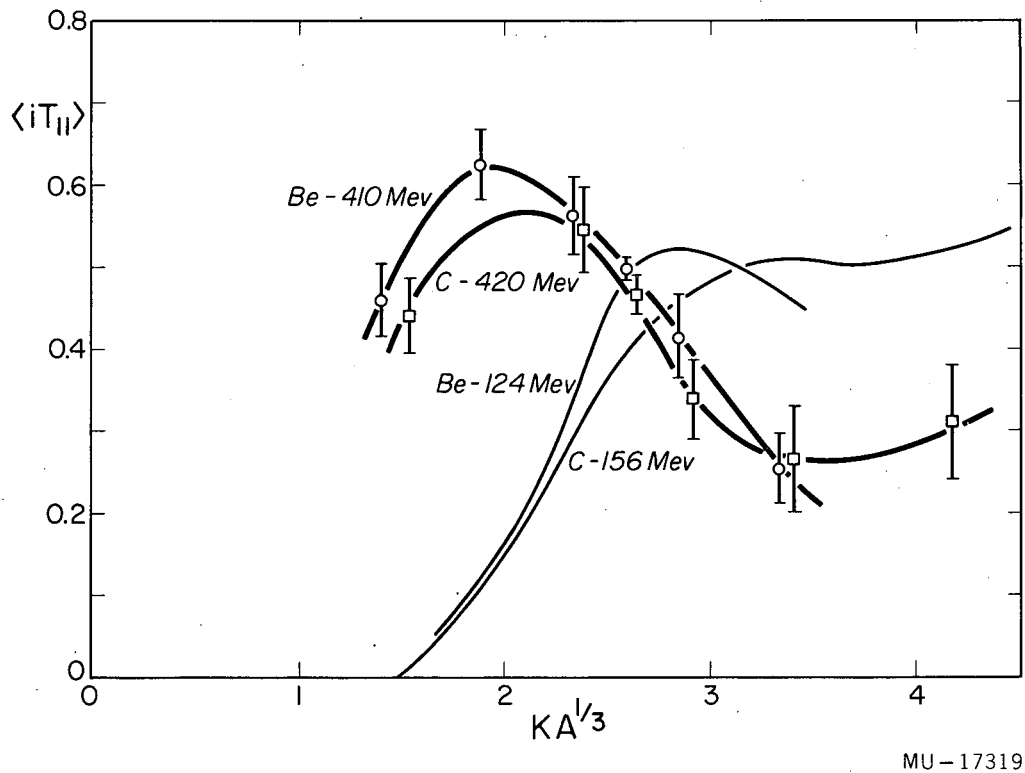
MU – 17318

Fig. 25. Vector polarization $\langle iT_{11} \rangle$ vs. momentum transfer times $A^{1/3}$.

If only S- and P-wave pions are produced, five parameters serve to describe the three possible types of transitions and thus to give information on differences between p-p phase shifts.[4,22,23] These five quantities can be taken as the parameters $\alpha$ and $\beta$ of the total cross section in terms of the center-of-mass pion momentum;[a] the A defined by the unpolarized differential cross section $(\sigma(\theta) \simeq A + \cos^2 \theta)$ in the center-of-mass system; the Q which derives from the asymmetry of pions produced by an incident unpolarized beam $(e = PQA \sin\theta/A + \cos^2 \theta)$; and finally a quantity $\omega_0$ which enters into the expression for vector polarization $\left\langle iT_{11} \right\rangle$ of the outgoing deuterons produced by an unpolarized proton beam. Analyses for these last quantities were performed by Crawford and Stevenson[24] and Tripp[4] at proton energies of 315 and 340 Mev; the latter was forced to accept an estimate by Stapp that $\left\langle T_{21} \right\rangle$ was much smaller than $\left\langle iT_{11} \right\rangle$, as he could analyze only for a combination of these components by utilizing Baldwin's results.[8]

Deuterons of 435 Mev would be produced by the $p + p \rightarrow \pi^+ + d$ reaction with the 740-Mev protons now available at the cyclotron. However, a determination of deuteron polarization using the known analyzabilities of carbon or beryllium at 410 to 420 Mev would be of no value unless the $p + p \rightarrow \pi^+ + d$ formalism could be revised. As suggested by Wolfenstein[22] and confirmed by Akimov, Savchenko, and Soyoko,[25] the D-wave production of pions becomes important above 400 Mev, as shown by the variation of asymmetry with angle; and further it becomes impossible to describe the $p + p \rightarrow \pi^+ + d$ cross section as $\alpha\eta + \beta\eta^3$ for a pion momentum above $\eta = 1.2$ (or proton energy above 490 Mev). Thus the parameters defined above can no longer describe the reaction.

Breakdown of the formalism at very high energies does not, however, preclude the possibility of extending knowledge of $\pi^+$-d transition amplitudes and p-p phase shifts above 400 Mev. Scattering

---

[a] For S- and P-waves, $\sigma(\eta) = \alpha\eta + \beta\eta^3$, with $\eta$ the pion momentum in units of $m_\pi c$.

of deuterons on carbon at an energy of 420 Mev, degrading, and analyzing at a much lower energy of 235 Mev could be done to obtain values of polarization components which would be useful for analyzing the $p + p \rightarrow \pi^+ + d$ reaction at proton energies of 415 Mev. The quantities $\alpha$, $\beta$, $A$, and $Q$ are already known at this energy; $A$ is approximately 0.22 and $Q$ is $0.45 \pm .08$.[26] A maximum $\langle iT_{11} \rangle$ would be obtained at a center-of-mass angle of about 60 deg, for which the deuteron would be emitted at an angle of about 7 deg in the laboratory system. The $\langle T_{21} \rangle$ produced in the reaction could be estimated in terms of $\langle iT_{11} \rangle$; and with knowledge having been obtained separately of the analyzing $\langle T_{21} \rangle$ and $\langle iT_{11} \rangle$, the $\langle iT_{11} \rangle$ produced in the $p + p \rightarrow \pi^+ + d$ reaction could be definitely determined.

Other polarization components could also be utilized for analysis. Usually there is calculated from the quantity $A$ a value for the parameter $X$, where the cross section for P-wave mesons produced is $\sigma_p \approx X + \cos^2 \theta$. $\langle T_{22} \rangle$, which is proportional to $X/A$ at $\theta = 90$ deg, might give a value for $X$ more nearly exact than asymmetry experiments with polarized protons. (Crawford and Stevenson found $X = 0.082 \pm .034$ from the latter.) $\langle T_{22} \rangle$ should have an appreciable value of approximately $0.3\sqrt{3}$ at a proton energy of 440 Mev;[23] however, $\langle T_{22} \rangle$ for the analyzer (e.g., beryllium or carbon) would very likely not have a value greater than 0.25 at a reasonable deuteron analyzing angle. $\langle T_{20} \rangle$ measured at $\theta = 0$ deg could also give $X/A$ and would be approximately equal to $-0.6\sqrt{2}$, but somewhat larger errors would be involved in the analysis, as it depends on absolute cross section. $\langle T_{21} \rangle$ measurements probably would not be helpful.

In conclusion, deuteron polarization components at the energies reported here are not directly useful for $p + p \rightarrow \pi^+ + d$ work unless the theory can be reformulated. Double scattering as described in this report could yield useful information through a degraded second scattering for $p + p \rightarrow \pi^+ + d$ analysis near 400 Mev; or remeasurement of tensor components at about 150 Mev through a degraded second scattering could be utilized to check the 315-Mev analysis with greater accuracy.

## ACKNOWLEDGMENTS

# APPENDIX A.

### Formulae for Nucleon and Deuteron Scatteron

As an aid in comparing nucleon and deuteron polarization on a mathematical and physical basis, the more important formulae are here summarized.

### General Formulae

Density matrix describing final polarization state of a beam of particles:

$$\rho_f = \frac{Tr\rho_i}{n_i} \sum_\mu \left\langle S^\mu \right\rangle \ S^\mu \quad \text{or} \quad M\rho_i M^\dagger.$$

Expectation value of any operator in terms of density matrix:

$$\left\langle A \right\rangle = \frac{Tr(\rho A)}{Tr\rho}.$$

Wolfenstein-Ashkin relation[6] describing beam after scattering:

$$I \left\langle S^\mu \right\rangle_f = \frac{1}{n_i} \sum_\nu \left\langle R^\mu \right\rangle_i \ Tr \ (MR^{\nu\dagger}M^\dagger S^\mu).$$

Here $n_i$ is the dimensionality of the initial spin space, M is the scattering matrix, and R or S is a set of basis operators in terms of which the density or scattering matrix may be expressed (for example, the Pauli matrices or the $T_{JM}$).

### Nucleon Formulae: (spin-zero nucleus)

Density matrix: $\rho = \frac{I_u}{2} \left(1 + \sum \left\langle \sigma_i \right\rangle \sigma_i \right) = \frac{I_u}{2} \ (1 + \overline{P} \cdot \overline{\sigma})$.

Polarization of singly scattered beam: $P_y = \dfrac{N_+ - N_-}{N_+ + N_-}$

(with $N_+$ the number of particles with spin up;

$N_-$, the number with spin down).

Cross section after second scattering: $I_2 = I_u (1 + e \cos \theta)$.

Asymmetry: $e = P_1 P_2 = \dfrac{I_L - I_R}{I_L + I_R}$ .

In terms of quantities obtained from impulse approximation,

$$M_{sc} = g(\theta) + h(\theta) \, \overline{\sigma} \cdot \overline{n} ,$$

$$I_u = g^2 + h^2$$

$$P_y = 2 \operatorname{Re} g^* h / (g^2 + h^2)$$

## Deuteron Formulae (spin-zero nucleus)

Density matrix: $\rho = 1/3 \displaystyle\sum_{JM} \left\langle T_{JM} \right\rangle T_{JM}^\dagger$ .

Polarization of singly scattered beam: $P_y = \dfrac{N_+ - N_-}{N_+ + N_- + N_0}$

(with $N_0$ the particles having spin in
  plane of scattering).

Cross section after second scattering: $I_2 = I_u (1 + d + e \cos \phi$

$+ f \cos 2\phi)$.

Asymmetry of second scattering:

$$e = 2 \left( \left\langle iT_{11} \right\rangle_1 \left\langle iT_{11} \right\rangle_2 - \left\langle T_{21} \right\rangle_1 \left\langle T_{21} \right\rangle_2 \right)$$

$$= (I_L - I_R)/2 I_u ,$$

where $\left\langle iT_{11} \right\rangle$ equals $\dfrac{\sqrt{3}}{2} P_y$ .

In terms of quantities obtained from impulse approximation,

$$M_{sc} = a + b \, \overline{S} \cdot \overline{n} + C_{ij} S_{ij} \text{ or } \simeq f^{1/2}(K) \left[ 2 g_d + h_d \, \overline{S} \cdot \overline{n} \right] ,$$

$$I_u \simeq f(K) \left[ 4 g_d^2 + 2/3 \, h_d^2 \right] ,$$

$$P_y \simeq 4/3 \ f(K) \ 2 \ \mathrm{Re} \ g_d^* \ h_d \ / \ I_u$$

(f(K) being the sticking factor).

Polarization expressions may be written in terms of spin wave functions:

$$\eta_i = \begin{pmatrix} a_1^i \\ a_2^i \end{pmatrix} \qquad \text{for the } \underline{i}\text{th nucleon,}$$

$$\chi_i = \begin{pmatrix} a_1^i \\ a_2^i \\ a_3^i \end{pmatrix} \qquad \text{for the } \underline{i}\text{th deuteron.}$$

Then

$$P_y^n = \frac{\sum_i \eta_i^\dagger \ \sigma_y \ \eta_i}{\sum_i \eta_i^\dagger \ \eta_i} = \frac{\sum_i \eta_i^\dagger \begin{pmatrix} 1 & 0 \\ 0 & -1 \end{pmatrix} \eta_i}{\sum_i \eta_i^\dagger \ \eta_i} = \frac{\sum a_1^{i2} - a_2^{i2}}{\sum a_1^{i2} + a_2^{i2}}$$

and

$$P_y^d = \frac{\sum \chi_i^\dagger \ S_y \ \chi_i}{\sum \chi_i^\dagger \ \chi_i} = \frac{\sum_i \chi_i^\dagger \begin{pmatrix} 1 & 0 & 0 \\ 0 & 0 & 0 \\ 0 & 0 & -1 \end{pmatrix} \chi_i}{\sum_i \chi_i^\dagger \ \chi_i} = \frac{\sum a_1^{i2} - a_3^{i2}}{\sum a_1^{i2} + a_2^{i2} + a_3^{i2}},$$

with the sums taken over all particles in the beams.

# APPENDIX B. 1.

## Operators in the Deuteron Spin Space

### Usual Spin Operators

$$S_x = \frac{1}{\sqrt{2}} \begin{bmatrix} 0 & 1 & 0 \\ 1 & 0 & 1 \\ 0 & 1 & 0 \end{bmatrix} \qquad S_y = \frac{1}{\sqrt{2}} \begin{bmatrix} 0 & -i & 0 \\ i & 0 & -i \\ 0 & i & 0 \end{bmatrix} \qquad S_z = \begin{bmatrix} 1 & 0 & 0 \\ 0 & 0 & 0 \\ 0 & 0 & -1 \end{bmatrix}$$

$$S_x^2 = \frac{1}{2} \begin{bmatrix} 1 & 0 & 1 \\ 0 & 2 & 0 \\ 1 & 0 & 1 \end{bmatrix} \qquad S_y^2 = \frac{1}{2} \begin{bmatrix} 1 & 0 & -1 \\ 0 & 2 & 0 \\ -1 & 0 & 1 \end{bmatrix} \qquad S_z^2 = \begin{bmatrix} 1 & 0 & 0 \\ 0 & 0 & 0 \\ 0 & 0 & 1 \end{bmatrix}$$

$$S_x S_y = \frac{1}{2} \begin{bmatrix} i & 0 & -i \\ 0 & 0 & 0 \\ i & 0 & -i \end{bmatrix} \qquad S_y S_z = \frac{1}{\sqrt{2}} \begin{bmatrix} 0 & 0 & 0 \\ i & 0 & i \\ 0 & 0 & 0 \end{bmatrix} \qquad S_x S_z = \frac{1}{\sqrt{2}} \begin{bmatrix} 0 & 0 & 0 \\ 1 & 0 & -1 \\ 0 & 0 & 0 \end{bmatrix}$$

$$S_y S_x = \frac{1}{2} \begin{bmatrix} -i & 0 & -i \\ 0 & 0 & 0 \\ i & 0 & i \end{bmatrix} \qquad S_z S_y = \frac{1}{\sqrt{2}} \begin{bmatrix} 0 & -i & 0 \\ 0 & 0 & 0 \\ 0 & -i & 0 \end{bmatrix} \qquad S_z S_x = \frac{1}{\sqrt{2}} \begin{bmatrix} 0 & 1 & 0 \\ 0 & 0 & 0 \\ 0 & -1 & 0 \end{bmatrix}$$

### $T_{JM}$ (Irreducible) Operators

$$T_{00} = 1 = \begin{bmatrix} 1 & 0 & 0 \\ 0 & 1 & 0 \\ 0 & 0 & 1 \end{bmatrix}$$

$$T_{11} = -\frac{\sqrt{3}}{2} (S_x + i S_y) = -\frac{\sqrt{3}}{2} \begin{bmatrix} 0 & 1 & 0 \\ 0 & 0 & 1 \\ 0 & 0 & 0 \end{bmatrix} = -T_{1,-1}^\dagger$$

$$T_{10} = \sqrt{\frac{3}{2}} \; S_z$$

$$T_{22} = \frac{\sqrt{3}}{2} (S_x + i S_y)^2 = \sqrt{3} \begin{bmatrix} 0 & 0 & 1 \\ 0 & 0 & 0 \\ 0 & 0 & 0 \end{bmatrix} = T_{2,-2}^\dagger$$

$$T_{21} = - \frac{\sqrt{3}}{2} \left[ (S_x + i S_y) S_z + S_z (S_x + i S_y) \right] = -\sqrt{\frac{3}{2}} \begin{bmatrix} 0 & 1 & 0 \\ 0 & 0 & -1 \\ 0 & 0 & 0 \end{bmatrix} = - T_{2,-1}^\dagger$$

$$T_{20} = \frac{1}{\sqrt{2}} (3 S_z^2 - 2) = \frac{1}{\sqrt{2}} \begin{bmatrix} 1 & 0 & 0 \\ 0 & -2 & 0 \\ 0 & 0 & 1 \end{bmatrix}$$

## APPENDIX B. 2.

### Eigenfunctions in the Deuteron Spin Space

It is convenient to know the eigenfunctions of the spin operators in a representation having the z axis as the axis of quantization. These may be found by solving eigenvalue equations or by transforming the usual $S_z$ eigenfunctions by performing a rotation about the x or y axis; for example,

$$\chi_i^y = \exp\left(iS_x\,\theta\right)\chi_i^z = \left[1 + (\cos\theta - 1)\,S_x^2 + i\sin\theta\,S_x\right]\chi_i^z .$$

The eigenfunctions found are given in the following table. Those associated with $S_y$ give the spin functions used by Baldwin,[7] while the usual $S_z$ eigenfunctions are special cases of the functions discussed by Lakin.

| Eigenvalues | Operators | | |
|---|---|---|---|
| | $S_x$ | $S_y$ | $S_z$ |
| +1 | $\dfrac{1}{2}\begin{bmatrix} 1 \\ \sqrt{2} \\ 1 \end{bmatrix}$ | $\dfrac{1}{2}\begin{bmatrix} 1 \\ i\sqrt{2} \\ -1 \end{bmatrix}$ | $\begin{bmatrix} 1 \\ 0 \\ 0 \end{bmatrix}$ |
| 0 | $\dfrac{1}{\sqrt{2}}\begin{bmatrix} 1 \\ 0 \\ -1 \end{bmatrix}$ | $\dfrac{1}{\sqrt{2}}\begin{bmatrix} 1 \\ 0 \\ 1 \end{bmatrix}$ | $\begin{bmatrix} 0 \\ 1 \\ 0 \end{bmatrix}$ |
| -1 | $\dfrac{1}{2}\begin{bmatrix} 1 \\ -\sqrt{2} \\ 1 \end{bmatrix}$ | $\dfrac{1}{2}\begin{bmatrix} 1 \\ -i\sqrt{2} \\ -1 \end{bmatrix}$ | $\begin{bmatrix} 0 \\ 0 \\ 1 \end{bmatrix}$ |

## APPENDIX C. 1.

### Density Matrix

The density matrix in the representation in which the z axis is the axis of quantization and is parallel to incident momentum, but the y axis is the normal to the scattering plane, takes the form

$$\rho = 1/3 \sum_{JM} \left\langle T_{JM} \right\rangle T^{\dagger}_{JM}$$

$$= \frac{1}{3} \begin{bmatrix} 1 + \frac{1}{\sqrt{2}} \left\langle T_{20} \right\rangle & -\sqrt{\frac{3}{2}} \left( \left\langle T^{\dagger}_{11} \right\rangle + \left\langle T^{\dagger}_{21} \right\rangle \right) & \sqrt{3} \left\langle T^{\dagger}_{22} \right\rangle \\ -\sqrt{\frac{3}{2}} \left( \left\langle T_{11} \right\rangle + \left\langle T_{21} \right\rangle \right) & 1 - \sqrt{2} \left\langle T_{20} \right\rangle & \sqrt{\frac{3}{2}} \left( -\left\langle T^{\dagger}_{11} \right\rangle + \left\langle T^{\dagger}_{21} \right\rangle \right) \\ \sqrt{3} \left\langle T_{22} \right\rangle & \sqrt{\frac{3}{2}} \left( -\left\langle T_{11} \right\rangle + \left\langle T_{21} \right\rangle \right) & 1 + \frac{1}{\sqrt{2}} \left\langle T_{20} \right\rangle \end{bmatrix}$$

($I_u$ is taken as 1; $\left\langle T_{10} \right\rangle$ does not appear because it is zero in this representation). The deuteron wave function in this system for time = 0 ( or $\lambda = \mu H_z t / \hbar = 0$ ) as expressed by Baldwin[2] is

$$\Psi_d = \begin{bmatrix} -\frac{i}{\sqrt{2}} \cdot (a-b) \\ a + b \\ \frac{i}{\sqrt{2}} (a-b) \end{bmatrix}$$

and follows from the combination of y-axis wave functions (Appendix B. 2) given by

$$\Psi = i \sqrt{2} \left( -a \, \chi^y_{+1} \, e^{i\lambda} + b \, \chi^y_{-1} \, e^{-i\lambda} + c \, \chi^y_0 \right).$$

Taking $c$ as zero and hence eliminating the trivial case when $\langle S_y \rangle$ must equal zero gives the self-adjoint form of the density matrix:

$$\rho = \frac{1}{2} \begin{pmatrix} a^2 + b^2 & i\sqrt{2}\,(a^2 - b^2 & -a^2 - b^2 \\ -a^*b - ab^* & +a^*b - ab^*) & +a^*b + ab^* \\[2ex] -i\sqrt{2}\,(a^2 - b^2 & a^2 + b^2 & i\sqrt{2}\,(a^2 - b^2 \\ -a^*b + ab^*) & +a^*b + ab^* & -a^*b + ab^*) \\[2ex] -a^2 - b^2 & -i\sqrt{2}\,(a^2 - b^2 & a^2 + b^2 \\ +a^*b + ab^* & +a^*b - ab^*) & -a^*b - ab^* \end{pmatrix}$$

where the definition of $\rho$ given in Section II.B has been used.

Comparison of these two forms of the density matrix yields values of the tensor components for special states, for example, the $+1$ state when $b = 0$ and $a = 1/\sqrt{2}$. (Compare Section II.E.)

## APPENDIX C. 2.

### Lakin Inequality

In another representation, that with the z axis along the normal to the scattering plane, the density matrix takes quite a different form and permits the derivation of an inequality given by Lakin and useful for restricting the values of tensor components. If the pure states of polarization are described by

$$\psi_1 = \chi_0 \, ,$$

$$\psi_2 = A\chi_{+1} + B\chi_{-1} \, ,$$

$$\psi_3 = B^*\chi_{+1} - A^*\chi_{-1} \, ,$$

with $\chi_{+1}$, $\chi_0$, and $\chi_{-1}$ the eigenstates of $S_z$, and if these states have statistical weights of $\lambda_1$, $\lambda_2$, and $\lambda_3$, the density matrix has the form

$$\rho = \begin{pmatrix} \lambda_2 A^2 + \lambda_3 B^2 & 0 & \lambda_2 AB^* - \lambda_3 B^* A \\ 0 & \lambda_1 & 0 \\ \lambda_2 BA^* - \lambda_3 A^* B & 0 & \lambda_2 B^2 + \lambda_3 A^2 \end{pmatrix}.$$

Equating terms in this matrix to those in the $T_{JM}$ representation and noting that $\langle T_{11} \rangle = \langle T_{21} \rangle = 0$ (also making $A$ and $B$ real by choosing the X and Y axes in the plane of scattering as the tensor principal axes) gives

$$1/3 \left( 1 + \sqrt{\tfrac{3}{2}} \langle T_{10} \rangle + \tfrac{1}{\sqrt{2}} \langle T_{20} \rangle \right) = \lambda_2 A^2 + \lambda_3 B^2 \, ,$$

$$1/3 \left( 1 - \sqrt{\tfrac{3}{2}} \langle T_{10} \rangle + \tfrac{1}{\sqrt{2}} \langle T_{20} \rangle \right) = \lambda_3 A^2 + \lambda_2 B^2 \, ,$$
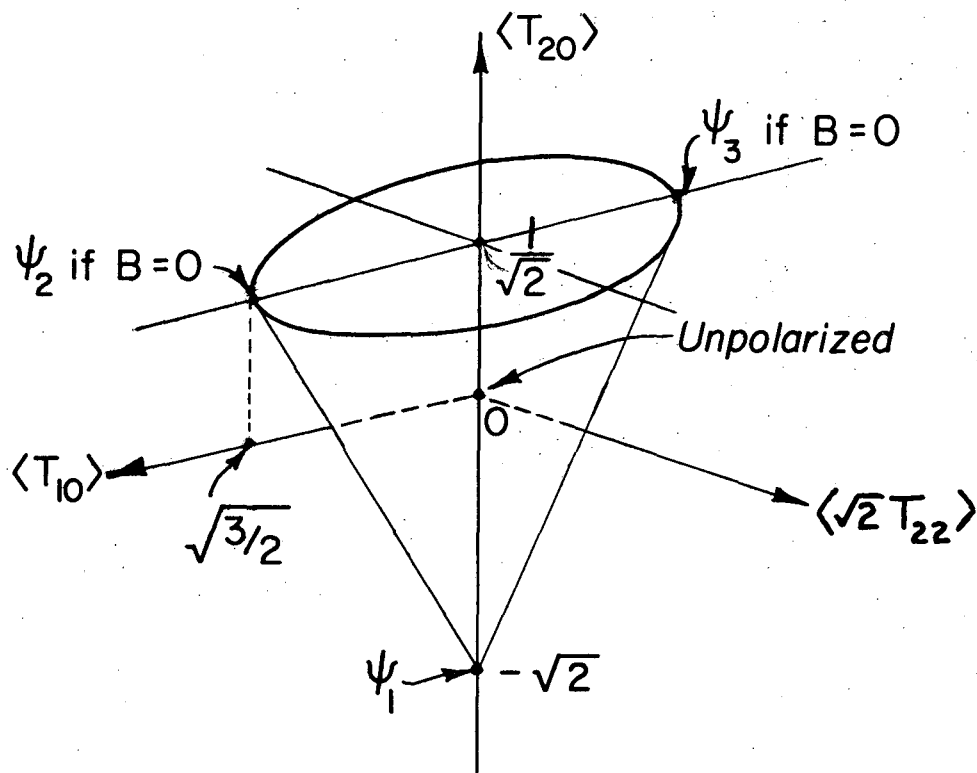
$$\langle T_{22} \rangle = \sqrt{3} (\lambda_2 - \lambda_3) AB \, ,$$

Obviously, then, since $(\lambda_2 - \lambda_3)^2 \leq (\lambda_2 + \lambda_3)^2$, there results

$$\langle T_{10} \rangle^2 + \left[ \sqrt{2} \ \langle T_{22} \rangle \right]^2 \leq \frac{1}{3} \left[ \langle T_{20} \rangle + \sqrt{2} \right]^2.$$

This inequality is represented by Fig. 26, which shows the cone containing all possible states. Pure states are at extreme points on the cone, as indicated.

MU-17320

Fig. 26. Lakin cone showing restriction of $\langle T_{JM} \rangle$ values in the spin space defined by the choice of z axis normal to the scattering plane. The $\psi$'s refer to the pure polarization states described in the Lakin article.

APPENDIX D. 1.

Rotation of the Polarization Tensor by a Magnetic Field

Three methods may be used to transform the $\langle T_{JM} \rangle$ :

(a) Finding the expectation values of spin operators as transformed in coordinate space with the use of precessed spin wave functions; i.e., making separate spin-system and coordinate-system transformations.

(b) Transforming the $\langle T_{JM} \rangle$ directly for a relative spin rotation $\lambda = \gamma(\mu-1)\eta$ by means of the Kramers method of transforming the spherical harmonic $Y_{JM}$, which uses the analogy between the three-dimensional rotation of the $Y_{JM}$ and a two-dimensional transformation of $\xi^{J+M}\eta^{J-M}$, where $\xi$ and $\eta$ are unit vectors of the spinor plane. (An equivalent method is the use of the $\mathcal{D}$ rotation matrix given by Fano and Racah.[27])

(c) Expressing $S_i S_j$ (like Stapp's $S_i S_j$, but without his $-2/3\ \delta_{ij}$) in terms of the $T_{JM}$ and carrying out an orthogonal transformation representing rotation through the angle $\lambda$.

The last is most easily understood physically. Just as a spin vector expressed in the x-y-z coordinate system can be transformed for rotation $\lambda$ about the y axis by taking

$$S'_i = \sum_m a_{im} S_m \quad \text{or} \quad \underline{S}' = \begin{bmatrix} \cos\lambda & 0 & -\sin\lambda \\ 0 & 1 & 0 \\ \sin\lambda & 0 & \cos\lambda \end{bmatrix} \begin{bmatrix} S_x \\ S_y \\ S_z \end{bmatrix},$$

so the tensor spin products can be transformed with the same matrix $\underline{A}$:

$$(S_i S_j)' = \sum \sum a_{im} a_{mn} S_n S_j \quad \text{or} \quad (\underline{S}\,\underline{S})' = \underline{A}\,(\underline{S}\,\underline{S})\,\underline{A}^{-1}.$$

The first problem is to express $S_i S_j$ in terms of $T_{JM}$.

By using

$$S_x^2 + S_y^2 + S_z^2 = S(S+1) = 2$$

and

$$S_x S_y - S_y S_x = i S_z \text{ , etc.,}$$

it can be shown on combining the $T_{JM}$ and $T_{J,-M}$ terms, that

$$S_x^2 = 1/\sqrt{3} \; T_{22} + 2/3 - (1/3\sqrt{2}) \, T_{20} \text{ ,}$$

$$S_x S_y = 0$$

$$S_x S_z = (1/\sqrt{3}) \, (-T_{21} - 2 \, T_{11}) \text{ , etc.}$$

Carrying out the above transformation, one obtains $(\underline{S}\,\underline{S})'$ in terms of the original $\underline{S}\,\underline{S}$ $(T_{JM})$ and trigonometric functions of $\lambda$. Equating the $T_{JM}$ expression for each $(\underline{S}\,\underline{S})'$ term to the associated $(T_{JM,}\,\lambda)$ expression then gives the formulae included in Baldwin's appendix (though with opposite signs for the $\sin 2\lambda$ terms). For example, the $S_x S_z$ element gives

$$(1/\sqrt{3}) \left( - \langle T_{21} \rangle' - 2 \langle T_{11} \rangle' \right) = \left[ -(1/\sqrt{2}) \langle T_{20} \rangle + (1/\sqrt{3}) \langle T_{22} \rangle \right] (\sin 2\lambda/2)$$

$$+ (1/\sqrt{3}) \left( \langle T_{21} \rangle - 2 \langle T_{11} \rangle \right) \sin^2 \lambda + (1/\sqrt{3}) \left( - \langle T_{21} \rangle - 2 \langle T_{11} \rangle \right) \cos^2 \lambda.$$

Thus,

$$\langle T_{21} \rangle' = \langle T_{20} \rangle \, (1/2) \sqrt{3/2} \; \sin 2\lambda + \langle T_{21} \rangle \cos 2\lambda - \langle T_{22} \rangle (\sin 2\lambda/2).$$

## APPENDIX D. 2.

### Polarization Ellipsoid

The ellipsoid representing the polarization tensor provides a simple way of performing the above transformation by geometry rather than algebra. This ellipsoid is analogous to the moment of inertia ellipsoid.

The moment of inertia for rotation of a body about an axis $\underline{n}$ is

$$I_n = I_{xx}x^2 + I_{yy}y^2 + I_{zz}z^2 + 2 I_{xy} xy + 2 I_{xz} xz + 2 I_{yz} yz,$$

and if an ellipsoidal surface is represented by

$$1 = I_{xx}\rho_x^2 + I_{yy}\rho_y^2 \cdots + 2 I_{xy}\rho_x\rho_y \cdots$$

with $\bar{\rho} = \bar{n}/\sqrt{I,}$ then $I$ for this particular axis $\underline{n}$ can be found by taking $1/\rho^2$ in the direction of $\underline{n}$.

Similarly, the spin tensor $\underline{SS}$ can be represented by a surface whose equation is

$$1 = \left\langle S_x^2 \right\rangle \rho_x^2 + \left\langle S_y^2 \right\rangle \rho_y^2 \cdots + \left( \left\langle S_{xy} \right\rangle + \left\langle S_{yx} \right\rangle \right) \rho_x\rho_y \cdots .$$

The effects of rotating the polarization tensor (with a magnetic field) about one of its principal axes can be easily determined by consideration of the effect of rotation of the ellipsoid cross section in the plane perpendicular to this axis. (See Fig. 3b.)

# APPENDIX E.

## Errors in Cross-Section Parameters

The expressions for the d, e, and f cross-section parameters were given in Section III. J. Errors entering into the determination of these quantities were caused by three factors: statistics, normalization, and misalignment.

For statistical error, the usual expression for error in a quantity A dependent upon variables $x_i$ was used:

$$(\Delta A)^2 = \sum_i \left(\frac{\partial A}{\partial x_i}\right)^2 (\Delta X_i)^2 .$$

This resulted in the following expressions for the errors in the quantities d, e, and f:

$$\Delta d = 1/I_u \cdot \sqrt{(\Delta \bar{I}_p)^2 + (1+d)^2 (\Delta I_u)^2} ,$$

$$\Delta e = 1/2I_u \sqrt{(\Delta I_0)^2 + (\Delta I_{180})^2 + (2e)^2 (\Delta I_u)^2} ,$$

$$\Delta f = 1/4I_u \sqrt{(\Delta I_0)^2 + (\Delta I_{180})^2 + (\Delta I_{90})^2 + (\Delta I_{270})^2 + (4f)^2 (\Delta I_u)^2} .$$

The polarized and regenerated beams differed in their degree of contamination by low-energy particles, and in calculations which compensated for this by "normalizing" the unpolarized to the polarized cross sections by the ratio of values at $\theta_2 = 6$ deg (where d could be considered almost zero), the error was at least that resulting from the statistical uncertainty of the ratio of the 6-deg cross sections. If $\bar{I}_p/I_u$ was equal to $r + \Delta r$, the relative error in 1+d, e, and f due to normalization was $\Delta r/r$.

For error in alignment, $I_0$ and $I_{180}$ and also $I_{90}$ and $I_{270}$ could not be considered as independent variables, as the associated errors were determined by horizontal and by vertical alignments, respectively. The effects of the latter cancelled, since

$$\frac{\partial}{\partial \theta} I_{90} = -\frac{\partial}{\partial \theta} I_{270} ; \text{ and because the unpolarized cross section}$$

was corrected for misalignment on the basis of the $\phi$-dependence at one $\theta$ (beryllium) or by averaging over $\phi$ for every $\theta$ (carbon), only the horizontal setting for the polarized beam caused error. The expressions for the misalignment errors obtained were

$$\Delta d = \Delta f = \frac{1}{4 I_u} \left( \frac{\partial}{\partial \theta} I_0 - \frac{\partial}{\partial \theta} I_{180} \right) \Delta \theta,$$

$$\Delta e = \frac{1}{2 I_u} \left( \frac{\partial}{\partial \theta} I_0 + \frac{\partial}{\partial \theta} I_{180} \right) \Delta \theta.$$

## APPENDIX F.

**Formulae for $T_{JM}$ $(\theta_1)$ in Terms of Cross-Section Parameters**

("$\beta\gamma\delta$ Formulae")

If internal and external angles of scattering are the same,

$$\langle T_{21}\rangle \ (\theta_1) = \pm \left(\frac{\left|e^m\right| - e^d}{2\eta}\right)^{1/2},$$

$$\langle T_{20}\rangle \ (\theta_1) = \pm \gamma/\beta \ \left(\frac{\left|e^m\right| - e^d}{2\eta}\right)^{1/2},$$

$$\langle T_{22}\rangle \ (\theta_1) = \pm \delta/\beta \ \left(\frac{\left|e^m\right| - e^d}{2\eta}\right)^{1/2},$$

$$\langle iT_{11}\rangle \ (\theta_1) = \pm \left[e^{d}/2^{m} + \epsilon^{d}/2\eta^{m} \left(\left|e^m\right| - e^d\right)\right]^{1/2},$$

where

$$\beta = \left(a_{00}^{\mathbf{d}} - \frac{d^d}{d^m}\, a_{00}^{m}\right)\left(a_{22}^{d} - \frac{f^d}{f^m}\, a_{22}^{m}\right) - \left(a_{02}^{d} - \frac{d^d}{d^m}\, a_{02}^{m}\right)\left(a_{20}^{d} - \frac{f^d}{f^m}\, a_{20}^{m}\right),$$

$$\gamma = \left(a_{02}^{d} - \frac{d^d}{d^m}\, a_{02}^{m}\right)\left(a_{21}^{d} - \frac{f^d}{f^m}\, a_{21}^{m}\right) - \left(a_{01}^{d} - \frac{d^d}{d^m}\, a_{01}^{m}\right)\left(a_{22}^{d} - \frac{f^d}{f^m}\, a_{22}^{m}\right),$$

$$\delta = \left(a_{01}^{d} - \frac{d^d}{d^m}\, a_{01}^{m}\right)\left(a_{20}^{d} - \frac{f^d}{f^m}\, a_{20}^{m}\right) - \left(a_{00}^{d} - \frac{d^d}{d^m}\, a_{00}^{m}\right)\left(a_{21}^{d} - \frac{f^d}{f^m}\, a_{21}^{m}\right),$$

$$\eta = \left[\left(a_{10}^{d} - a_{10}^{m}\right)\frac{\gamma}{\beta} + \left(a_{11}^{d} - a_{11}^{m}\right) + \left(a_{12}^{d} - a_{12}^{m}\right)\frac{\delta}{\beta}\right],$$

$$\epsilon^{d,m} = a_{10}^{d,m}\frac{\gamma}{\beta} + a_{11}^{d,m} + a_{12}^{d,m}\frac{\delta}{\beta},$$

with the $a$ coefficients defined as functions of tensor rotation angle by

$$\langle T_{2M'}\rangle' = \sum_{M} a_{M'M}\ \langle T_{2M}\rangle. \qquad \text{(Section II. F)}$$

Although these expressions give direct $\left\langle T_{JM} \right\rangle$ evaluation, they are not very useful because of producing considerably biased results owing to the combination of $d$ and $f$ errors.

# BIBLIOGRAPHY

1. Riesenfeld and Watson, Phys. Rev. 102, 1161 (1956);
   Robert D. Tripp, Elastic Scattering of High-Energy
   Polarized Protons by Complex Nuclei (thesis),
   UCRL-2975, April 1955.

2. Baldwin, Chamberlain, Segrè, Tripp, Wiegand, and
   Ypsilantis, Phys. Rev. 103, 1502 (1956).

3. Henry P. Stapp, The Theory and Interpretation of Polarization
   Phenomena in Nuclear Scattering (thesis), UCRL-3098,
   Aug. 1955; H. P. Stapp, Phys. Rev. 107, 607 (1957).

4. R. D. Tripp, Phys. Rev. 102, 862 (1956).

5. W. Lakin, Phys. Rev. 98, 139 (1955).

6. Wolfenstein and Ashkin, Phys. Rev. 85, 947 (1952).

7. A. Garren, Phase Shifts and Coulomb Interference Effects
   for High Energy Proton-Proton Scattering, NYO-7102,
   Appendix B.2, January 1955;
   J. Simmons, Phys. Rev. 104, 416 (1956).

8. John Baldwin, Experiments on Polarization in Scattering
   Deuterons from Complex Nuclei and in Proton-proton
   Scattering (thesis), UCRL-3412, May 1956.

9. Henley and Jacobsohn, Phys. Rev. 113, 225 (1959).

10. Chamberlain, Segrè, Tripp, Wiegand, and Ypsilantis,
    Phys. Rev. 102, 1659 (1956).

11. Gordon H. Pettengill, Measurements on Proton-Proton
    Scattering in the Energy Region 150 to 340 Mev (thesis),
    UCRL-2808, Dec. 1954, Appendix C.

12. Chamberlain, Segrè, and Wiegand, Phys. Rev. 83, 928
    (1951).

13. Fermi, Metropolis, and Alei, Phys. Rev. 95, 1581 (1954).

14. Cziffra and Moravcsik, A Practical Guide to the Method
    of Least Squares, UCRL-8523, Oct. 1958;
    P. G. Hoel, Introduction to Mathematical Statistics
    (John Wiley and Sons, Inc., London, 1947), p. 134.

15. Anderson, Davidon, Glicksmann, and Kruse, Phys. Rev. 100, 279 (1955).

16. E. M. Hafner, Phys. Rev. 111, 297 (1958), and private communication.

17. L. Wolfenstein, Polarization of Fast Nucleons, Ann. Rev. Nuclear Sci. 6, 43 (1956).

18. E. Fermi, Lectures on Pions and Nucleons, Nuovo cimento Suppl. 2, Series X, 75 (1955).

19. Fernbach, Heckrotte, and Lepore, Phys. Rev. 97, 1059 (1955).

20. G. Chew, Phys. Rev. 74, 809 (1948).

21. Fernbach, Serber, and Taylor, Phys. Rev. 75, 1352 (1949).

22. L. Wolfenstein, Phys. Rev. 98, 766 (1955).

23. F. Mandl and T. Regge, Phys. Rev. 99, 1478 (1955).

24. F. S. Crawford and M. L. Stevenson, Phys. Rev. 97, 1305 (1955).

25. Akimov, Savchenko, and Soyoko, Nuclear Phys. 8, No. 6, 637 (1958); also Proceedings of 1958 Annual International Conference on High-Energy Physics at CERN, Geneva, Switzerland, p. 51.

26. Fields, Fox, Kane, Stallwood, and Sutton, Phys. Rev. 96, 812 (1954).

27. Fano and Racah, Irreducible Tensors (Academic Press, Inc., New York, 1958).